INFORMATION TO USERS

This manuscript has been reproduced from the microfilm master. UMI films the text directly from the original or copy submitted. Thus, some thesis and dissertation copies are in typewriter face, while others may be from any type of computer printer.

The quality of this reproduction is dependent upon the quality of the copy submitted. Broken or indistinct print, colored or poor quality illustrations and photographs, print bleedthrough, substandard margins, and improper alignment can adversely affect reproduction.

In the unlikely event that the author did not send UMI a complete manuscript and there are missing pages, these will be noted. Also, if unauthorized copyright material had to be removed, a note will indicate the deletion.

Oversize materials (e.g., maps, drawings, charts) are reproduced by sectioning the original, beginning at the upper left-hand corner and continuing from left to right in equal sections with small overlaps. Each original is also photographed in one exposure and is included in reduced form at the back of the book.

Photographs included in the original manuscript have been reproduced xerographically in this copy. Higher quality 6" x 9" black and white photographic prints are available for any photographs or illustrations appearing in this copy for an additional charge. Contact UMI directly to order.

UMI

A Bell & Howell Information Company
300 North Zeeb Road, Ann Arbor MI 48106-1346 USA
313/761-4700 800/521-0600

A

Endothelial-Dependent, Shear-Induced Vasodilation is Rate-Sensitive

By

Peter Butler

A dissertation submitted to the Graduate Faculty in Engineering of The City University Of New York in partial fulfillment of the requirements for the degree of Doctor of Philosophy

1999

This manuscript has been read and accepted by the Graduate Faculty in Engineering in satisfaction of the dissertation requirement for the degree of Doctor of Philosophy.

1/21/99 — Sheldon Weinbaum (mentor) — Chair of Examining Committee
Date

1/21/99 — Mumtaz Kassir — Executive Officer
Date

Daniel Lemons (co-mentor)

Shu Chien

Stephen Cowin

Charles Maldarelli

The City University of New York

Abstract

Title: Endothelial-Dependent, Shear-Induced Vasodilation is Rate-Sensitive

By: Peter J. Butler

Mentor: Professor Sheldon Weinbaum, Mechanical Engineering

Co-mentor: Professor Daniel E. Lemons, Biology

In this dissertation, we begin by presenting a background on blood-flow regulation, shear sensitivity of the endothelium, and endothelial mechanics. We then demonstrate, for the first time in arterioles, the existence of an endothelial mechanism to sense shear-stress magnitude and shear-stress rate-of-change and we proceed to quantify the arterioles' response. Finally, we describe a novel experimental technique to measure the membrane fluidity of cells under shear; membrane fluidity is a cell parameter which is hypothesized to play a role in endothelial shear mechanotransduction.

To evaluate the relative roles of shear magnitude and rate of change of shear in endothelial mediated vascular dilation, we developed a novel feedback control system in which shear stress (τ) and the temporal shear gradient (TSG) were prescribed and dynamically controlled in isolated rat cremaster 1A arterioles. This system was used to assess the roles of τ and TSG in the initial, transient vasodilations and the secondary, sustained vasodilations in response to steps and ramps in shear stress. Results showed that there exist two fundamentally different vasodilatory responses to shear stress which are mediated by microvascular

endothelium: one being potent, transient, and rate-sensitive and the other being more modest, sustained, and magnitude-sensitive.

Finally, we hypothesize that the cell membrane may be a shear sensitive organelle and that shear stress may alter cell membrane fluidity, a parameter known to modulate membrane protein function. We proceeded to develop a system in which cell membrane fluidity was measured on the confocal microscope using fluorescent recovery after photobleaching (FRAP) while the cells were sheared in a parallel plate flow chamber. Results show that this system can enable us to obtain fluidity measurements in as little as one second and will therefore be useful in measuring the time rate-of-change of membrane fluidity during various shear transients.

To Ana

Acknowledgments

I would like to acknowledge the following people who coaxed, supported, endured, learned with, studied with, laughed with, and supported me either directly or indirectly in the preparation of this research:

My parents, Ruthanne and Anthony, my step mother, Tanja, my wife, Ana, and sons, Peter Andrew and Matthew, and my wife's family.

My fellow graduate students: Yulong Wu, Liang Zhu, and Ji Song.

My student assistants: Christina Guillen, Chirag Shah, Boaz Francois, Rima Shah, and Megha Manik

Researchers from the New York Medical College: Dong Sun, Ed Messina, Gabor Kaley, Researchers from the Departments of Bioengineering, UCSD: Jerry Norwich, Julie Li, John Shyy, Shunichi Usami, and Jeff Price.

And my advisors and mentors: Daniel E. Lemons, Sheldon Weinbaum, Latif Jiji, Stephen Cowin, Charles Maldarelli, and Shu Chien

Grants: NIH, NASA, PSC-CUNY

Table of Contents

Lists of Illustrations, Charts, and Diagrams

Chapter 1: Introduction and Background

1.1 Introduction

It has long been hypothesized that the vascular system modulates its diameter to optimize the tradeoff between cardiac work and systemic blood volume in the steady state (54). Such optimization principles have led to the "Murray's Law" and form the basis of an hypothesis of Kamiya *et al.*, which states that the shear stress imparted by blood flow on the arterial side is maintained within a narrow range from a parent blood vessel to its daughter branches (37). While most studies on the modulation of vascular tone are directed at responses to stimuli such as pressure, pH, Po_2, temperature, and neurotransmitters, Murray's law as adapted by Kamiya has also fostered a number of investigations into the mechanism by which vascular tone is regulated to maintain the homeostasis of shear stress (reviewed in (9)).

Blood flow imparts shear stress, which has both steady and transient components, on vascular endothelial cells. Moderate rates of increase of shear stress may occur during exercise; more rapid rates of increase may occur during reperfusion after ischemia, following the release of experimental arterial occlusion (48), at arterial bifurcations over the cardiac cycle, and during flow intermittency in capillaries. In response to step-shear changes, endothelial cells produce nitric oxide (NO) (20) and prostacyclin (PGI_2) (26,4) within minutes, and alter their expression of

many genes to produce new proteins (68) over hours or days. While the dynamic responses of endothelial cells to sudden, step-shear changes have been studied extensively, there has been little experimental investigation of the rate-dependence of the endothelial responses to more gradual changes in shear stresses. Since ramped shear changes are likely to be far more common in the microvasculature than are step changes in shear stress, understanding these temporal aspects is essential to formulating a realistic picture of how endothelial cells regulate vascular tone and the attendant control of organ blood flow.

There is evidence for a rate-sensitivity in the NO release by cultured human umbilical vein endothelial cells (HUVECs) in response to shear: a stepped shear elicits a large and transient burst in NO, while a shear ramped over 5 minutes elicits a more moderate NO production (20). The physiological implications of such rate-sensitivity in the regulation of microvascular diameter, however, remain, until now, unknown. Although it has been reported that endothelial prostaglandin production is sensitive to shear histories (18) and that large vessel caliber may be modulated differently according to flow histories (57), the quantitative relationship between shear or shear transients and the resulting vasodilation in the microcirculation has not been established.

It is the subject of this dissertation, therefore, to demonstrate and quantify the rate-sensitive mechanism by which microvascular endothelial cells respond to elevated shear. *Ex vivo* studies were conducted which showed that the response to shear stress is biphasic with time with the initial peak depending on both the shear magnitude and a newly defined stimulus: the Temporal Shear Gradient (TSG). The

TSG is the final shear stress magnitude divided by the duration of the ramp used to achieve that magnitude. Finally, we hypothesize that changes in membrane fluidity induced by shear stress could, in part, explain rate and magnitude sensitivity of endothelium to shear stress, and proceed to develop a method to measure the changes in membrane-lipid and protein diffusion (measures of membrane fluidity) during shear stress imposition. Preliminary results are presented.

Regarding the *ex vivo* studies, we report three novel achievements. First, we describe a new experimental design in which the shear stress and the time rate of change of shear stress are prescribed and dynamically controlled in an *ex vivo* arteriolar preparation (with an accuracy previously achieved only in cell culture systems). Second, we present data revealing the biphasic nature of arteriolar dilation in response to a sustained shear stress: an initial, transient response which had a much higher peak value in response to step-shear than to a slowly ramped shear, and a later, sustained response which was essentially similar for both modes of shear. Third, by refining the time scale of the shear ramping system, we were able to quantify the roles of the shear magnitude and the newly defined stimulus, the temporal shear gradient (TSG), in the vasodilatory response to shear stress.

With respect to the *in vitro* studies we demonstrate for the first time that a Confocal-FRAP system can be used to measure lipid dynamics in as little time as 1 second. With this new method, we will be able to evaluate the time rate of change of the diffusion coefficient for membrane lipids (a direct indicator of membrane fluidity) and the mobile fraction. We will also be able to evaluate whether the membrane reacts differently to different shear histories gaining us insight into

endothelial rate sensitivity to shear stress. We present preliminary results that suggest a time rate of change of both the diffusion coefficient and the mobile fraction of lipids in the membranes of bovine aortic endothelial cells after a step in shear stress.

1.2 Background

1.2.1 Vasoregulation

Vasoregulation is essential to tissue homeostasis. Adjustment of microvascular diameter ensures that organ tissues receive enough blood to carry out important physiological functions. Oxygen delivery and CO_2 washout (25), as well as capillary pressure maintenance (36), luminal shear stress control (37), and heat transfer (80) all have been implicated as important physiological functions carried out by blood flow. Regulation of blood flow to the tissues is therefore an important physiological phenomenon. In addition, minimizing blood volume and the resistance to blood flow have the benefit of minimizing the work the heart has to do to maintain the circulatory pattern (54).

Vasoregulatory mechanisms have therefore been the subject of extensive research. In the short term, elevated tissue CO_2 may serve to dilate vessels in order to allow more oxygenated blood to flow into the tissue. The decrease in feed arteriole luminal pressure resulting from the fall of downstream vascular resistance may be counteracted by a myogenic phenomenon which dilates the vessels in

response to lower pressures (50). Finally, blood flow imparts shear stress on the endothelial lining and the endothelium responds by secreting vasodilator substances such as nitric oxide and/or prostaglandins (41). These shear-stress-induced vasodilations counteract the myogenic constriction to increases in intraluminal pressure. Remarkably, vasoactive stimuli combine to result in a relatively constant shear stress throughout the vasculature, a constant capillary pressure, and adequate oxygen supply to the tissues. In the long term the vascular bed may react to increased tissue demand by generating more blood vessels, by increasing smooth muscle cell proliferation to the walls of existing blood vessels, and endothelial cells may adjust their ability to secrete vasodilators after chronic elevations in shear stress (71). An interesting summary of these phenomenon is that while the stimuli are numerous the response, vessel diameter change, is singular. Therefore, an important experimental advance would be to monitor the vessel diameter response while keeping all vasoregulatory stimuli constant except one. This problem will be addressed later in this paper.

Two principal vasodilators secreted by the endothelium in response to shear stress are prostaglandins and nitric oxide. Their effects on smooth muscle cell contractile state are summarized in figure 1. Briefly, an arteriole is made up of one layer of confluent endothelial cells on a basement lamina surrounded by one or two layers of smooth muscle cells (fig. 2). The long axis of is aligned with the flow direction while ten to fifteen smooth muscle cells intersect with it circumferentially (fig. 4 a,b). The mechanisms by which shear stress initiates the biochemical pathway leading to vasodilator production are still poorly understood. The

hypothesized mechanism is illustrated in figure 3. It is thought that once activated, the affinity of the α subunit for its β/γ subunit in the G-protein is reduced and the α subunit with bound GTP diffuse through the membrane (73) to activate a potassium channel and/or phospholipase C (PLC). The subsequent conversion of PIP_2 to IP_3 leads to the efflux of calcium from the endoplasmic reticulum into the intracellular cytoplasm. Calcium activates the Ca^{2+}/calmodulin system which aids in the conversion of L-arginine to L-citrulline and the production of nitric oxide. Nitric oxide activates the cGMP pathway which leads to smooth muscle relaxation. Similarly, for prostaglandin production, calcium assists in the release of arachodonic acid from phospholipids via phospholipase A_2. Arachodonic acid is a substrate for the subsequent cyclooxygenase pathway which produces PGI_2, a prevalent prostaglandin. PGI_2 binds to a membrane receptor on the smooth muscle to activate the cAMP pathway which also causes smooth muscle relaxation. Smooth muscle relaxation, because of the smooth muscle cell orientation and outward luminal pressure, results in vasodilation.

1.2.2 Problems with "steady state"

Whether one looks at the long term or short term, vasoregulation is a dynamic process. Although in many cases the changes are so slow that a quasi-steady state can be assumed, this approximation misses the important dynamic changes occurring during vasoregulation. The vasoregulatory scenarios outlined in the preceding section occur within minutes and concurrently the endothelium

transiently experiences a wide range of shear stresses; the smooth muscle first distends then constricts in response to pressure increases, and the vascular bed as a whole experiences a large fluctuation in resistance that is brought back to control levels (17,28). In the long term, endothelial cells exposed to chronic alterations in shear adjust their alignment with the flow direction, move their stress fibers (24), and even alter their genetic expressions of certain molecules (76,55). All these events point to the dynamic nature of vessel and cellular function and the existence of multiple time scales (11).

While the mechanisms endothelial cells use to transduce shear stress into biological signals remain elusive, shear stress has been shown to initiate many physiological processes. Shear induces G-protein hydrolysis within seconds (30), endothelial NO and prostaglandin production within minutes (41), changes in vascular adhesion molecule expression within hours (55), and cell realignment within a day (24). Even longer term experiments (days, weeks) have demonstrated that chronic exercise may affect the efficacy with which endothelial cells secrete vasodilators in response to shear (71). Certainly, atherosclerosis is a disease in which a lifetime of relatively low and oscillating shear results in a serious obstruction of large arteries, an effect which may propagate to the microcirculation (46).

The current understanding for shear induced dilation is that within a minute, endothelial cells release NO and/or prostaglandins (PGI_2 or PGE_2) in response to elevated shear. In isolated coronary arterioles in which the vasodilator is NO (43) and in isolated cremasteric arterioles in which the vasodilator is a prostaglandin (42) an increase in flow causes vasodilation which reduces the shear stress back to near

control levels within 3-5 minutes. A rate sensitive mechanism for NO production in response to shear has been demonstrated in cultured endothelial cells but its physiological implications have only been speculated (20). It is also unclear whether these results for NO carry over to prostaglandin production. Two interesting differences exist between the isolated vessel results and the cell culture results. First, that while the stimulus (shear) and the response (vasodilator production) were the same between the two studies, in the isolated vessel, the steady state was assumed to have been reached within minutes while in the cell culture results the steady state was reached only after one hour. Second, the shear stress was not constant in the isolated vessels because of the associated vasodilation. For this reason we later present experimental data showing responses to shear changes both in the early phase (~4 minutes) and the later phase (15-30 minutes) of vasodilation.

1.2.3 The cell membrane and associated cytoskeleton as a mechanotransducer

The endothelial lining of blood vessels is the primary transducer of shear induced dilation. Its cells experience shear stress and produce vasodilators in response. Some have hypothesized that flow causes the washout of metabolic products and that the cells sense the changes in local concentrations and that the delivery of substances such as ATP are affected by the flow rate (12). Local ATP concentrations may influence vasodilator production. However, in studies where flow rate is kept constant and shear is increased by increasing medium viscosity,

investigators have shown that it is shear to which the cells are responding and not to changes in flow rate (1,42). How might a cell experience shear stress or its accompanying strain? Many investigators have demonstrated the presence of stress fibers which are linked both to luminal membrane proteins and cross the cytoplasm and connect to abluminal focal adhesion proteins (fig. 5) (10,23). These stress fibers may also be connected to cell organelles such as the nucleus and directly transduce force to them. Alternatively, these fibers may be part of a system that provides support for a cell type that is constantly experiencing out side forces (shear and pressure). In this case, it is likely that the cell membrane would experience stress (and strain) as it resists shear stress with the aid of the cytoskeleton.

Because of the possible contributions of cytoskeletal and cytoplasmic components to the cell response to mechanical stimuli formulation of the problem becomes complicated. However, Frangos *et al.* have suggested that the membrane and G-proteins are essential components of a shear stress sensing system (19). These investigators have also shown that the cells respond differently to different time histories of shear (20). Finally, they have attempted to establish the primacy of the membrane as the shear sensor by demonstrating that NO production in response to shear is independent of an intact cytoskeleton (39). In those studies, preincubation of confluent endothelial cells with cytochalasin D, which disrupts actin filaments, did not affect nitric oxide production in response to shear stress while disruption of microtubules with colchicine enhanced shear induced NO production. Missing from these studies, however, is an evaluation of whether or not the

cytoskeleton plays a role in the rate sensitive mechanism of shear induced responses.

Seemingly contradictory results come from an *ex vivo* study using rabbit aortas and cytoskeletal disrupting agents (32). Both microfilament disruption with cytochalsin B and microfilament stabilization with phalloidin attenuated endothelial NO dependent aortic relaxations suggesting that dynamic microfilament turnover is necessary for shear induced NO production. Similarly, microtubule disruption attenuated NO dependent aortic ring relaxations. In a similar study, pH and tyrosine phosphorylation and not an intact cytoskeleton determined shear induced NO production (Ayajiki, K.M. in (39)). Methodological differences may explain the differing results in the aortic preparations while it is possible that lack of alignment with the flow direction of stress fibers in confluent endothelial monolayers as contrasted with stress fiber alignment in aortic endothelial cells (38) may explain discrepancies between cell culture and *ex vivo* results. Stress fiber alignment in the direction of flow is likely a method the cells use to better resist shear stress. Therefore, stress fibers may be more important in signal transduction in *in vivo* preparations (aligned) than in (non-presheared) endothelial cells in culture (non-aligned).

Additionally, it has been suggested that the extracellular matrix - integrin - cytoskeleton system (at the focal adhesions) form a stress sensing system (53). In studies on isolated coronary arterioles, Muller *et al.* found that disrupting extracellular matrix binding through integrins inhibited shear induced vasodilation and reduced tyrosine phosphorylation (necessary for shear induced vasodilation in

these arterioles). Such studies, however, do not preclude the presence of a G-protein - membrane stress sensing system because it is likely that any disruption of stress bearing elements in the cell would affect how the cell membrane responds to luminal shear stress.

1.2.4 Shear stress and cell viscoelasticity

Finally, it will be useful to summarize previous models of endothelial cells and their mechanical properties. Sato *et al.* (63) modeled as a viscoelastic (modified kelvin) solid the endothelial membrane and its accompanying actin rich cortical layer. Their modified kelvin solid is one in which a viscous dashpot (with a coefficient of viscosity μ) in series with an elastic spring (k_2) is in parallel with another elastic spring (k_1). The dashpot's force against deformation is proportional to the rate of deformation whereas the springs' force is proportional to their elongation. A viscoelastic body modeled in such a way will exhibit strain growth with constant applied stress. By fitting to the model the data from micropipette suction experiments they calculated a coefficient of viscosity (μ) and a k_1 elastic coefficient that depended strongly on the presence of actin filaments but depended less strongly on an intact microtubule network. The k_2 elastic coefficient was not dependent on either cytoskeletal component. It was concluded that the membrane is primarily elastic and the cytoskeleton serves to stiffen it (by increasing the values of the elastic coefficients) and to damp its response to stress (by increasing the

value of the coefficient of viscosity).

In the first paper to attempt a biomechanical model for an endothelial cell exposed to shear stress, Fung and Liu (1993) predicted the tension field present in the cell membrane in response to fluid shear and suggested a role in this tension in the deformation of the nucleus (22). Furthermore they suggested that transmission of force to the sidewalls may influence the stress distribution among neighboring cells. In this light, tension may be additive from one cell to the next. However, the role of the cytoskeleton was introduced only as a parameter that might reduce membrane tension by transmitting it to the cell interior or to the focal adhesion sites on the abluminal side. This transmission of force did not have a viscoelastic component. It seems likely that most of the force generated by fluid shear is transmitted to the cell interior (79) and to the basement membrane because of the orientation of the stress fibers and that abluminal focal adhesion reorient when cells are exposed to luminal shear stress (9). Finally, a time component to force generation and strain in the cell is likely to be necessary to explain the different cellular responses to different stress time histories.

Recently, Satcher and Dewey (61) suggest that the filamentous actin (F-actin) can be modeled as a foam while stress fibers connect to it intermittently to form the endothelial cell cytoskeleton. Modeled as such they estimate the mechanical properties of the cytoskeleton when the cell undergoes shear stress. They concluded that the cell is relatively stiff and does not strain appreciably in response to shear stress. There are difficulties, however, in their implicit assumption that the cell is a static mechanical system. The stiffness measured by a mechanical model

which gained geometric parameters (fiber orientation etc.) from fixed cells via electron microscopy ignores the possibility that the cells react in a time dependent manner to a mechanical stimulus. This time-dependent reaction could be a passive response (a deformation) or an active response (a contraction, relaxation, or generation of molecules affecting the cells mechanical properties).

Recently, Wiesner *et al.* (79) presented a model to explain calcium transients in cells exposed to shear stress including mass transport effects of shear at the cell surface and mechanical straining effects on the cell membrane. They used the approximation of Liu in which most (90%) of the membrane tension is taken up by the cell interior (assumed to be solid). To account for the transient relationship between membrane permeability and membrane potential with shear stress they used empirical relationships.

The properties of the cell membrane and how it responds to fluid shear remain poorly understood. Although some have hypothesized that it acts as an elastic solid, its fluid properties cannot by ignored. Most soft biological tissues are viscoelastic because they have the feature that under constant strain their stress relaxes over time (21). The sources of cell membrane viscoelasticity are likely to be numerous. Both invaginations and evaginations of the cell membrane require tension to open (65), protein movement through the membrane is resisted by membrane viscosity (16), and stress fibers may not be linearly elastic. These features and others are likely to contribute to the viscoelastic nature of cell membranes.

To understand the dynamic nature of strain in a stressed cell it is helpful to

analyze the models governing stress induced strain. Furthermore, solving this model for a ramp in stress may give insight into the rate sensitivity to shear demonstrated in this dissertation.

Viscoelasticity theory contributes a constitutive equation relating the imposed stress to the strain in the material. Unlike linear elasticity which assumes equilibrium conditions, viscoelasticity contains time dependent strains to imposed stresses (creep). In the following analysis, the reaction of a viscoelastic material to a stress (τ) applied at the ends and in the plane of the material is investigated to illustrate the reactions of a viscoelastic material to time varying shear. For an elastic material in equilibrium this equation is simply Hook's law,

$$\sigma^{ij} = C^{ijkl} e_{kl} \tag{1}$$

For a kelvin viscoelastic solid there exists a time dependent relationship between stress and strain which is given by the differential equation (in one dimension),

$$\sigma + \lambda_1 \dot{\sigma} = -\frac{2}{3} E \left[\lambda_2 \dot{v} + v\right] \tag{2}$$

where

$$\lambda_1 = \frac{\mu}{k_2}, \quad \lambda_2 = \frac{\mu}{k_1}\left(1 + \frac{k_1}{k_2}\right), \quad E = \frac{3}{2} k_1 \tag{3}$$

and where μ, k_1, and k_2 are material constants described above. Equation 2 has a different solution depending on the time course of stress imposition. For a step

stress from 0 dynes/cm^2 to $\Delta\tau$ at time zero $\tau=\Delta\tau \cdot H(t)$, where $H(t)$ is the Heaviside step function, we obtain as a relation between stress and displacement,

$$v=\frac{3}{2}\frac{\Delta\tau}{E}\left[e^{-t/\lambda_2}\left(\frac{\lambda_1}{\lambda_2}-1\right)+1\right] H(t) \qquad (4)$$

A ramped stress can be described by,

$$\tau(t)=\frac{\Delta\tau}{t_s}\, t\,[H(t)-H(t-t_s)]+\Delta\tau\; H(t-t_s) \qquad (5)$$

where t_s is the time to finish a steady ramp increase in stress from zero to $\Delta\tau$ (45). The solution to equation 2 using equation 5 is,

$$v=\frac{3}{2}\frac{\Delta\tau}{Et_s}\left[H(t)[t+(\lambda_1-\lambda_2)(1-e^{(-t/\lambda_2)})]-H(t-t_s)[(t-t_s)+(\lambda_1-\lambda_2)(1-e^{-(t-t_s)/\lambda_2)})]\right] \qquad (6)$$

Figure 6 illustrates the estimates of strain in a membrane subject to either step changes in stress or ramp stress. They also illustrate the difference in response between confluent endothelial cells under static conditions and the response of those that had been previously sheared at 20 dynes/cm^2 for 24 hours. Constants for k_1, k_2 and μ are from (62) and are 450 dynes/cm^2, 750 dynes/cm^2 , and 65,000 dyne-s/cm^2 respectively for unsheared cells and are 1050 dynes/cm^2, 1800 dynes/cm^2, and 100,000 dyne-s/cm^2 respectively for sheared cells. The cells in the isolated arteriole are likely to behave more like the sheared cells because they

have undergone a lifetime of shear and change very little during the equilibrium period. As illustrated in figure 6 pre-exposure to shear stress (designated as "sheared") seems to decrease the steady state strain. This figure also illustrates another phenomenon in which cells reduce the time it takes to reach maximum strain. It would appear that endothelial cells adjust in the long term their material properties to minimize strain magnitude as well as to shorten the time to reach a steady state strain.

Such analysis demonstrates that the strain in a cell subjected to a step in shear stress is not maximal initially but rises over time. The rate of change of strain (given by the first derivative with time of equation 4, however, is maximal at the instant after the step in stress (time=0^+) and falls off exponentially with time thereafter:

$$\left[\frac{dv}{dt}\right]_{0^+} = \frac{3}{2}\frac{\Delta\tau}{E}\left[e^{-t/\lambda_2}\left(1-\frac{\lambda_1}{\lambda_2}\right)\frac{1}{\lambda_2}\right]. \qquad (7)$$

This exponential decay is used later as the form of the equation for the decay of the experimentally determined vasodilatory response to shear stress.

Chapter 2: *Ex vivo* demonstration of Shear Stress Magnitude and Rate-Dependence

2.1 Background

It was the goal of this study to investigate the rate-sensitivity of shear-induced, prostaglandin-mediated arteriolar dilation in a realistic, *ex vivo* physiological setting. To this end, we used isolated 1A cremaster arterioles because first, this isolated arteriole preparation allows definitive quantification of the dilatory response of a microvessel to a variety of TSGs. Such results are more physiologically relevant than those obtained on cell cultures. Second, previous experiments have shown that shear-induced vasodilation is dependent on an intact endothelium and a prostaglandin (possibly prostacyclin) is the principal shear-induced vasodilator released by the endothelium in this vascular bed (42).

2.2 Methods

2.2.1 Isolated Arteriole Preparation

Rat cremaster arterioles (1A) were used to investigate the rate-sensitivity of arteriolar endothelium to shear stress (see figure 7). Male Sprague-Dawley rats (160±6gm, n=39) were anaesthetized by intraperitoneal injections of sodium

pentobarbitol (50 mg/kg body weight). The left cremaster muscle was exposed by a mid-scrotal incision, cut longitudinally, splayed flat, and excised by a lateral cut at its base. After the muscle excision, the rat was euthanized with an overdose of sodium pentobarbitol I.P. The muscle was rinsed with cold saline solution and immediately placed in a 0-4°C physiological saline solution (pH=7.4) with the following composition: 145mM NaCl, 4.7mM KCl, 2mM $CaCl_2 2H_20$, 1.2mM $MgSO_4$, 1.2mM NaH_2PO_4, 5mM dextrose, 2mM pyruvate, 0.02mM EDTA, and 3mM MOPS [3-(N-morpholino)propanesulfonic acid]. The muscle was pinned flat and allowed to equilibrate with the solution for 10 minutes. Under a Nikon dissecting scope, a 1.5-2 mm-long arteriole section was selected and carefully cut away from the skeletal muscle and connective tissue by using sharpened forceps and microscissors. The excised arteriole was transferred via a 10-µl pipette into a cannulating chamber which contained a modified Krebs bicarbonate buffer (room temperature, pH=7.4) with the following composition: 118mM NaCl, 4.7mM KCl, 2.5mM $CaCl_2 2H_20$, 1mM $MgSO_4$, 1mM KH_2PO_4, 25mM $NaHCO_3$ and 11.1mM dextrose.

The upstream side of the arteriole was cannulated by using an 80-µm o.d. glass cannula connected to silicone tubing filled with Krebs solution. The arteriole was then secured around the cannula by tightening a knot made from a single strand of 6-O silk suture. Upstream pressure was increased to ~5cmH_2O to flush the arteriolar contents. The downstream end of the blood vessel was cannulated by a similar glass cannula connected to silicone tubing. The chamber-arteriole assembly was then moved to a Nikon Diaphot inverted microscope stage. While open to atmospheric pressure, the tubing ends were connected to the pressure/flow

system which contained gravity-feed upstream and downstream reservoirs (see figure 8). At this time the cannulating chamber was connected to the recirculating reservoir and the blood vessel was suffused with Krebs buffer at room temperature. The luminal pressure was raised to 20mmHg and a slight pressure gradient (<2mmHg) was imposed along the length of the vessel and maintained for 3 minutes to eliminate debris and non-equilibrated solutions from the vessel lumen. Finally, the downstream stopcock was closed and the vessel was pressurized from the upstream side for the entire equilibration period.

The cannulating chamber was filled with Krebs buffer equilibrated remotely in the recirculating reservoir via a feedback control system. The solution properties were monitored by an Anafaze 8LS controller (Par Associates) which received inputs from P_{O_2}, pH, and temperature sensors and modulated N_2 valve, CO_2 valve, and the on/off rates of the heater thus controlling P_{O_2} (65-75mmHg), pH (7.4), and bath temperature, respectively (33). The recirculating reservoir, heat exchangers, and cannulating chamber were jacketed with water from the temperature-controlled bath to maintain the desired chamber temperature (80). The total volume of the cannulating chamber, recirculating reservoir, and associated tubing was 150ml, and the solution was recirculated at a rate of 50ml/min. Every hour the suffusion solution was exchanged with a fresh solution which had been pre-equilibrated for P_{O_2}, pH, and temperature.

During the equilibration period, with the chamber temperature maintained at 25°C, the luminal pressure was raised in 10mmHg increments, each lasting 5 minutes, to the final pressure of 65mmHg found *in vivo* (49). The arteriole was

stretched to its *in vivo* length and assessed for leaks by closing the upstream stopcock (upstream of the upstream pressure sensor) and monitoring the pressure for 1 minute. A fall in pressure of $\geq$1mmHg was indicative of a leak, and the experiment was terminated. For those vessels without leaks, the stopcock was opened and the temperature was raised from room temperature to 34°C over a half hour. During this time the vessel usually constricted to 50-60% of its passive diameter; this diameter represented the intrinsic tone for these blood vessels as was taken as the control diameter ($d_{control}$). Blood vessels lacking this intrinsic tone (about 20% of all vessels) were not investigated further. Those showing this tone were allowed to have an additional half-hour equilibration prior to the start of experiments.

2.2.2 Instrumentation

The variables measured were blood vessel diameter, upstream pressure, and differential pressure across the pipettes and blood vessel assembly. The blood vessel image was projected on a video screen (SONY) via an Hitachi CCD color video camera mounted on a Nikon Diaphot microscope. A time generator (For-A Video Timer, Japan), synchronized with the computer clock, placed a time stamp on the image, and the experiments were recorded on a VCR (Panasonic). Blood vessel dimensions were measured using a video caliper (Microcirculation Research Institute, College Station, TX) calibrated with a micrometer scale. Vessel length (0.8-1.5mm), taken as the distance between the ends of the pipettes, was measured

using the 4x objective when the vessel was first pressurized to 65mmHg and then straightened. A 10x objective was used for the measurement of diameter which was taken as the distance between the inside edges of the vessel wall at the midpoint of the vessel length. Upstream pressure and differential pressure were measured using a flow-through pressure transducer (World Precision Instruments (W.P.I.)) and a differential pressure transducer (W.P.I.), respectively, each coupled to an amplifier (W.P.I.). All electrical signals from the video caliper and the amplifier were routed to a Macintosh IIci computer equipped with a National Instruments A/D converter board and converted via LABVIEW® software into diameter and pressure measurements. To avoid contamination of the transducers with physiological saline solution and to minimize surface tension effects between the tubing and the fluid, all pressure reservoirs, transducers, and associated tubing were filled with mineral oil, with the oil/saline solution interface kept remote from the blood vessel and cannulae.

In order to definitively study the effects of shear stress in the absence of pressure changes, it was necessary to control luminal pressure and shear stress independently. This requirement was met by independently adjusting inflow and outflow pressures (see figure 9). Because the system geometry on the upstream and downstream sides of the vessel midpoint nearly mirrored each other, equal and opposite adjustments of upstream and downstream pressures, with some modifications as described below, allowed the modulation of flow while maintaining intraluminal pressure. Similarly, equal adjustments of upstream and downstream pressures allowed changes in intraluminal pressure while maintaining the pressure gradient and hence flow.

From the known resistances of system components, the pressure drops in the system at various flow rates were calculated. The flow rate (Q (nl/sec)) was calculated from the pressure drop measured with the differential pressure transducer (ΔP (mmHg)) using the equation $Q=\Delta P/(R_{ca} + R_v + R_{cb})$ (13) where R_v was the blood vessel resistance and R_{ca} and R_{cb} were the upstream and downstream cannula resistances, respectively. The resistances (mmHg/(nl/sec)) were calculated as described below.

Cannula resistances, R_{ca} and R_{cb}, were measured using a Harvard perfusion pump and the upstream pressure transducer. Prior to resistance measurements, pump flow rates were verified by measuring the rate of movement of a water/air interface through a small-bore polyethylene tubing of known diameter. To measure cannulae resistances, fluid was pumped through each cannula into the water filled reservoir at four different flow rates ranging from 266 to 2660 μl/sec, with the downstream (chamber) pressure set at atmospheric. Because $\Delta P=R_c \cdot Q$ where $\Delta P = P_{up}$, and Q is the pump flow rate, the slope of the ΔP versus Q line yields the cannula resistance (R_{ca} or R_{cb}). The same upstream and downstream cannulae were used in every experiment and their resistances (and correlation coefficients) were: R_{ca}=0.0095 mmHg/(nl/sec) (r^2=0.98 for ΔP vs Q) and R_{cb}=0.0075 (mmHg/(nl/sec) (r^2=0.96 for ΔP vs Q). The two cannulae resistances were not equal even though great care was used in fabricating them to have the same inside diameters. These discrepancies were compensated for by including the measured cannula resistances into the calculations for pressure and flow rate.

The pressure drop from the point of upstream measurement to the midpoint

of the blood vessel (P_{u-m}) was calculated as $P_{u-m}=Q(R_{ca}+1/2R_v)$, and the mean intraluminal pressure P_{lumen} was given by the pressure at the midpoint of the vessel: $P_{lumen}=P_{up}-P_{u-m}$, where P_{up} was the pressure measured by the upstream pressure transducer. The blood vessel resistance (R_v) was given by the Hagen-Poiseuille relationship: $R_v=750x128\mu L/(\pi d^4)$ mmHg/(nl/sec), where 750 is a factor to convert the units into mmHg/(nl/sec), μ is the perfusate viscosity (0.008 poise at 34°C), L is the vessel length (μm), and d is the vessel inner diameter (μm). For an arteriole 1000μm long and 80μm in diameter, R_v= 0.006 mmHg/(nl/sec); this was comparable to the cannular resistances, indicating the importance of knowing R_{ca} and R_{cb}. Our approach allowed the determination of pressure drops throughout the system from the upstream pressure and differential pressure at a given flow rate. In these experiments, intraluminal pressure was controlled by raising and lowering the reservoirs connected to the inflow and outflow cannulae of the blood vessel, via motors, strings, and pulleys. Similarly, vessel wall shear stress [τ (dynes/cm^2) $=10^6x32\mu Q/(\pi d^3)$] was dynamically controlled by continually adjusting upstream and downstream pressures (and therefore Q) in response to deviations from a prescribed set point for shear stress by using the feedback control system described below.

2.2.3 Feedback control of shear stress and pressure

The solenoid valves and motors were controlled by a Macintosh computer based on the data collected with the aid of LABVIEW® software. In a feedback

control loop, the vessel diameter, pressure, and differential pressures were recorded, and the resistance, luminal pressure, flow rate, and shear stress were calculated. The motors were appropriately adjusted, via strings and pulleys, by the computer through an HP relay board (3488A) to bring luminal pressure and shear stress to prescribed set points (see figures 8,9, and 12).

2.2.4 Imposing steep and gradual temporal shear gradients

To impose a step change in shear stress, both upstream and downstream stopcocks were closed off, and upstream and downstream pressures were adjusted to generate a pressure gradient that would impose the desired shear stress. Immediately, the stopcocks were simultaneously opened, and the shear stress was imposed. In all cases, the blood vessel would dilate within 10-30 seconds. Therefore, it was necessary to adjust the pressure difference across the blood vessel to keep the shear stress constant in the face of vasodilation. Intraluminal pressure was kept constant at 65mmHg during the entire experiment (see figure 12C).

Slow-ramp and a fast-ramp systems were used. To impose a slow ramp (>16sec in duration), an algorithm was devised in which the shear stress set point was increased in small steps over the entire ramp duration to yield low TSGs. In order to cover the high TSG range, a fast ramping system was developed (figure 8). On the upstream side, a secondary supply reservoir (H_2 in figure 8), which was made of a large (50ml) syringe barrel filled with mineral oil to a prescribed height,

was connected to the upstream feed tube (H_{up} in figure 8); flow to the upstream feed tube was controlled by the computer and a solenoid pinch valve. The upstream feed tube was a 1/8" or 1/16" i.d. mineral oil-filled length of tygon tubing with a mm-scale; it imparted the H_2 height as the upstream pressure (P_{up}) during and after filling by the secondary supply reservoir. By adjusting the relative heights of the fluid in the upstream feed tube and in the secondary supply reservoir, the rate of filling of the upstream feed tube by the secondary supply reservoir when the solenoid opened could be precisely controlled. For example, if the upstream feed tube was nearly empty the rate of filling from the secondary reservoir would be maximal; whereas if the fluid height in the upstream feed tube approached that of the secondary supply reservoir, the filling rate would approach zero. Using the mm scale on the upstream feed tube and assuming that, during filling, the height of the secondary supply reservoir remained constant, a calibration graph relating the upstream feed tube initial fluid height (h_i) and the upstream feed tube filling speed (dh/dt) was constructed for two different diameters of upstream feed tubes (see figure 10). A three-way stopcock allowed switching from one upstream feed tube (1/16" i.d. for faster ramps) to the other feed tube (1/8" i.d. for slower ramps) as needed. These calibration curves were programmed in the computer and the opening of the solenoid valve was also timed and controlled by the computer.

With this system it was possible to impose a prescribed TSG to reach a prescribed maximum shear stress over a prescribed duration. To induce a shear stress that started at 0 dynes/cm^2 and rose to a maximum value (τ_{max}) over a ramp duration (= τ_{max}/TSG): 1) the solenoid valve and the stopcocks to the blood vessel

were closed, 2) a pressure gradient sufficient to impose τ_{max} was computed via LabVIEW® (knowing current vessel diameter), 3) the rate of change of the upstream feed tube column height (dh/dt) was computed from this pressure gradient and the ramp duration, 4) the proper starting column height in the upstream feed tube (h_i) was computed from the regression curve (figure 10), 5) h_i was set and upstream and downstream pressures were adjusted so that Q=0 nl/sec and P=65 mmHg, 6) the stopcocks regulating flow to and from the vessel were opened, and then the computer-controlled solenoid valve was opened for the specified ramp duration. It should be noted that the opening of the solenoid valve, the inertia to start the column of mineral oil in motion, and the surface forces between the mineral oil and the tubing, would cause an initial spike in the pressure reading when the valve was opened. To mitigate this spike, a T connection was made in the line by attaching a piece of closed-end tubing containing an air column as a damping dashpot. By adjusting the height of the air column, we were able to completely eliminate this spike (see figure 11) without changing the slope or shape of the ramp.

2.2.5 Protocols: step, slow ramp, and fast ramp

Three protocols were employed to assess the response of arterioles to different rates of shear stress application. First, the slow-ramp system was used to carry out the experiments in the step-protocol and the slow-ramp protocol. In the step-protocol, shear stress was stepped to 20 dynes/cm^2 and maintained for 30 minutes. In the slow-ramp protocol, shear stress was ramped to 20 dynes/cm^2 over

a period of 5 minutes (TSG = 0.067 dynes/cm^2/sec) as described above and then held constant for 30 minutes (n=8). Time equals zero was taken either at the instant just before the step in shear or when the five-minute ramp was initiated. In half the experiments, the shear was stepped first, followed by a 20-minute recovery period, and then the shear was ramped (step/recovery/slow ramp). In the other half, the shear was ramped first, followed by the 20-minute recovery period, and then the shear was stepped (slow ramp/recovery/step).

In the fast-ramp protocol, the fast-ramp system was used. Shear stress was ramped with a TSG of greater than 0.067 dynes/cm^2/sec to assess the effects of different TSGs on maximal dilation. Preliminary experiments showed that there was little difference in the vasodilatory response of blood vessels to a shear stress of 20 dynes/cm^2 whether it was ramped over 5 minutes, 2 minutes, 1 minute, 30 seconds, or 10 seconds (i.e TSG from 0.067 to 2 dynes/cm^2/sec). However, there existed a substantially greater vasodilation in response to a step-shear as compared to that elicited by any of the aforementioned TSGs. To explore this transition in greater detail we imposed a shear stress, using the fast-ramp system described above, with a ramp duration of 16, 8, 4, 2, 1, or 0.5 seconds to reach a maximum shear stress of either 10, 20, or 40 dynes/cm^2 (n=8 for each maximum shear stress unless otherwise noted). Step-protocol experiments were also carried out on the same arterioles used for the fast-ramp protocol, and the results were the same as the step-protocol experiments carried out with the slow-ramp system. Between successive experimental interventions was a five-minute equilibration period during which the arteriole returned to its control diameter. These ramp durations and

maximum shear stresses were selected so that similar TSGs with different combinations of ramp durations and maximum shear stresses could be compared. Because of system limitations, we could not impose a 0.5-second ramp to 40 dynes/cm^2, and hence this data point is absent.

In order to confirm previous results regarding the role of the shear-induced vasodilators NO and prostaglandin, L-NAME (10^{-3}M), which blocks NO production, was added to the bath at the end of two experiments. After an equilibration period of 15 minutes, the responses of the vessel to a ramp or step to a maximum shear stress of 40 dynes/cm^2 were assessed. At the end of two other experiments, the vessels were bathed in 10^{-5}M indomethacin, which blocks prostaglandin production, and equilibrated for 30 minutes. Responses to a step or ramp to 40 dynes/cm^2 were then assessed.

Preliminary experiments were conducted to assess the reproducibility of the step response. In these experiments (n=7) the shear stress was first stepped, maximal diameter measured over 5 minutes while the shear stress was maintained, and during a 5-minute recovery period during which there was no flow through the blood vessel. This cycle was repeated four times. The results showed that the 5-minute recovery period between interventions was sufficient as indicated by the finding that the responses were reproducible and not affected by previous cycles (data not shown).

At the end of all experiments, the blood vessels were equilibrated for 15 minutes in Ca^{2+}-free solution containing 10^{-3}M EGTA to obtain the passive diameter at 65mmHg. Removal of all extracellular Ca^{2+} caused complete relaxation of

vascular smooth muscle and thus maximum arteriolar distension. This passive diameter was equivalent to that measured at 65mmHg and 25°C at the beginning of the experiment.

2.2.6 Drugs, Statistics

All chemicals were purchased from Sigma, Fisher Scientific, or Boehringer Mannheim.

In experiments under step and slow-ramp protocols, the vessel diameters (d) were normalized to the control diameter ($d_{control}$) and the results at each time point (at one-minute intervals) were averaged over the eight experiments and are expressed as the mean ± SEM in figure 13. A paired t-test was used to assess the significance of differences between average responses to ramped and stepped shear stress at each time point. For the fast-ramp experiments, the maximal diameters reached within 5 minutes were normalized to the control diameters and the results for eight experiments were averaged. Control diameters were average values obtained at the end of the recovery periods (i.e., just prior to the next experimental interventions) when the pressure was 65 mmHg with no flow. For comparisons of more than two groups, a one-way analysis of variance (ANOVA) was used to assess the significance of differences among the groups, followed by a t-test modified by the Bonferoni procedure. $P<0.05$ was the criterion for statistical significance unless otherwise specified (75). Equation coefficients were calculated using least-squares regression with the help of Slidewrite software (Advanced Graphics Software,

Carlsbad, CA).

2.3 Results

2.3.1 Testing the system

To assess whether the intraluminal pressure was held constant during flow changes, two arterioles were maximally dilated with 10^{-6}M nitroprusside, which caused complete vascular smooth muscle relaxation, and flow was set to various levels while the computed intraluminal pressure was held constant. In no case was there any observable change in arteriolar diameter as the flow was varied from zero to a maximal level; indicating the absence of passive changes in vessel diameter and hence the constancy of the intraluminal pressure.

To verify our calculations of the flow rate through an arteriole, in two other arterioles we compared the flow value calculated by using the pressure drop across the blood vessel as described in Methods with the prescribed flow rate delivered by the Harvard pump (260 nl/sec). Even during different levels of vasodilation, the calculated flow rate agreed with the flow set by the pump to within 5%.

Finally, to verify whether we achieved a linear ramp to a maximum shear stress with the fast-ramp system, we measured the differential pressure across the blood vessel and the cannulae during the ramping. Figures 4 A-D show various TSGs to a common maximum shear stress. These shear stress tracings were

obtained by transforming the continuous pressure gradient measurements as described in Methods.

2.3.2 Arteriolar tone and repeatability of step response

The average passive diameter of the vessels in experiments using the fast-ramp system (obtained at the end of each experiment by bathing arterioles in Ca^{2+}-free Krebs bicarbonate buffer containing 1mM EGTA) was 138±2μm and they achieved a stable control diameter ($d_{control}$) averaging 69±2μm. The passive and control diameters for the vessels in experiments using the slow-ramp system were 145±4μm and 77±5μm, respectively.

Repeatability of the step response was shown in seven experiments by noting that the dilatory response to a step-shear stress and the return to control values were reproducible within 7.7% and 4.6%, respectively, for four cycles of repetition (n=7, data not shown).

2.3.3 Vasodilatory responses to step shear and fast ramp shear

Figure 5 is an example of the time course of the responses to a step-shear stress of 20 dynes/cm^2 and to a shear stress ramped to 20 dynes/cm^2 over 5 minutes. The graphs are superimposed at time = 0, which was either when the step-shear or the ramp-shear stress was initiated by prescribed flow changes. The step-shear led to an increase in diameter from 90μm to over 100μm in 1 minute

(figure 12A), and this was accompanied by a further increase in flow (Fig. 12B); with time, both the diameter and flow decreased to settle at steady levels higher than their respective controls despite the maintenance of the step-shear stress at 20 dynes/cm^2. In the experiment shown here, the slow ramping of flow and shear did not cause any change in vessel diameter during the first 5 minutes, but a vasodilation later occurred with the diameter rising to level comparable to that observed in the step-shear experiments (figure 12A); between 15 and 30 minutes the flow rate was also similar in the two experiments (figure 12B). Note that, despite the large differences in the early phases of the responses of the diameter and flow to the two modes of shear, the shear stress was maintained at the same constant level of 20 dynes/cm^2 once that was attained (figure 12D), and the luminal pressure was also kept constant at 65 mmHg throughout in both experiments (figure 12C).

Composite plots of the time courses of diameter changes for all step and slow-ramp experiments are shown in figure 13. Each point represents the mean diameter of eight experiments at the specified time point, each normalized to their control diameter. In this composite plot, the diameter showed an increase with shear during the slow-ramp period (not seen in the one experiments shown in figure 12A), but began to decrease following the attainment of the maximum shear stress. The step-shear caused a peak vasodilation (1.28±0.05 times control) at 4-5 minutes, and this vasodilation was significantly greater that seen in response to a slow-ramp shear (1.13±0.05 times control). In both groups of experiments, the diameter decreased from the peak value to about 1.10 times control at 10-15 minutes. Thereafter the diameter of both groups showed a tendency to rise toward a plateau

level, and they were not significantly different from each other. These results indicate that the vasodilatory response was biphasic. In the early phase the step-shear response was significantly greater than the slow-ramp shear response, while the magnitude of shear response in the later, long-term phase was independent of the rate of shear application.

To analyze further this biphasic nature of the vasodilatory response, we used two curve fits, one for the early transient phase and one for the later sustained phase. The curve fits took the form of : $d/d_{control}=1+[G(t)\cdot H(t)]_{early}+[G(t)\cdot H(t)]_{late}$ where 1 is the normalized control diameter, G(t) is a delay function characterizing the delay between the stimulus and the response, and H(t) is a dissipation function characterizing the dissipation of the stimulus (τ or TSG) and the total response is a linear superposition of the early and late phase responses. This approach is based on the assumption that the initial vasodilation decays exponentially with time, that the early and late vasodilation exhibit a sigmoidal behavior, and that there is a delay in the response due to factors such as the time needed for shear-induced production of vasodilator by the endothelium, diffusion of vasodilator to the smooth muscle, and relaxation of the smooth muscle. H(t) is a dissipation function characterizing the subsidence of the initial response over time. For the early phase (0 to 15 minutes for the step-shear response and 0 to 17 minutes for the ramp-shear response) $G(t)_{early}$ is assumed to be sigmoidal starting at a minimum and rising to a maximum plateau over some time (45). G(t) and H(t) take on the forms:

$$G(t)_{\text{early or late}} = \frac{(t/a_0)^{a_1}}{1+(t/a_0)^{a_1}}$$

and

$$H(t)_{\text{early}} = e^{-t/a_2} \quad \text{and} \quad H(t)_{\text{late}} = a_3,$$

where a_0, a_1, a_2, and a_3 are curve fitting constants and t is the time. This method of curve fitting is consistent with our hypothesis for rate-sensitivity in which the effects of the initial, fast rates of change of shear stress are dissipated yielding to a later, sustained response. Figure 14 shows that such decomposition of the vasodilatory responses to step- and ramp-shear fits very well with the experimental data. The results indicate the initial vasodilation was much larger in the step-shear than in the ramp-shear experiments, whereas the late vasodilation are essentially the same for both the types of experiments.

2.3.4 Vasodilatory response to different rates of ramp shear

The rates of shear ramping were varied by changing the duration and the maximum level of shear stress. In figure 15 the peak vessel diameter (d_{max} normalized by $d_{control}$) is plotted against the ramp duration. For all ramp durations tested, the magnitude of the $d_{max}/d_{control}$ curves increased with increases in the magnitude of the maximum shear stress. However, the steepness of the increase in $d_{max}/d_{control}$ with decreasing ramp duration (under 4 seconds) was greatest for the

lowest maximum shear stress.

We found that indomethacin (10^{-5}M) completely eliminated the vasodilatory response to both a step and a ramp to a maximum shear stress of 40 dynes/cm^2 (n=2), whereas 10^{-3}M L-NAME had no effect (n=2) (data not shown). These results confirm the results of Koller *et al.* (42) regarding the nature of the shear-induced vasodilator.

2.3.5 Rate sensitivity

Plotting of the maximum changes in vessel diameter as a function of TSG (figure 16), shows that the maximum vasodilation generally increased with increasing TSG with the greatest increase occurring for a shear magnitude of 20 dynes/cm^2. Significant differences in vasodilation as a function of the maximum shears were observed for a TSG of 2.5 dynes/cm^2/sec, indicating that a magnitude-sensitive mechanism became more dominant for this slow TSG (see figure 17). Furthermore, the response to ramp-shear with a maximal shear of 40 dynes/cm^2 was independent of the TSG. When changes in maximum vessel diameter are presented as a function of shear magnitude the maximum vasodilation was also found to increase with increasing magnitude of the maximum shear stress at given TSGs; significant differences occurred between responses to TSGs of 2.5 versus 10 and 2.5 versus 20 dynes/cm^2/sec when τ_{max} was 20 dynes/cm^2. These results suggest that both magnitude-sensitive and rate-sensitive mechanisms might be operative for TSG$\geq$5 dynes/cm^2/sec. In summary, rate sensitivity was most

pronounced for the intermediate shear stress of 20 dynes/cm^2 and all but absent for low shears (10 dynes/cm^2) and high shears (40 dynes/cm^2).

2.4 Discussion

Our goals in this study were threefold. First, we investigated the relationship between shear magnitude and the diameter of arterioles *ex vivo* by clamping the shear stress in the face of compensatory vasodilation to increases in flow. Second, we investigated the possibility that the shear-induced vasodilation may be rate-dependent by comparing the effects of a step change in shear stress to those from a slowly rising shear stress. Third, having shown that these vessels are sensitive to shear transients, we sought to assess the roles of TSG and shear stress magnitudes on vasodilation.

The results indicate a significant rate sensitivity of vascular diameter to shear stress when shear is applied as a step or at high rates of ramp. The shear-magnitude sensitivity, on the other hand, is more prominent for slower rates of ramp. The results also support the hypothesis that TSG and shear stress magnitude are distinct and different types of activators of vasodilator production in vascular endothelium, with the former acting on a time scale of seconds and contributing most pronouncedly to the early vasodilatory response and the latter contributing to both the early and late response. It is possible that, via endothelial cell regulation, microvessels use this rate-sensitive enhancement in dilation to respond to rapid increases in blood flow, while they maintain their steady state caliber in part through

the shear-magnitude sensitive mechanism.

The present *ex vivo* investigations into how shear magnitude and shear transients affect microvascular tone serve to bridge the gap between *in vitro* (cell culture) and *in vivo* studies. First, in this system, shear stress and TSG can be prescribed and dynamically controlled; hence we are able to tightly control the shear environment of our *ex vivo* preparation as they are in cell culture studies conducted in flow chambers. Such an approach allows the study of shear-induced production of vasoactive substances in a relatively physiological setting. Second, the present *ex vivo* study has the advantage over *in situ* investigations in that we were able to control pressure, PO_2, and other parameters which tend, in *in situ* preparations, to undergo fluctuations in response to experimental interventions. It is possible that the surgical manipulation itself could have affected the reactivity of these blood vessels. However, these *ex vivo* vessels respond to vasoactive stimuli such as acetylcholine (endothelial dependent) and adenosine, nitroprusside, and pressure (endothelial independent) in the same manner as microvessels *in vivo* (data not shown). Furthermore, these vessels maintain stable tone between interventions for a number of hours, and they often exhibit vasomotion. All these factors indicate that these arterioles behave normally and are suitable for the measurements of shear modulation of vascular tone.

These is a large body of evidence implicating shear stress as a potent modulator of endothelial cell biology (9). It has also been shown that flow itself modulates endothelial function by influencing local agonist and antagonist

concentrations (12). To exclude from consideration the flow-induced effects on local concentrations of these substances (and the subsequent effects on endothelial function), we excluded all known vasoactive substances from the bath: there was no ATP, NO, bradykinin, adenosine or any precursors of constrictors. It is possible, however, that an autocrine mechanism could play a role here in which initial production of prostacyclin could enhance subsequent production. In consideration of this possibility Koller *et al.*, in an apparatus similar to ours, used increases in viscosity of the perfusate (rather than flow increases) to increase luminal shear stress and found that similar dilation-versus-shear graphs were obtained whether shear was raised by increasing perfusate viscosity or by increasing luminal flow rate (42). Such studies implicate shear stress as a vasoactive stimuli in favor of flow-induced modulation of local agonist concentrations. Their studies also suggested that shear stress is regulated (although not precisely) by a negative feedback control mechanism in which an increase in shear stress from an increase in luminal flow is mitigated by the resulting increase in diameter. We sought to evaluate the roles of the rate of change of shear stress and the shear-stress magnitude in vasodilation by prescribing and dynamically controlling both the TSG and the shear stress. In order to completely rule out flow as the modulator rather than shear stress we would need to carry out studies in which shear is adjusted dynamically by altering viscosity.

The effects of shear stress on vascular tone reported here represent the first published report on blood vessels showing that (a) a slow ramp in shear stress leads to an attenuated initial dilatory response when compared to the response from a step to the same shear stress, and (b) sustained shear stress leads to a later,

secondary vasodilatory response. It is clear from our results (figure 6) that a step in shear stress induced vasodilation that peaked in 4 minutes, subsided in about 10 minutes, and then rose to a new plateau. Such time-dependent responses to shear may involve shear-mediated prostacyclin production (26). Although the cellular pathway mediating shear induced prostacyclin production has not been resolved, a likely scenario involves, in order, G-protein activation, elevated IP_3 levels, the release of Ca^{2+} from the endoplasmic reticulum (ER), the formation of prostaglandins (possibly prostacyclin) from arachodonic acid, and sustained Ca^{2+} entry from outside the cell. Therefore, it is interesting to note that time-dependent responses to shear are reported in the literature for IP_3 levels (peaking at ~15 seconds) (58), intracellular Ca^{2+} (peaking at ~60 seconds) (15), and prostacyclin production (peaking at ~1-2 minutes) (26), and dilation (peaking at 4-5 minutes). Currently, others are measuring the cytosolic flux of intracellular free calcium concentrations, $[Ca^{2+}]$, in cells subjected to various TSGs and preliminary results reveal a complicated dependence of peak calcium levels on TSG and shear magnitude in which rate sensitivity is more pronounced at intermediate (5 and 10 dynes/cm^2) than at high (30 dynes/cm^2) shear stress magnitudes (6) (Blackman, personal communication). The observation that the initial peak in dilation subsides after the disappearance of TSGs at constant shear stress suggests that the results of the TSG dissipate, leaving the only remaining stimulus to be the shear magnitude. The method of curve fitting used in figure 14 and the excellent fit of the data lend further credibility to this hypothesis.

A slow startup rate to the same elevated shear stress results in a much

attenuated peak, but is followed by a plateau equivalent to that resulting from a stepped shear. Such results suggest that the mechanisms mediating the response to rapid changes in shear stress are fundamentally different from those mediating the response to slow shear adjustments. A similar phenomenon has been shown in NO production of cultured cells in response to shear stress (20). In those studies, NO production in response to stepped shear was G-protein dependent, while NO production in response to slowly ramped shear was not. It is likely that prostacyclin production in response to a stepped shear is also G-protein dependent (4), but whether elevated steady state prostacyclin production depends on G-proteins is not known. There is also no direct evidence that a ramp-shear initiates a fundamentally different endothelial pathway leading to prostacyclin production from that initiated by a step-shear.

In the fast-ramp protocols in which the early phase vasodilation was analyzed for rate and magnitude sensitivity, it was shown that, while the vasodilatory response to 20 dynes/cm^2 increased markedly with increasing TSG, this enhancement of shear-induced dilation by the TSG-stimulated pathway was less pronounced when the maximal shear stress was 10 dynes/cm^2 and virtually absent when shear stress was 40 dynes/cm^2. Such results indicate that a minimum and maximum shear stress exist for which the TSG enhances vasodilation. Furthermore, since the response to 40 dynes/cm^2 was not maximal ($d_{max}/d_{control} < 2$) the lack of vasodilatory enhancement with the TSG was not due to the attainment of a maximum dilation state. Further analysis of such interplay between the effectiveness of shear magnitude and TSG in eliciting a vasodilatory response might help in clarifying how

cells transduce shear stress into chemical signals.

The present study confirmed the previous findings (42) that both the dilation in response to a step-shear and to a ramp-shear are abrogated by indomethacin, a cyclooygenase inhibitor(42). Neither response was affected by L-NAME, an NO synthase inhibitor. These results indicate that step-shear and ramp-shear both initiate prostaglandin production. It is still possible, however, that this prostaglandin production in response to a stepped shear is accomplished through a different cellular pathway than that elicited by a ramped shear. Many investigators have implicated G-proteins as a common element in the shear transduction pathway but it should be noted that for NO production (20) and possibly for prostaglandin production, G-proteins play a role only if shear is rapidly elevated (large TSGs). In the vasoactive portion of the microcirculation (e.g. arterioles), small TSGs are likely to occur far more frequently than large TSGs. Therefore, it is possible that G-proteins are not part of the steady-state, shear-magnitude-sensitive mechanisms that lead to prostaglandin production by the vascular endothelium.

In vivo, shear stress transients are documented but not implicated as vasoactive stimuli in their own right. *In situ* studies in which shear transients were induced by removing an occluding micropipette from an arteriole resulted in a TSG of approximately 18.6 dynes/cm^2/sec (shear rose from 0 to 93 dynes/cm^2 in 5 seconds (μ=0.042 poise) (48). In other studies, the micropipette occlusion of one of two daughter arterioles resulted in a TSG of 14.4 dynes/cm^2/sec in the unoccluded daughter arteriole (40) and this intervention caused a large transient dilation. When increases in shear were induced pharmacologically by application of a metabolic

stimulator 2,4 dinitrophenol (DNP) to the distal portion of a hamster cremaster muscle preparation, the resulting TSG in the upstream arterioles was less than 1.2 dynes/cm^2/sec and was followed by a dilation that could not be blocked by either L-NAME (an NO synthase inhibitor) nor indomethacin (a prostaglandin inhibitor) (60). These *in situ* data suggest, indirectly, that gradual increases in shear stress did not elicit the production of NO nor prostaglandin by the endothelium. This result could be explained partly by our results showing that, in the rat cremaster preparation, only large TSGs yield large prostaglandin-mediated dilations while slow TSGs yield modest dilations. *In situ* diameter changes are induced by a number of vasoactive stimuli concurrently with the shear-magnitude-sensitive component being modest.

It is important to note that TSGs are probably small in the majority of the shear-induced vasodilations in the microcirculation, *in vivo.* Therefore, the postulated magnitude-sensitive mechanism is likely to be of primary importance under normal regulatory conditions. Occlusive events and other abnormal conditions producing larger TSGs which may invoke the rate-sensitive mechanism are probably rare in pre- and post-capillary blood vessels. In the capillary microcirculation, where flow intermittency could occur and theoretically cause abrupt changes in shear stress, the rate sensitivity of endothelium to shear stress could be important. No studies we are aware of, however, have investigated shear effects on capillary endothelium with regards to prostaglandin production.

In a related mathematical model on the myogenic response, the role of pressure in modulating vascular tone was reduced to one parameter relating the smooth muscle contractile state to intraluminal pressure (45). The authors

hypothesized that this parameter could be made dependent on other stimuli that affect smooth muscle tone. We suggest that shear magnitude and the TSG, via endothelial derived vasodilators, may be these factors.

Finally, we would like to speculate on the origin of the rate-sensitive mechanism. A number of cellular elements have been proposed as shear sensors (9). A transmembane, yet unidentified shear stress receptor (72), a stretch activate potassium channel (56), integrins (67,53), the cytoskeleton (77,32), the membrane itself with associated G-proteins (29), the glycocalyx (78) and others. Many of these proposed receptors are likely to be viscoelastic or contained in a viscoelastic medium. For example, the cell membrane with associated cytoskeleton has been shown to behave viscoelastically (62). In a viscoelastic material, energy is dissipated during stretch. Furthermore, in reaction to a step in stress, the rate of change of strain falls off exponentially with time. This observation prompted the use of an exponential decay function for H(t) (the dissipation function for the initial response to shear stress in this study). An impulse load might result in a greater transfer of energy to the membrane or entire endothelial cell than that of a slowly applied stress. For an impulse load, this energy might be sufficient to initiate the rate- and magnitude- sensitive mechanisms, while a slowly applied load may initiate only the magnitude-sensitive mechanism.

In conclusion, the important findings of the present study are as follows. There exists a mechanism for shear-induced vasodilation that is time-dependent and rate-sensitive. While other investigators have considered endothelial sensitivity

to the rate of change of shear under *in vitro* conditions, the present studies, carried out *ex vivo*, represent an important reference point for future studies, because they relate two physiological relevant stimuli, TSG and shear magnitude, to a physiologically relevant parameter, vessel diameter.

Chapter 3: Development of a FRAP / Shear-Stress system

3.1 Overview of Membrane Fluidity

3.1.1 Chapter overview

In this chapter, we hypothesize that membrane fluidity may be altered by shear stress and that these change in membrane fluidity may confer alterations in membrane-bound protein function (see figure 18). We begin by defining fluidity, and describe various ways an optimal fluidity is maintained by the cell. We then proceed to describe a method by which fluidity can be measured at various time points after the imposition of shear stress and present preliminary results which show a change in membrane fluidity shortly after a step in shear stress.

3.1.2 Defining fluidity

It was Singer and Nicholson (69) who first proposed a working model of the

cell membrane that allowed for in-plane movement of its components. This model hypothesized that the cell membrane is a thin layer of lipid molecules with protein molecules interspersed throughout. Further studies have revealed that the distribution of lipid molecules is heterogeneous and that the protein molecules, being bound to an underlying cytoskeleton, are not always free to move (34).

For the purposes of this paper, we will define fluidity as a measure of the lateral mobility of a fluorescent lipid probe inserted into the membranes of live bovine aortic endothelial cells. Lateral mobility will be assessed by measuring the rate of fluorescent recovery of a small spot which had been rapidly bleached with a high power laser. This recovery of fluorescence is due to the lateral diffusion of unbleached fluorophore into the bleached region (see figure 19) (3).

3.1.3 Factors affecting membrane fluidity

Animal-cell membrane fluidity, in the steady-state case, is determined primarily by three factors: the amounts and types of phospholipids, the membrane cholesterol content, and the interaction of lipids with membrane bound proteins (and the interactions of these proteins with the cytoskeleton) (see figure 20). A phospholipid is composed of a hydrophilic head region which is in contact with the extra- or intracellular space and two fatty acid chains which are hydrophobic and arranged on the interior of the membrane and interact with other phospholipid tails. Variations in these tails determine the type of phospholipid. If the tails are saturated with hydrogen (*i.e.* with no carbon-carbon double bonds), then they are straight and

many of these types of phospholipids can pack closely together leading to a high resistance to lateral movement of membrane constituents and hence to a low membrane fluidity. Similarly, increasing the degree of unsaturation, by increasing the number of carbon-carbon double bonds, puts kinks in the otherwise straight chains and makes it more difficult for these types of phospholipids to pack in an orderly fashion. In this case, the membrane would be made more fluid. Similarly, cholesterol binds via a hydrogen bond to the carboxyl group on the base of the fatty aid and thus intercalates itself into the hydrophilic portion to the membrane (3). In doing so it restricts the movement of lipids and thus confers a stiffening property to the membrane at physiological temperatures.

Although little appreciated until recently, proteins can also affect membrane fluidity via their interactions with their surrounding lipids (52). It is thought that the perturbation of a protein in the lipid medium disturbs the orderly packing of the lipids in an annular region around the protein. Generally, the hydrophilic portion of the lipids are attracted to the hydrophilic part of the protein. Since many proteins protrude out of the membrane, the lipid environment immediately surrounding the protein is fluidized (made less dense). Maintaining a separation between fatty acid chains of lipids from opposing leaflets is a high energy process. To compensate for this disturbance, and to minimize the energy necessary to maintain the membrane integrity around the protein, often only lipids with longer fatty acid tails will surround protruding proteins. In this way, proteins determine what type of lipids will surround them. Furthermore, with a high concentration of proteins, these annular regions may overlap and therefore there is a potential for protein-protein interaction via the

annular lipid regions. For proteins that are bound to the cytoskeleton, the presence of proteins may confer an overall stiffening of the membrane.

Each of these properties, fatty acid chain saturation, cholesterol content, and protein content (and protein interaction with the cytoskeleton), are known to be tightly regulated by the cell. When these systems are chronically perturbed, cells can potentially adjust these properties to maintain an "optimal" fluidity. This regulation is known as homeoviscous adaptation (47). While the notion of a fluidity set-point is still controversial, the homeoviscous adaptation theory has been shown to apply in poikilotherm's adaptation to chronic temperature changes and to cells of hibernating animals. Both poikilotherms and homeotherms adapt to the cell fluidity decreases induced by cold by synthesizing a greater proportion of unsaturated fatty acids which, when incorporated into the cells, stabilize membrane fluidity as the temperature falls (3). If shear stress really alters membrane fluidity in a chronic manner, than the cells could potentially adjust their membrane components to adapt to this chronic stress. Such adaptation (or lack of) could be an, as yet undiscovered, proclivity to atherosclerosis.

3.1.4 Shear stress and membrane fluidity

Outside to inside cell signaling is regulated primarily by the cell membrane. The cell membrane houses, in a lipid bilayer environment, proteins, some peripheral, and some membrane spanning, which can behave as channels, receptors, second messengers, substrates, or structural components linking

extracellular matrix and intracellular cytoskeleton. Some functions clearly relegated to the cell membrane are selective permeability to ions via selective channels, detection of signaling chemicals via ligand-specific receptors, and the G-protein second-messenger system linking receptor activation to channel activity. For some stimuli, however, it is more difficult to know on which cellular organelles they act. Many of these stimuli are not true "outside" stimuli because their effects can potentially be sensed throughout the cell. For example, temperature changes are transmitted throughout the cell and can potentially affect many cellular systems. Since endothelial cells are compliant, shear stress can deform the whole cell and affect any of the many internal cell structures. Indeed, the reactive force necessary to withstand shear stress must come from the stress necessary to cause shearing strain in the cell, from interactions with neighboring cells, and from the abluminal side of the cell which then transmits force to the substratum. Therefore, shear stress induced by blood flow acts on endothelial cell surfaces; but because of the interconnectedness of cell organelles, it can potentially be sensed by a number of organelles. While shear stress induces a myriad of cellular changes it is still unknown which system or systems transduce them.

Recent discoveries that endothelial cells also react to rapid shear transients differently than steady-state shear stress and that vascular endothelium is subjected to both shear transients and steady shear, depending on the location in the vasculature, suggest that shear transients and endothelial reactions to them may have important physiological and pathophysiological implications. Some of the first work to be done in this regard has showed that the cell membrane dependent

processes NO (20) and prostacyclin production (18), are sensitive to shear transients and these results have led to investigations into the role of G-proteins in distinguishing between stepped shear stress and shear stress that is slowly ramped (19). Knudsen *et al.* have investigated the roles of cytoskeletal elements in transducing shear induced NO production and found that neither actin microfilaments nor microtubules were necessary for shear mechanotransduction (39), although the physiological implications for this finding were disputed by a similar study using intact aortic segments (32). More recent studies, outlined in this proposal, have shown that vascular endothelium is sensitive to the rate of change of shear stress for fast ramps and magnitude sensitive for slower ramps.

In any event, while many cellular structures have been shown to be shear sensitive, a likely candidate for rate-sensitivity, due to its viscoelasticity and proximity to the shear stress stimulus, is the cell membrane itself. Finally, in support of the hypothesis that membrane fluidity is modulated by luminal shear stress, Berthiaume & Frangos (1994) reported that shear increased the permeability of the membrane to a lipophilic dye merocyanine 540 (5). They suggested that shear disrupted the normal packing of lipids allowing for increased insertion of the foreign dye into the membrane. These studies, however, lacked time resolution of this change or any analysis of whether this permeability was affected differently by different rates of change of shear stress.

3.1.5 How does lipid fluidity affects proteins?

Lipid fluidity can potentially affect protein function in three ways. First, by restricting (or allowing) movement in the plane of the membrane, changes in lipid fluidity can restrict or enhance protein lateral mobility and thus might affect diffusion-dependent protein functions. This property is less important for proteins that are bound to the underlying cytoskeleton. For G-protein hydrolysis, a process necessary for many agonist induced change in the cell, G-proteins must diffuse from the receptor to a downstream effector. Alterations in this diffusion could potentially affect the equilibrium between receptor/G-protein complexes and effector/G-protein complexes.

Second, changes in lipid fluidity can change the proteins local energy environment by either changing the phase of the lipid immediately surrounding the protein and thus altering the protein conformation by altering the hydrophobic mismatch. The former effect has been hypothesized to cause the anesthetic effects of haloalthane on nerve function; haloalthane fluidizes the entire membrane and thus negates the phase change from the protein annular region to the rest of the lipid bilayer and thus prevents the opening of sodium channels in neurons (74). Sodium channel opening and closing is necessary for action-potential transmission. The latter effect suggests that lipid fluidity changes can affect the hydrophobic mismatch between the lipids and the protein and alter the free energy state of the protein (51). Such changes in free energy may be sufficient to cause a receptor protein, for example, to initiate downstream signaling even in the absence of a

ligand.

Finally, it thought that lipid fluidity may affect the accessibility of proteins to ligands. In accordance with an Archimedes-like principle, tighter packing of lipids might cause integral membrane proteins to be pushed out of the membrane and thus make their active sites more available to ligand binding (66). The converse might also be true. This mechanism seems unlikely to be involved in shear transduction because shear transduction has been shown to occur in the absence of known endothelial ligands. However, increased protrusion of integral proteins out of the membrane could increase their hydrophobic mismatch and thus alter protein free energy.

Because of the importance that membrane fluidity plays in determining protein function, it remains an important endeavor to measure the time-course of membrane- fluidity changes under time varying shear stress.

3.2 Confocal-FRAP as a means to measure membrane fluidity

It was desired to develop a technique by which the hypothesized time rate of change of membrane fluidity with shear stress application could be measured. In order to perform such experiments we needed a system which could easily accommodate a monolyaer of cells cultured in a flow chamber, a flow apparatus, and a means by which membrane fluidity could be measured on a small, pre selected, area of a cell. Furthermore, our current experiments on isolated arterioles suggests that endothelial cells are sensitive to rates of change of shear stress of

greater than 5 dynes/cm^2/sec. Such results suggest that the cell has a reaction time roughly of the same order of magnitude (~2 seconds for a shear ramped to 10 dynes/cm^2). In any event, we needed a system which could take a sufficiently rapid measurement of membrane fluidity so that the diffusion constant, although hypothesized to be time dependent, could be considered quasi-steady. To meet these requirements we used flow chambers and a Biorad-1024 confocal microscope to measure lipid diffusivities in cell membranes of endothelial cells while they were being sheared (see figure 21).

Of the many techniques available to measure membrane properties, confocal-FRAP was the most suitable method because, as will be discussed later, it had all the necessary features for measuring rapidly changing diffusion constants on pre-selected subcellular membrane areas while the cells were being sheared. We present some preliminary data regarding the effects of shear stress on membrane lipid diffusivity before and after a step in shear stress. This method is refined to demonstrate that measurements of diffusivity can be made in less than one second, thus demonstrating that, with this method, we will be able to detect time-rates-of-change of diffusivity that occur with characteristic times of as little as one second.

3.2.1 Fluorescence recovery after photobleaching

The two cellular components whose diffusivities are most commonly measured are lipids and proteins. While other components undergo diffusion (such as intercellular components (microtubules, actin filaments)) the application of the

theory is much more difficult because, first, these components diffuse in three dimensions and second, there distribution is highly localized. Membrane components, on the other hand are confined to the membrane and diffuse only laterally (2-D) and are more evenly dispersed in the sample area monitored. Recently, however, advances have been made using the confocal microscope to conduct FRAP experiments making the measurement of three dimensional diffusion feasible (70,31). Currently, because of the system limitations of most confocal microscopes, only slower diffusion rates can be made in three dimensions.

The theory for two dimensional diffusion of a translating species into a circular photobleached spot has been worked out by Axelrod *et al.* (2) and is based on the following assumptions. First, the bleaching time must be much faster than the characteristic diffusion time. This requirement must be met because if the bleaching time is close to the diffusion time, then bleached fluorophore will diffuse to the immediate vicinity of the spot and affect the local concentration of unbleached fluorophore. The theory assumes that the surrounding concentrations of unbleached fluorophore equals the pre-bleach concentration. Second, the bleaching intensity must be such that the resulting distribution of the fluorophore in the bleached region approximates a Gaussian distribution being a minimum in the center of the spot and abruptly approaching the outside fluorescence near the edges (see figure 23). Third, although the data can be adjusted for photobleaching during the monitoring phase, it is best if the fluorophore is resistant to bleaching when the laser power is low. Finally the theory assumes that the bleach spot is circular and that unbleached fluorophore diffuses into the spot in the radial direction

only. This assumption holds very well in traditional FRAP experiments where a traditional fluorescent microscope with a Gaussian beam laser is used to bleach the spot. For the confocal microscope, however, the bleach area is generally a square or a line.

Others have used alternative geometries and variations on the FRAP techniques to accommodate convection of fluorophore and geometries that are alternatives to a circular spot. Jain *et al.*, for example, solved the convection diffusion equation in two directions (x and y) for a circle to derive an expression for the fluorescence concentration as a function of a spot radius as assessed on individual frames of a video tape (35). This method had the advantage that other geometries could be used (they also solved the equations for an elliptical bleached spot) and the flow direction did not need to be known *a priori*. Furthermore, it was not necessary to know whether convection or diffusion dominated the fluorescent recovery process because the diffusion was related to the spot radius and the flow was assessed by measuring the movement of the spot centroid over time. Their method had the disadvantage that acquisition rate was limited to the video frame rate and that post-experiment data analysis was labor intensive. However, it is possible that their method could be useful to detect membrane flow in the presence of shear stress.

Others have developed a means by which the confocal microscope could be used as a FRAP apparatus. Blonk *et al.* were the first to use the confocal laser scanning microscope to measure fluorescence recovery after photobleaching (7). They pointed out that the confocal microscope is well suited for FRAP experiments

because it has the necessary lasers, attenuating devices, and photodetection equipment. Furthermore, it has the advantage of being able to scan the recovery in a volume element and these authors proceeded to work out the theory for 3-D diffusion dominated fluorescent recovery.

In the experiments we outline here, we choose to bleach and scan the exact same line and can therefore accomplish mush faster bleaching speeds and shorter recovery times. These short recover times are essential in order to measure the time rate of change of the diffusion constant. A new theory will be worked out covering the diffusion in one direction in a line scan and two directions for a rectangular bleach.

3.2.2 *Theory for fluorescence recovery after photobleaching*

The following is the solution to the convection diffusion equation for a FRAP experiments employing a confocal microscope using a rectangular bleach and a line scan bleach.

1. First we define the geometry:

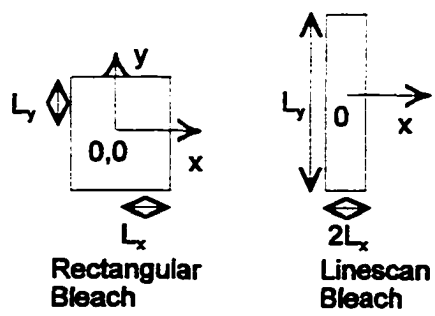

Note that L_x and L_y are the half-widths of the scanning area. We will see later that they are also assumed to be equal to the half-widths of a Gaussian concentration profile evaluated at e^{-2} times the profiles depth. This assumption will be verified later experimentally.

2. We then write the convection-diffusion equation:

$$\frac{Dc}{Dt} = D\nabla^2 c \tag{8}$$

where c is the fluorophore concentration and D is the diffusion coefficient (cm^2/sec). In two dimensions and using an assumption of isotropic diffusion, this equation becomes:

$$\frac{\partial c}{\partial t} = D\left(\frac{\partial^2 c}{\partial x^2} + \frac{\partial^2 c}{\partial y^2}\right) - v_x\frac{\partial c}{\partial x} - v_y\frac{\partial c}{\partial y} \tag{9}$$

where v_x and v_x are the flow velocities in the x and y directions, respectively.

3. As a first approximation, we then set total fluorescence to be proportional to the concentration integrated over the viewing area. This assumption is an approximation because generally the laser intensity is not spatially uniform. Mathematically, the above statement is given by:

$$f \propto 4 \int_0^{L_x} c_x dx \cdot \int_0^{L_y} c_y dy \qquad (10)$$

For a rectangular scan and:

$$f \propto 2L_y \int_0^{L_x} c_x dx \qquad (11)$$

for a line scan.

4. The solution must satisfy the boundary conditions:

$$B.C.: \quad \frac{\partial c}{\partial x}\Big|_{x=0} = 0 \quad , \quad \frac{\partial c}{\partial y}\Big|_{y=0} = 0 \quad , \quad c(x, y \to \infty) = c_\infty \qquad (12)$$

and initial condition:

$$I.C.: \quad c(x,y,0) = c_0(x,y) \qquad (13)$$

5. We will begin by assuming that the initial profile of the bleach pattern mirrors the laser's spatial profile which is Gaussian (35):

   a) for the line scan this becomes:

$$c_{ls0}(x) = c_0(0) + (c_\infty - c_0(0))(1 - e^{-2\frac{x^2}{L_x^2}}) \tag{14}$$

c) and for the rectangular bleach:

$$c_{rs0}(x,y) = c_0(0,0) + [c_\infty - c_0(0,0)][1 - e^{-2\frac{x^2}{L_x^2}} e^{-2\frac{y^2}{L_y^2}}] \tag{15}$$

6. To simplify equation 9 and I.C.'s we define the following variables:

$$Let \quad \theta_{ls} = \frac{c - c_\infty}{c_0(0) - c_\infty} \quad , \quad \theta_{rs} = \frac{c - c_\infty}{c_0(0) - c_\infty} \tag{16}$$

7. Equation 9 becomes:

$$\frac{\partial \theta}{\partial t} = D\left(\frac{\partial^2 \theta}{\partial x^2} + \frac{\partial^2 \theta}{\partial y^2}\right) - v_x \frac{\partial \theta}{\partial x} - v_y \frac{\partial \theta}{\partial y} \tag{17}$$

where $\theta = \theta_{ls}$ or θ_{rs}.

8. The initial conditions become:

$$\theta_{ls}(x,0)=\theta_{ls0}=e^{-2\frac{x^2}{L_x^2}} \quad , \quad \theta_{rs}(x,y,0)=\theta_{rs0}=e^{-2\frac{x^2}{L_x^2}}e^{-2\frac{y^2}{L_y^2}} \tag{18}$$

9. Finally we define the following dimensionless variables:

$$\xi=\frac{x-v_x t}{L_x} \quad , \quad \eta=\frac{y-v_y t}{L_y}$$
$$\tau_x=\frac{Dt}{L_x^2} \quad , \quad \tau_y=\frac{Dt}{L_y^2} \tag{19}$$

10. Upon substitution and rearrangement we obtain:

$$\frac{\partial\theta}{\partial\tau}=\frac{\partial^2\theta}{\partial\xi^2}+\frac{\partial^2\theta}{\partial\eta^2} \tag{20}$$

with initial conditions:

$$\theta_{ls0}(\xi)=\theta_{\xi 0}=e^{-2\xi^2} \quad , \quad \theta_{rs0}(\xi,\eta)=\theta_{\xi 0}\theta_{\eta 0}=e^{-2\xi^2}e^{-2\eta^2} \tag{21}$$

where θ_{rso} is given using Gaussian approximation for the laser profile.

11. Because of the form of the initial conditions and governing equation we see that equation 20 is separable. We therefore define the following function:

$$\theta(\xi,\eta,\tau)=\theta_{\xi}(\xi,\tau)\theta_{\eta}(\eta,\tau) \tag{22}$$

12. Upon substituting equation 22 into 20 we obtain:

$$\frac{\dfrac{\partial\theta_{\xi}}{\partial\tau}-\dfrac{\partial^2\theta_{\xi}}{\partial\xi^2}}{\theta_{\xi}} = -\frac{\left(\dfrac{\partial\theta_{\eta}}{\partial\tau}-\dfrac{\partial^2\theta_{\eta}}{\partial\eta^2}\right)}{\theta_{\eta}} = F(\tau) \tag{23}$$

where $F(\tau)$ is an arbitrary function giving the general solution. Since we desire only a particular solution, inspection of the initial conditions suggests that we can set $F(\tau)$ to 0 to obtain:

$$\frac{\partial\theta_{\xi}}{\partial\tau}=\frac{\partial^2\theta_{\xi}}{\partial\xi^2} \quad , \quad \theta_{\xi 0}=e^{-2\xi^2} \tag{24}$$

and

$$\frac{\partial\theta_{\eta}}{\partial\tau}=\frac{\partial^2\theta_{\eta}}{\partial\eta^2} \quad , \quad \theta_{\eta 0}=e^{-2\eta^2} \tag{25}$$

where the initial conditions are given as Gaussian profiles.

13. Therefore, we need to solve equation 24 with each initial condition and we

can construct the solution of 25 with the appropriate change of variables. The solution to 24 with the Gaussian distribution will generate the solution for the line scan profile. We can then construct solution for the rectangular scan using equation 22 with the Gaussian initial condition.

14. We solve 24 using the Fourier transform:

$$\Theta(\lambda,\tau)=\frac{1}{\sqrt{2\pi}}\int_{-\infty}^{\infty}\theta(\xi,\tau)e^{i\lambda\xi}d\xi \qquad (27)$$

15. Upon substituting 27 into 24, we obtain:

$$\frac{d\Theta}{d\tau}=-\lambda^2\Theta \qquad (28)$$

which has the solution:

$$\Theta(\lambda,\tau)=\Theta_0(\lambda)e^{-\lambda^2\tau} \qquad (29)$$

with the initial condition:

$$\Theta_0(\lambda)=\frac{1}{\sqrt{2\pi}}\int_{-\infty}^{+\infty}\theta_{\xi 0}(\xi)e^{i\lambda\xi}d\xi \qquad (30)$$

and with $\theta_{\xi 0}$ given in equation 24.

16. To solve equation 29 we use the inverse Fourier transform:

$$\theta(\xi,\tau)=\frac{1}{\sqrt{2\pi}}\int_{-\infty}^{+\infty}\Theta_0(\lambda)e^{-\lambda^2\tau}e^{-i\lambda\xi}d\lambda \qquad (31)$$

17. We change ξ to s in equation 30 and substitute 30 into 31 to obtain:

$$\theta(\xi,\tau)=\frac{1}{\sqrt{2\pi}}\int_{-\infty}^{+\infty}\int_{-\infty}^{+\infty}\theta_{s0}(s)e^{i\lambda(s-\xi)}e^{-\lambda^2\tau}d\lambda ds \qquad (32)$$

18. From the integral tables (27) we have:

$$\int_{-\infty}^{+\infty}e^{(-p^2\lambda^2\pm q\lambda)}d\lambda=\frac{\sqrt{\pi}}{p}e^{\frac{q^2}{4p^2}},\quad p>0 \qquad (33)$$

19. Using 33 we solve the inner integral of 32 to obtain

$$\theta(\xi,\tau)=\frac{1}{\sqrt{2\pi}}\int_{-\infty}^{+\infty}\frac{\sqrt{\pi}}{\sqrt{\tau}}e^{-\frac{(\xi-s)^2}{4\tau}}\theta_{s0}(s)ds \qquad (34)$$

20. We substitute the Gaussian initial condition from 24 (changing ξ to s) into 34 and, using equation 33 along with algebraic manipulation and rearrangement, we arrive at the solution:

$$\theta(\xi,\tau)=\frac{1}{\sqrt{8\tau+1}}e^{\left(\frac{-2\xi^2}{8\tau+1}\right)} \qquad (35)$$

which is the solution for a line-scan bleach.

21. From equation 22, 24 and 35 we construct the solution for a rectangular bleach assuming a Gaussian profile for each coordinate:

$$\theta(\xi,\eta,\tau)=\frac{1}{\sqrt{8\tau_x+1}}e^{\left(\frac{-2\xi^2}{8\tau_x+1}\right)}\frac{1}{\sqrt{8\tau_y+1}}e^{\left(\frac{-2\eta^2}{8\tau_y+1}\right)} \qquad (36)$$

22. From equations 10 through 16 we see that the fluorescence, *f*, normalized to its value before bleaching, f_0, will have the form:

$$\frac{f}{f_0} = a_0 + (a_1 - a_0) \cdot a_2 \cdot \int_0^{L_x} \theta(x,\tau)\, dx \tag{37}$$

for the one dimensional problem (line scan) and:

$$\frac{f}{f_0} = a_0 + (a_1 - a_0) \cdot a_2 \cdot \int_0^{L_x} \int_0^{L_y} \theta(x,\tau_x)\, \theta(y,\tau_x)\, dx dy \tag{38}$$

for the rectangular bleach.

23. To integrate 35 we use the definition of the error function given by:

$$erf(\xi') \equiv \frac{2}{\sqrt{\pi}} \int_0^{\xi'} e^{-u^2} du \tag{39}$$

to obtain:

$$\int_0^{L_x} \theta_{ls} = \frac{L_x \sqrt{\pi}}{2\sqrt{2}} \left[erf\left(\frac{\sqrt{2}}{\sqrt{8\tau_x + 1}} \cdot \frac{L_x - v_x t}{L_x} \right) - erf\left(\frac{\sqrt{2}}{\sqrt{8\tau_x + 1}} \cdot \frac{v_x t}{L_x} \right) \right] \tag{40}$$

3.2.3 Interpreting the experimental results using the model

The three most important pieces of information that can be obtained from FRAP experiments are: 1) the diffusion coefficient 2) the mobile fraction, and 3) detecting the presence of membrane flow. The diffusion coefficient, D, governs the rate of recovery of fluorescence after photobleaching. The mobile fraction is defined as:

$$\Phi=\frac{f_\infty-f_i}{f_0-f_i}=\frac{\left(\frac{f}{f_0}\right)_\infty-\left(\frac{f}{f_0}\right)_i}{1-\left(\frac{f}{f_0}\right)_i}. \qquad \textbf{(41)}$$

Having solved the convection diffusion equation for two types of reasonable initial condition approximations, we now need to derive equations which can be used to fit the data and yield information on the above three quantities. We begin by noting that at t=0, $f/f_0=(f/f_0)_i$ and as $t\to\infty$, $f/f_0\to(f/f_0)_\infty$. For the line-scan bleach described by equation 37 we need to evaluate 40 at t=0 and $t\to\infty$. Noting that erf(0)=0 and erf(∞)=1 we see from 40 that:

$$\int_0^{L_x}\theta_{ls}(t=0)\,dx=\frac{L_x\sqrt{\pi}}{2\sqrt{2}}erf(\sqrt{2}) \qquad \textbf{(42)}$$

Similarly,

$$\int_0^{L_y} \theta_{ls}(t=0)\,dy = \frac{L_y\sqrt{\pi}}{2\sqrt{2}}\,erf(\sqrt{2}) \tag{43}$$

As $t \to \infty$ we have:

$$\int_0^{L_y} \theta_{ls}(t\to\infty)\,dy = 0 \tag{44}$$

Therefore, using equation 37 we see that $a_0=(f/f_0)_\infty$. If we let:

$$a_2 = \frac{2\sqrt{2}}{L_x\sqrt{\pi}} \cdot \frac{1}{erf(\sqrt{2})} \tag{45}$$

Then $a_1=(f/f_0)_i$. So equation 37 becomes, introducing the definition of τ_x:

$$\frac{f}{f_0} = \left(\frac{f}{f_0}\right)_\infty + \left[\left(\frac{f}{f_0}\right)_i - \left(\frac{f}{f_0}\right)_\infty\right] \cdot \frac{1}{erf(\sqrt{2})} \cdot \left[erf\left(\frac{\sqrt{2}}{\sqrt{\frac{8Dt}{L_x^2}+1}} \cdot \frac{L_x - v_x t}{L_x}\right) - erf\left(\frac{\sqrt{2}}{\sqrt{\frac{8Dt}{L_x^2}+1}} \cdot \frac{v_x t}{L_x}\right)\right] \tag{46}$$

To analyze the present experiments we make some simplifying assumptions. Preliminary curve fits showed that including flow as a parameter resulted in good curve fits but that had a more sigmoidal shape and deviated from experimental curves in the early and late phases of the recovery. Since we do not expect flow on the time scale of these measurements, we set v_x and v_y to 0 and obtain:

$$\left(\frac{f}{f_0}\right)_{ls} = \left(\frac{f}{f_0}\right)_{\infty} + \left[\left(\frac{f}{f_0}\right)_i - \left(\frac{f}{f_0}\right)_{\infty}\right] \cdot \frac{1}{erf(\sqrt{2})} \cdot \left[erf\left(\frac{\sqrt{2}}{\sqrt{8\frac{Dt}{L_x^2}+1}}\right)\right] \quad \textbf{(47)}$$

We used the Gaussian profile assumption to construct a solution for a square bleach ($L_x = L_y$):

$$\left(\frac{f}{f_0}\right)_{sqs} = \left(\frac{f}{f_0}\right)_{\infty} + \left[\left(\frac{f}{f_0}\right)_i - \left(\frac{f}{f_0}\right)_{\infty}\right] \cdot \left[\frac{1}{erf(\sqrt{2})} \cdot erf\left(\frac{\sqrt{2}}{\sqrt{8\frac{Dt}{L_x^2}+1}}\right)\right]^2 \quad \textbf{(48)}$$

Equations 47 and 48 are, then, 3 parameter curve-fit equations. We used Slidewrite software to perform a least squares regression analysis using $(f/f_0)_\infty$, $(f/f_0)_i$, and D as curve fitting parameters.

3.2.4 Experimental setup

Bovine aortic endothelial cells (passage 4-15) were grown on #1 glass coverslips in complete medium containing Dulbeccos modified eagle medium (DMEM) supplemented with 10% fetal bovine serum (pH=7.4). Coverslips were either uncoated or coated with gelatin. When the cells reached confluency, the coverslips were washed three times first with medium and then with Hanks buffered salt solution (without calcium or magnesium). For DiI staining (DiI C_{16}, Molecular

Probes, Oregon) the cells were incubated at room temperature in 10^{-4}M DiI for 10 minutes and immediately washed 3 times with HBSS (see figure 22 for staining results).

Immediately the cells were placed into the flow chamber such that the gap height between the cells and the opposite glass window was about 100um. This height was measured using a light microscope with a micrometer caliper attached to the stage and capable of measuring the vertical displacement of the stage. The displacement achieved when each glass surface came into focus gave the gap height. This height was used to predict the pump flow rate necessary to achieve shear stresses of 10 and 20 dynes/cm^2. The equation for shear stress is $\tau=3/2Q\mu/wh^2$ where Q is the flow rate, μ is the viscosity, w is the channel width, and h is the channel height.

The flow chamber was connected on the upstream side to a reservoir containing about 100ml of warm, pre-gassed, medium. This medium had been pre-equilibrated with 95% air and 5% CO_2 in an incubator. On the downstream side the chamber was connected to a Harvard infusion/withdrawal pump which had adjustable speed. The whole assembly was brought to the confocal microscope for FRAP analysis (see figure 21).

Analysis was done on a Nikon Diaphot inverted microscope equipped with Biorad confocal lasers and electronics. Two lasers were used: an argon-ion laser allowed bleaching at the 488nm wavelength of light while a krypton-argon laser allowed monitoring at the 514 wavelength. Two lasers were used because the Biorad 1024MRC system was fitted with fast shutters for all three laser ports (two on

the argon-ion, one on the krypton argon) allowing for fast switching from one laser to the other. In this way the specimen could be rapidly bleached and immediately afterwards, could be monitored for fluorescence recovery. Most researchers outfit the neutral density filters with a fast switching device (the neutral density filters are the means by which laser power is attenuated). This method was impractical for our purposes because the neutral density filters are located inside the Biorad unit.

For DTAF staining, cells were washed and then incubated in 10^{-5}M DTAF in saline (pH=9.5) and incubated on ice for 30 minutes. The reaction was stopped by washing with DMEM.

3.2.5 FRAP Protocols

Decay curves were first constructed by predicting the rate of monitoring to be used during the recovery period. The fastest rate possible was used during the initial phase of the fluorescence recovery while a less frequent monitoring pulse was used for the later phase of the recovery. Changing the monitoring frequency was necessary to minimize photobleaching during recovery. The frequency of monitoring refers to the scan frequency. The decay curves are shown in figure 24. The decay data was fitted with a 2^{nd} order polynomial and this polynomial was used to superimpose (1 minus the decay) onto the recovery curves. The rapid-monitor decay curve was superimposed on the early phase of the recovery curve while the less-frequent-monitoring decay curve was superimposed on the later phase of the recovery.

The recovery data was fitted with the appropriate fluorescent recovery equation from section 3.2.3 generated from the theory outlined in section 3.2.2.

To illustrate the differences in recovery between a square bleach and a line-scan bleach we constructed concentration profile plots that varied with time (figure 23). In these figures one can notice that the recovery for a line scan is much faster (nearly complete in 0.5 seconds) than the recovery for a square bleach. It also shows that the initial Gaussian profile decays to become more uniform over time.

3.2.6 Preliminary results

Results of FRAP experiments are shown in figures 25 through 27. In figure 25 are four panels illustrating corrected fluorescent recovery curves before, 10 seconds after, and five minutes after the imposition of a step in shear stress of 10 dynes/cm^2. The fourth panel is a fluorescent recovery curve performed one minute after shear was turned off. These results suggest that mobile fraction is reduced while the diffusion coefficient increases with shear stress and that these changes are reversible. Results illustrated in figure 26, however, suggest that the mobile fraction decreases and the diffusion coefficient decreases. Therefore reductions in the mobile fraction with shear stress seem consistent while changes in the diffusion coefficient with shear stress, as measured thus far, are not. Further experimentation is needed to sort out these discrepancies.

Figure 27 demonstrates the feasibility of performing FRAP experiments on a time scale of less than one second. Achieving this time scale shows that time rates

of change of membrane properties with shear stress are feasible.

3.2.7 Discussion of preliminary results

We hypothesize that the cell membrane may react differently to different rates of change of shear stress. To test this hypothesis we seek to directly investigate the role of shear in affecting the mechanical properties of the cell membrane. FRAP measurements coupled with shear system is an ideal combination to yield direct measurements of shear effects on both lipid properties and protein diffusion.

The preliminary results from FRAP experiments using DiI (lipid probe) stained BAECs under shear flow (figure 25 and 26) demonstrate the feasibility of this approach. The graphs show that flourescent recovery of a bleached spot and the calculated mobile fraction changes with shear stress. It should be noted however that the immobile fractions in most of these trials was less than what other investigators have found (Φ=~1) and the diffusion coefficients are also lower (Schlessinger *et al.* measured ~9 x 10^{-9} cm^2/sec (64)). But all values are the same order of magnitude. The likely reason for these discrepancies is that the cells were not maintained at 37°C but rather were at 25°C during the course of the experiment. Low temperatures are known to decrease membrane fluidity.

Chapter 4: Summary and Conclusions

In this research proposal the feasibility has been established of imposing different time courses of shear stress in isolated microvessels and measuring the resulting change in diameter. Using a novel feedback control system in which intraluminal shear stress and pressure were prescribed and controlled in vasoactive isolated arterioles, we conducted studies showing that shear induced vasodilation exhibited a complex dependence on the shear magnitude and the rate of change of shear stress. We proceeded to show that step-shear and ramp-shear induce biphasic vasodilatory responses which differed in the early phase but not in the late phase. In the early phase (0 to ~10 minutes), the vasodilation elicited by the step-shear (20 dynes/cm^2) was dramatically greater than that elicited by a shear ramped over five minutes to the same final shear stress. In the late phase (11-35 minutes), however, the plateau dilation for both step- and ramp-shears were equal. Furthermore, we showed, through a curve-fitting procedure, that the early phase was well represented by the product of a sigmoidal delay function and a negative exponential decay function while the late phase was well represented by the product of the delay function and a constant. The total response is a linear superposition of the early and late phase responses. Further analysis of the early phase revealed that shear-induced endothelial-mediated dilation is rate sensitive for intermediate shear magnitudes (20 dynes/cm^2) but not for lower (10 dynes/cm^2) and higher (40 dynes/cm^2) shear stresses and that it is magnitude sensitive when shear is ramped slowly (2.5 dynes/cm^2/sec). Additionally, we conclude that vascular endothelium

mediates a biphasic dilatory response to shear stress that depends, in the early phase but not in the late phase, on a newly defined stimulus for shear induced dilation: the temporal shear gradient (TSG).

We concluded that two fundamentally different vasodilatory responses to shear stress are mediated by microvascular endothelium: one activated by shear stress changes on a time scale of a few seconds or less and the other activated by shear stress changes on a longer time scale. The former response is potent, transient, and rate-sensitive and the latter is more modest, sustained, and magnitude-sensitive.

Finally, we set out to develop a method by which the hypothesis could be tested that the cell membrane is directly affected by shear stress and may confer rate sensitivity to shear stress to the endothelial cell. Using a confocal microscope to perform fluorescent recovery after photobleaching we measured diffusion coefficients in cells in static medium and cells subjected to shear stress. Furthermore we have demonstrated that we can take rapid measurements and thus can potentially evaluate the hypothesized time rate of change of the diffusion coefficient when cells are in shear flow. Such investigation represent not only a new method for evaluating membrane dynamics but represent as well a fundamental new thinking on how shear might lead to altered cellular mechanical properties.

Not only does this research have important implications for understanding the mechanical aspects of cellular biology but is also challenges the current understanding of how shear stress is controlled in a network. Instead of simply describing network vasoregulation as a proportional feedback control system as

Koller *et al.* have suggested (44), it may be necessary to include in such a model integral control (which looks at how long shear stress has strayed from the set point) and derivative control (which considers how quickly shear stress changes).

How might stretching a membrane change the energy state of an integral protein such as a receptor, a G-protein, or an ion channel? It has been suggested by Frangos *et al.* and Reich *et al.* (19,59) that the membrane fluidity plays a role in the shear stress response. Adjusting the membrane fluidity using cholesterol (which stiffens it) suppressed G-protein hydrolysis while adding benzyl alcohol (which makes it more fluid) enhanced G-protein hydrolysis in response to shear stress. However, they were not able to conclusively demonstrate that shear itself fluidizes the membrane.

It must be established initially, however, that cells do respond differently to different shear histories. For this reason we have developed the FRAP-confocal system that is capable of measuring the high diffusion constants for lipid mobility and doing so rapidly. With this technique we hope to determine if the diffusivity (and hence the membrane fluidity) changes over time after a step in shear stress and whether a ramp in shear stress affects membrane fluidity differently than a step. In this way we should be able to determine if the rate sensitivity to shear stress of endothelial cells resides, at least in part, in the mechanical properties of the cell membrane.

We have successfully demonstrated and quantified the rate sensitivity of endothelial cells to shear stress in s physiological setting. Second, we have devised a workable method to test the hypothesis that sheer stress alters the membrane

mechanical properties in a time dependent manner. Coupling these *ex-vivo* and *in vitro* approaches should lead us closer to discovering the mechanism by which shear stress is transduced into chemical signals in vascular endothelium.

5. Figure legend:

Figure 1: *Effects of NO and PGI_2 on smooth muscle:* Agonists (e.g. acetylcholine) bind to membrane bound receptors to initiate a cascade of events leading to smooth muscle relaxation. Many of the signaling events have been shown to be similar in shear induced dilation (illustration from (8)).

Figure 2: *Cross section of an arteriole:* Electron micrograph of 1A arteriolar cross section. BM (Basement membrane), E (endothelial cells), VSM (vascular smooth muscle) (EM micrograph from (14)).

Figure 3: *Mechanism of shear induced dilation:* Shear stress initiates increases in PKC (protein kinase C). Some believe that shear stress causes G-protein hydrolysis via changes in membrane fluidity. However, this mechanism has yet to be proven.

Figure 4: *Silver nitrate staining of arterioles:* A. Silver nitrate preferentially stains endothelial orders revealing that the cells are aligned in the flow direction. B. Permeabilizing the endothelium allows staining of endothelial cells and smooth muscle cells simultaneously.

Figure 5: *Stress fibers and cytoskeletal network:* Actin microfilaments furnish structural integrity of the endothelial cells. Stress fibers are made of bundles of actin and are aligned in the flow direction (illustration from (77)).

Figure 6: *Viscoelastic graphs:* A step in stress causes n initial rapid (elastic) deformation followed by a gradual deformation leading to a plateau strain. A ramp causes only the gradual strain but leads to the same plateau. Pre-shearing cells (sheared) makes them stiffer; they do not strain as much and reach the plateau earlier as compared to non-presheared cells (unsheared).

Figure 7: *Arteriole removed from a cremaster muscle:* The 1A arteriole is a long feed arteriole for the cremaster muscle and therefore has the potential for significant blood flow regulation.

Figure 8: *Experimental Setup:* Showing the perfusion and suffusion system for isolated arterioles. The suffusion solution, which was equilibrated for CO_2, O_2, pH, and temperature in the recirculating reservoir (H_r) was used to bathe the blood vessel. Perfusion solution was equilibrated by bathing with suffusion solution the CO_2 and O_2 permeable silicone tubing connecting the pressure reservoirs to the cannulating pipettes. To prevent upstream changes in perfusion solution, pH and O_2 gas-

impermeable tygon tubing was used to connect the pressure reservoirs to the vessel chamber. The fast-ramp apparatus was composed of an upstream feed tube (H_{up}) connected to a secondary supply (H_2) by a piece of tubing whose opening was controlled by a computer-controlled solenoid pinch valve. On the upstream side, the pulley system was connected to both the secondary supply reservoir and the feed-tube. Adjustments by the upstream motor caused equal movements of the reservoir and feed-tube, thus maintaining their heights relative to each other. This relative height determined upstream feed-tube filling rate by the secondary supply reservoir when the solenoid was opened. Gravity feed of solution into the upstream feed tube allowed fast and accurate ramps of P_{up} and ∴ flow and ∴ shear stress. Equal and opposite adjustment of the up and downstream pressure heads allowed dynamic flow adjustment without changing intra luminal pressure.

Figure 9: *Feedback control of pressure and shear:* Shear stress and pressure were dynamically controlled by measuring flow and diameter, calculating pressure and shear stress, and adjusting flow and/or pressure to bring them back to their set points. To make pressure or differential pressure adjustments in response to deviations from set points, the following algorithm was developed: For shear stress: if $|\tau - \tau_{set}| > \tau_{spread}$, then the computer adjusted the pressure reservoirs for $t^* \cdot (\tau -$

τ_{set}) seconds, where τ is the luminal shear stress, τ_{set} is the desired luminal shear, τ_{spread} is the tolerated error, and t* is a time constant (0.02 sec/dynes/cm^2). The adjustment took place when the computer activated a relay that turned on a constant speed DC (12V) motor that wound, through a pulley, a string attached to the reservoir. If τ-τ_{set}<0, then the upstream feed tube was raised and the downstream receiving tube lowered by an equal amount and τ-τ_{set} was checked again. A similar algorithm was used to adjust pressure and to equilibrate upstream and downstream pressures.

Figure 10: *Calibration curves for two different upstream feed tubes:* Curves were generated by measuring the filling rate for a short time (0.5-10 seconds) of the upstream feed-tube by the 2° supply reservoir. The height of the 2° supply reservoir remained constant during upstream feed tube filling (the 2° supply reservoir had a large volume). For short filling durations, the filling rate was nearly constant, ensuring a ramp in upstream pressure. Second order polynomial regressions yielded: (A) h_i=63-24(dh/dt)+1.9(dh/dt)^2 (r^2=1.0) for the 1/8" tubing and (B) h_i=55-14(dh/dt)+0.97(dh/dt)^2 (r^2=0.99).

Figure11: *Ramping shear from 0 to τ_{max}:* Voltage values from the differential pressure transducer were converted to differential pressures using a calibration curve established prior to experiments. Differential

pressures were converted to flow rate and subsequently to shear stresses using equations described in Methods and using measured diameters. For fast ramps, shear stress rose in a linear fashion with time, while for slower ramps shear approached τ_{max} more asymptotically. This result occurred because as the upstream feed tube filled, its height approached the secondary supply height. Thus, the driving force for upstream feed tube filling was reduced with time. However, even slow ramps were close to being linear.

Figure 12: *Representative experimental tracings:* In all tracings the step-shear experimental results are represented by solid lines and the results from ramp-shear experiments by dashed lines. (A) shows the diameter responses to both step-shear and ramp-shear. (B) shows that the increases in diameter were followed by increases in flow to keep shear constant. (C) shows that the intraluminal pressure was maintained at 65 mmHg. (D) indicates the maintenance of shear stress after it was stepped or ramped.

Figure 13: *Vasodilatory response to a step-shear (+ symbols) or ramp-shear (open circles) from 0 to 20 dynes/cm^2*: Zero time refers to either when shear was stepped or the when ramp was started, so that shear = 20 dynes/cm^2 for all t>5 minutes. Diameters were recorded continuously

but are here represented as averages of the normalized diameter at each minute interval. The mean control diameter was 77±5μm. Vertical bars represent standard errors. Asterisks indicate significant differences ($p<0.05$) between the two groups.

Figure 14: *Curve fitting of the experimental data in the step-shear and ramp-shear experiments as described in Results*: $d/d_{control} = 1+[G(t)H(t)]_{early}+[G(t)H(t)]_{late}$ ($r^2=0.95$) where $[G(t)H(t)]_{early} = (t/3.6)^{1.6}/(1+(t/3.6)^{1.6})]\cdot e^{(-t/5.7)}$, for the initial response to a step-shear to 20 dynes/cm^2 and $[G(t)H(t)]_{late} = (t/18)^{12}/(1+(t/18)^{12})]\cdot 0.11$ for the late phase. The vasodilatory response to a shear ramped over 5 minutes from 0 to 20 dynes/cm^2 was also characterized by $d/d_{control} = 1+[G(t)H(t)]_{early}+[G(t)H(t)]_{late}$ ($r^2=0.88$) where $[G(t)H(t)]_{early} = [(t/7.9)^{1.7}/(1+(t/7.9)^{1.7})]\cdot e^{(-t/5.5)}$ for the early phase and $[G(t)H(t)]_{late} = [(t/22)^{7.8}/(1+(t/22)^{7.8})]\cdot 0.11$ for the later phase.

Figure 15: *Effects of ramp duration and subsequent steady shear on maximum vessel diameter:* For these experiments (n=8 for each τ_{max}), shear was ramped to the stated shear stress over the time indicated by ramp duration. A ramp duration of 0 refers to a step change in shear stress although even a step-shear is a shear ramped over a very short (but un-specified) time.

Figure 16: *Effects of temporal shear gradient (TSG) on maximum vessel diameter three levels of maximum shear stresses.* Asterisks indicate significant differences between the means of the shear-magnitude groups at the same TSG ($P<0.05$).

Figure 17: *Effects of shear magnitude on maximum vessel diameter for equal TSGs.* Asterisks indicates significant differences between the means of the TSG groups at the same shear magnitude ($P<0.05$).

Figure 18: *Membrane structure and lipid protein interaction:* Increases in membrane fluidity may cause an increase in mismatch between protein hydrophobic cores and lid fatty acid chains because of an hypothesized thinning of the membrane. Increased membrane fluidity may also increase lateral motion of proteins(3).

Figure 19: *Fluorescence recovery after photobleaching and lipid mobility:* This illustration shows how fluorescence can recover in a spot where the lipid-like fluorophore was irreversibly bleached by an unattenuated laser beam. Unbleached fluorophore diffuses through lateral motion into the bleached area causing the recovery of fluorescence. The fluorescence recovery is detected using a second, attenuated, laser beam focused on the same spot.

Figure 20: *Determinants of membrane fluidity:* Saturated fatty acid chains pack more closely that unsaturated ones. Therefore unsaturation increases membrane fluidity. Cholesterol increases membrane fluidity (illustrations from (3)).

Figure 21: *Confocal-FRAP setup:* A flow chamber with bovine aortic endothelial cells is placed on the confocal microscope. Biorad Timecourse software enables timed bleaches by an Argon-ion laser followed by recovery monitoring by a Krypton-argon laser (Biorad configuration is from www.biorad.com)

Figure 22: *Stained BAEC's:* DiI readily intercalates itself in the cell membrane. Dead cells show up bright as they are more permeable to the dye. Furthermore, the dye provides an excellent way to stain the cell borders without the toxic effects of silver nitrate. DTAF is a non-specific fluorocine based stain for membrane bound proteins.

Figure 23: *Time evolution of concentration profiles:* These profiles were generated using equations 35 and 36 for the line scan and square scan respectively which are the solutions of the convection diffusion equation with a Gaussian distribution assumed for the initial condition. The following parameters are used: L_x (square scan) = 1.25 $x10^{-4}$ cm, L_x (line scan) = 0.225 $x10^{-4}$ cm, D = 4.8 x 10^{-9} cm^2/sec.

Figure 24: *Decay curves:* Decay curves were generated for rectangular curves for rapid monitoring and periodic monitoring. There data were curve fit and the curve fits were used to determine the photobleaching that occurred during the monitoring phase.

Figure 25: *Recovery curves:* Decay-corrected data (upper line) were curve fit using equation 48 to determine $(f/f_0)_\infty$, $(f/f_0)_i$ and D. Φ was calculated using equation 41. These curves represent the fluorescent recovery curves for cells in a flow chamber. $(f/f_o)_i$ refers to the normalized fluorescence immediately after bleaching. In each panel the lower curve is the raw data and the upper curve is the curve corrected for monitor photobleaching. The L_x dimension in these monitor areas was 1.25 μm.

Figure 26: *Recovery curves:* Decay-corrected data (upper line) were curve fit using equation 48 to determine $(f/f_0)_\infty$, $(f/f_0)_i$ and D. Φ was calculated using equation 41. In this experiments there is an apparent reduction in mobile fraction with shear stress as well as a reduction in the diffusion coefficient.

Figure 27: *Recovery curve for a line scan:* Data were curve fit using equation 47 to determine $(f/f_0)_\infty$, $(f/f_0)_i$ and D. Φ was calculated using equation 41. A line scan allows much faster analysis. Diffusion coefficients are

comparable to those measured by a square scan.

6. Figur

Figure 1: Effects of NO and PGI_2 on smooth muscle

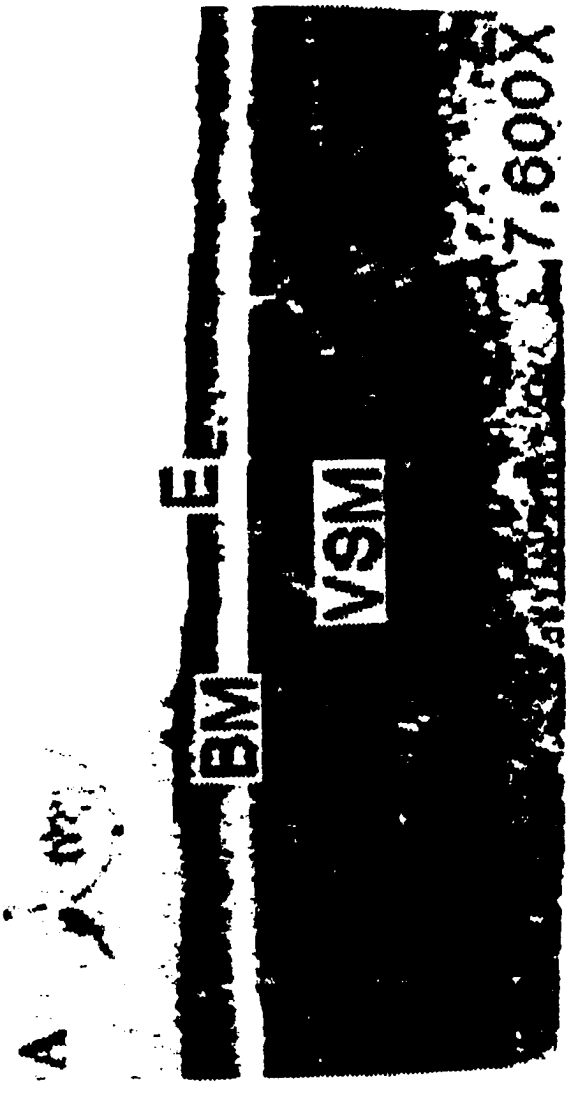

Figure 2: Cross section of an arteriole

Figure 3: Mechanism of shear-induced dilation

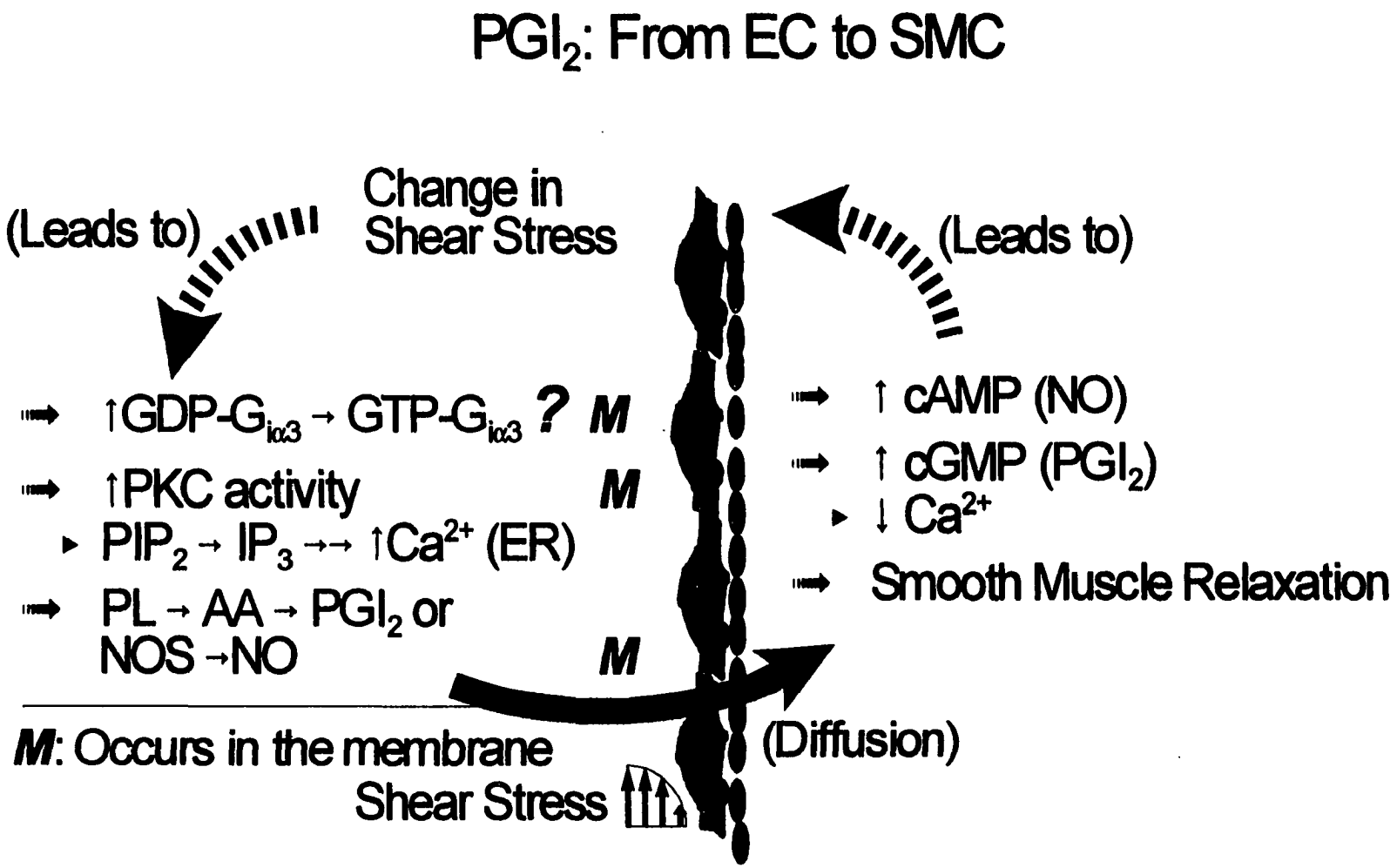

Figure 4: Silver nitrate staining of arterioles

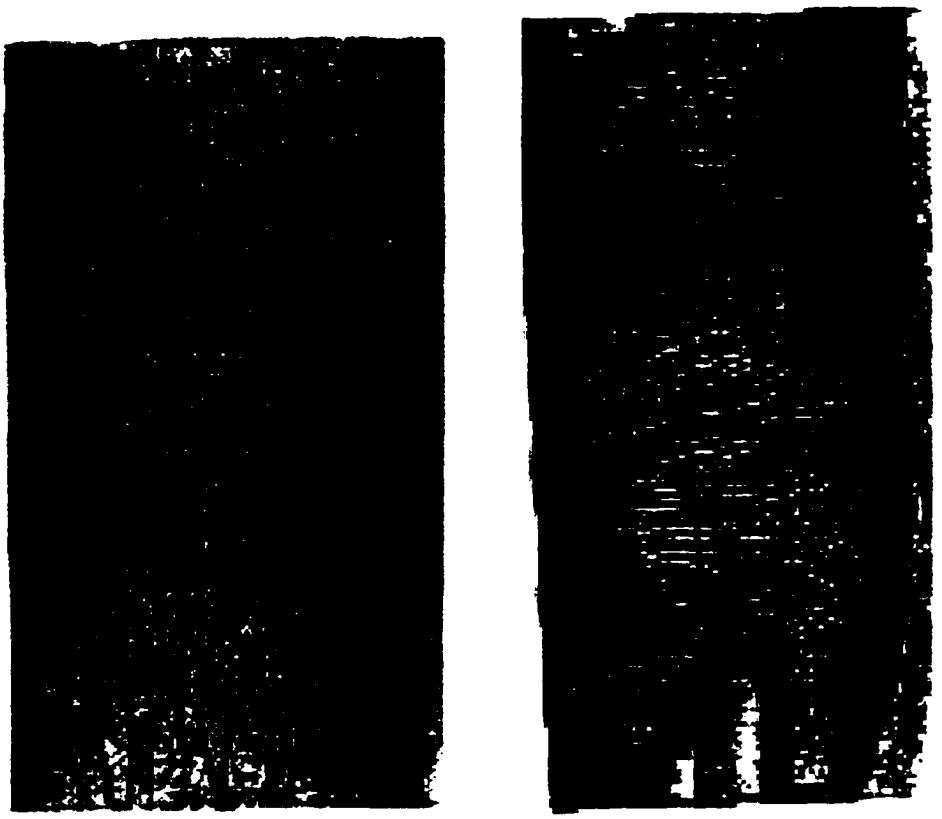

A

B

Figure 5: Stress fibers and the cytoskeletal network

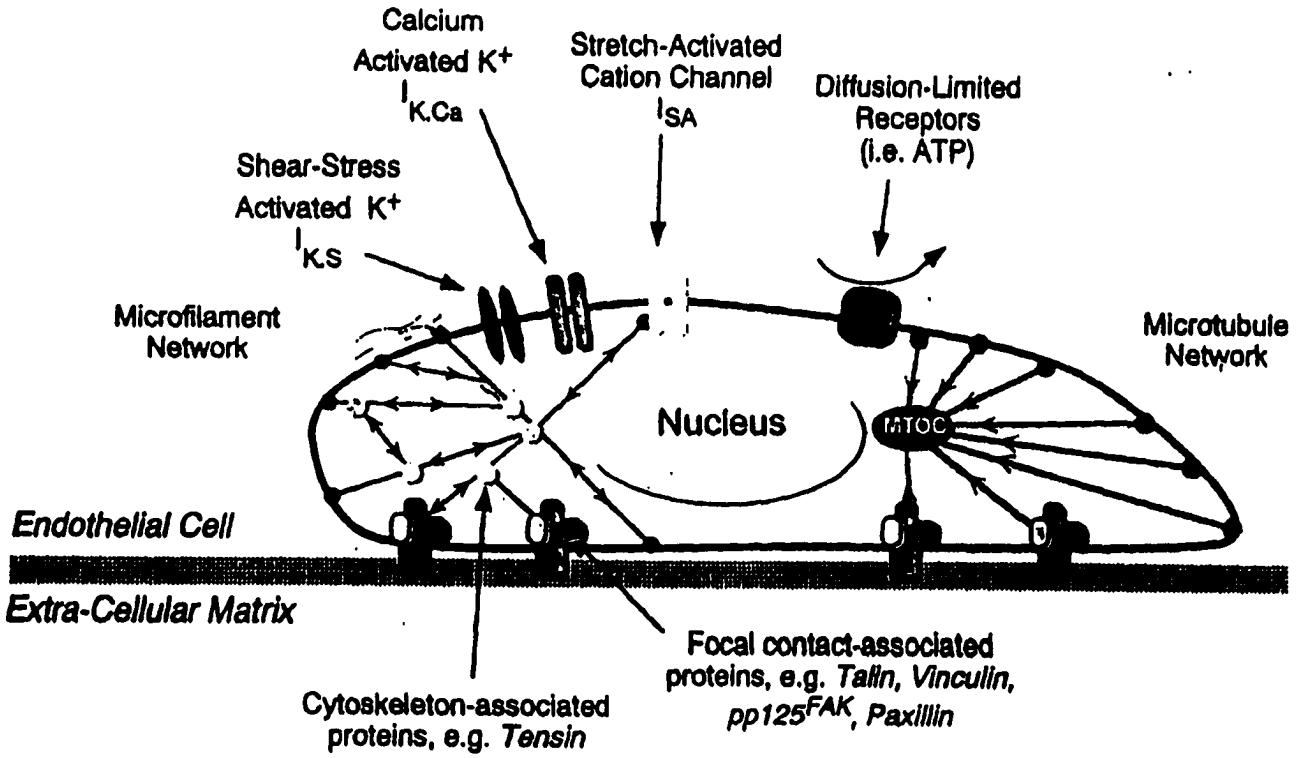

Figure 6: Viscoelastic graphs

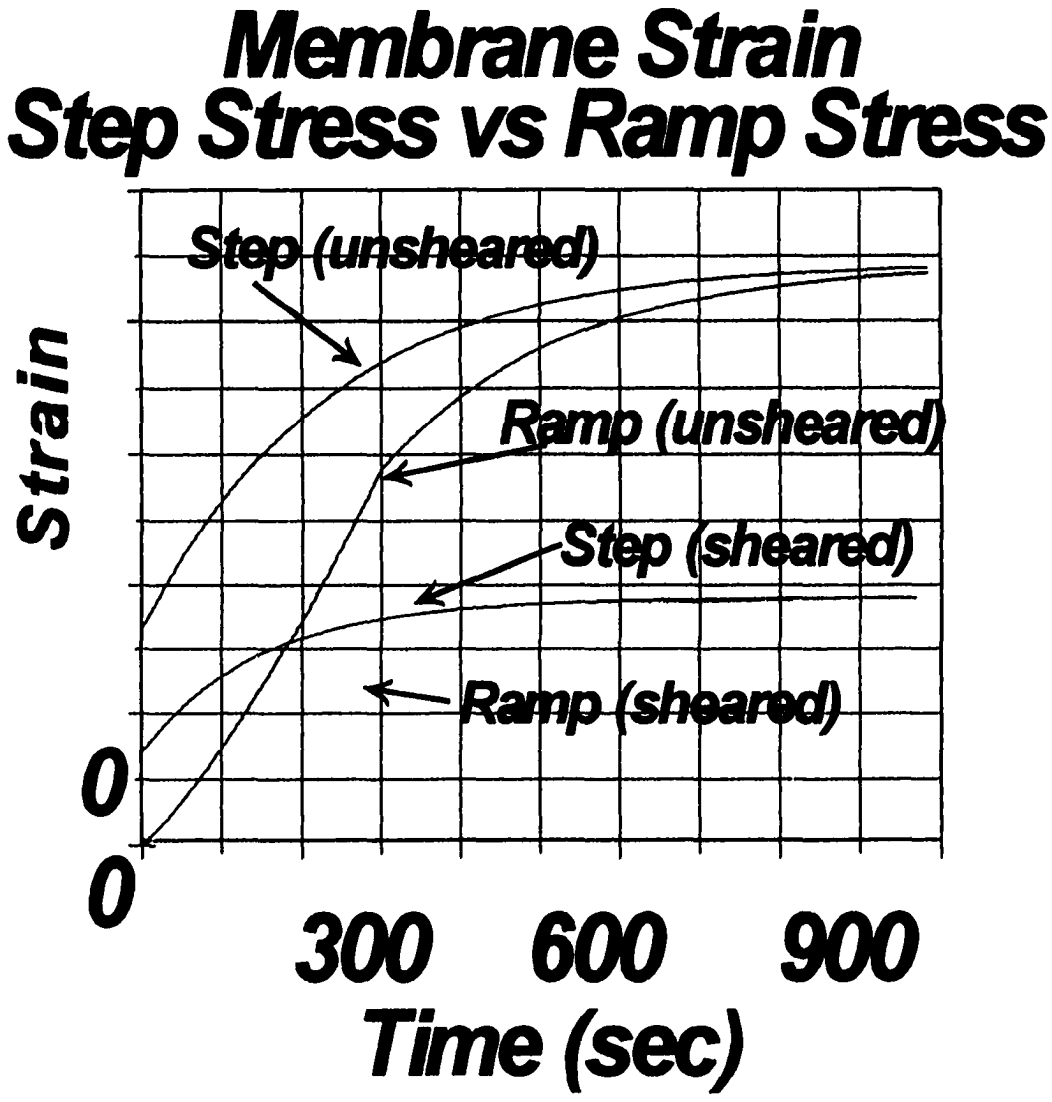

Figure 7: Arteriole removed from cremaster muscle

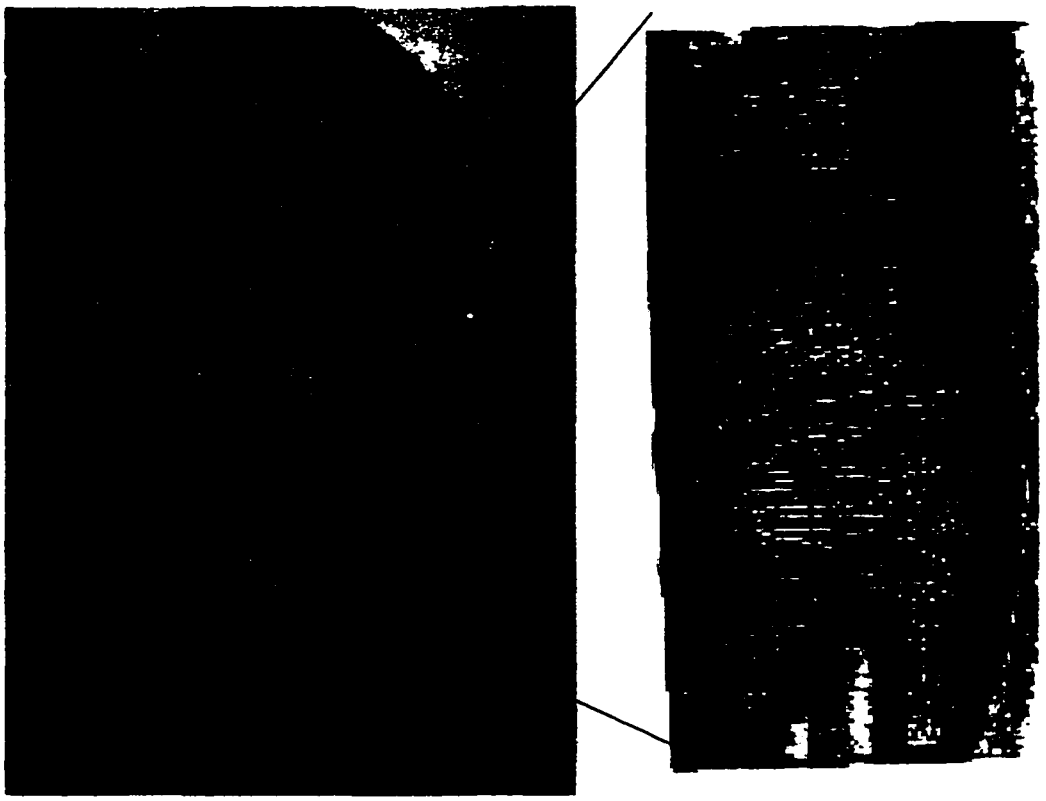

Figure 8: Experimental setup

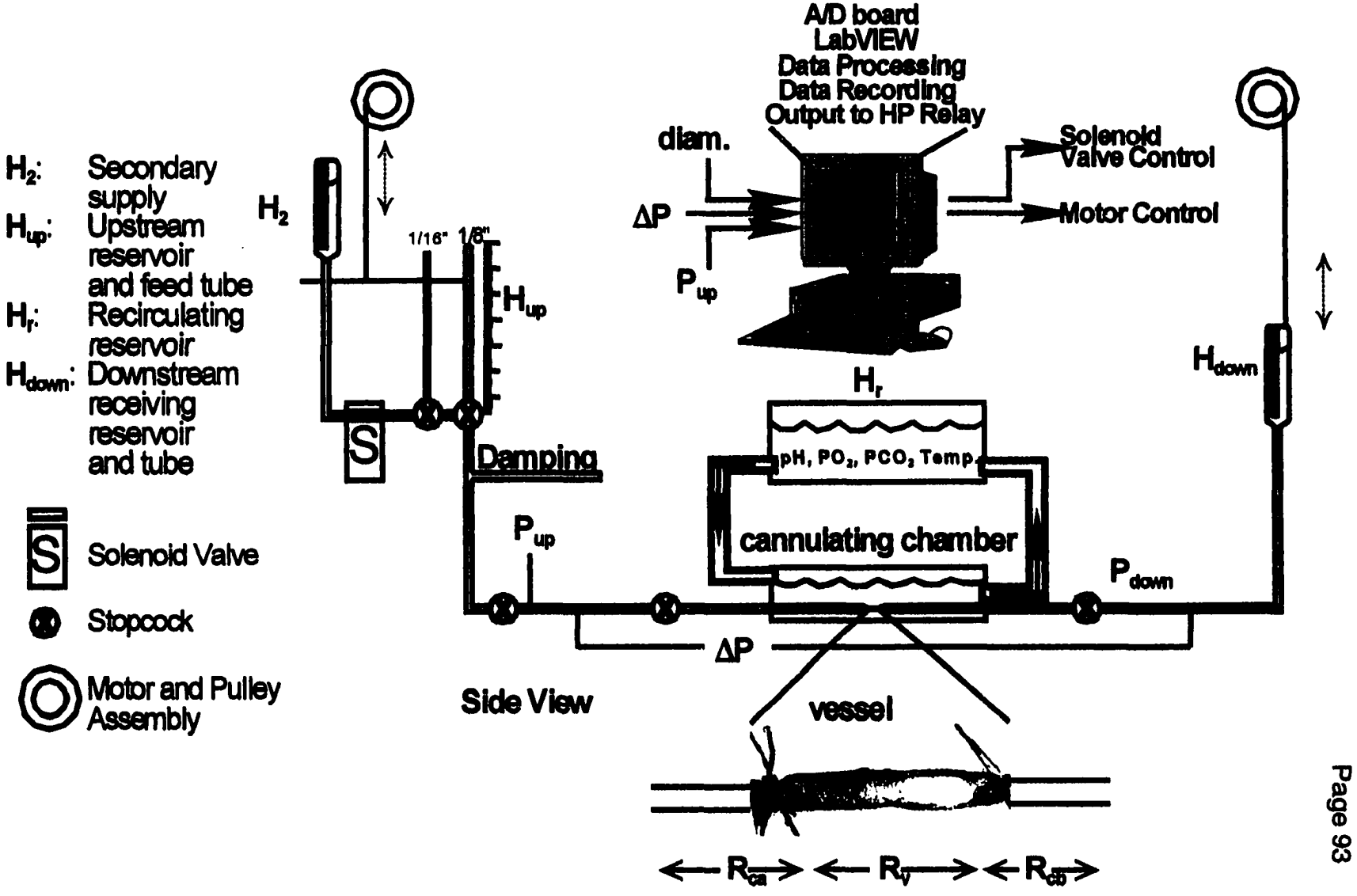

Figure 9: Feedback Control of Shear Stress

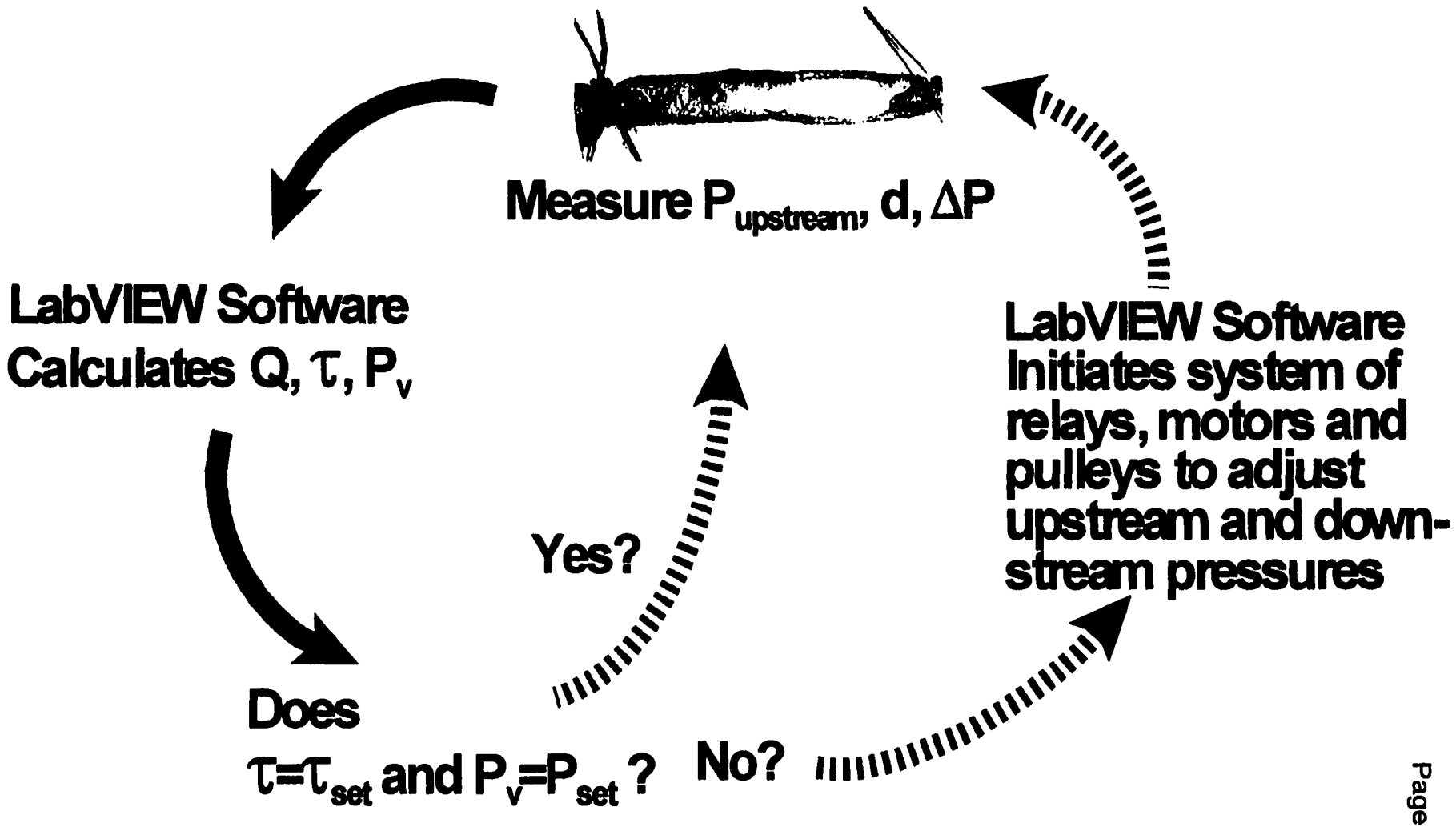

Figure 10: Calibration Curves for upstream feedtubes

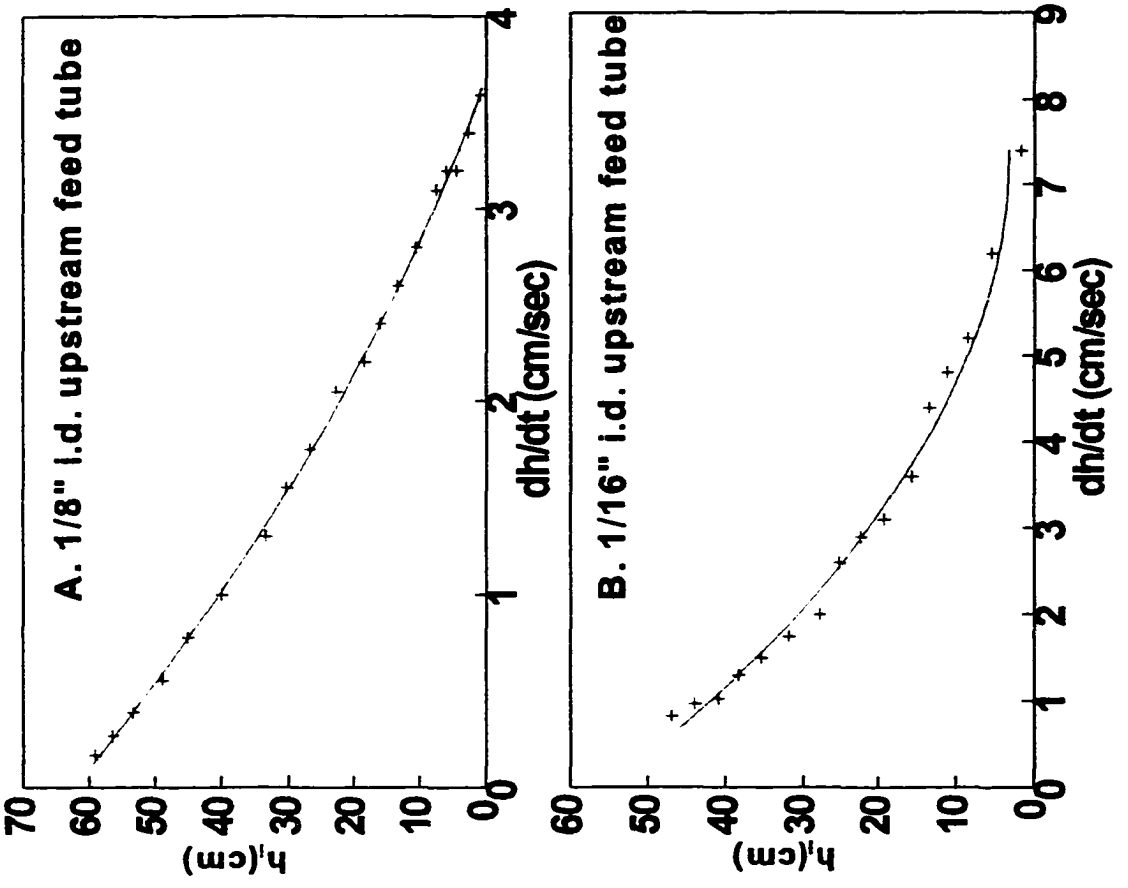

Figure 11: Ramping shear from 0 to τ_{max}

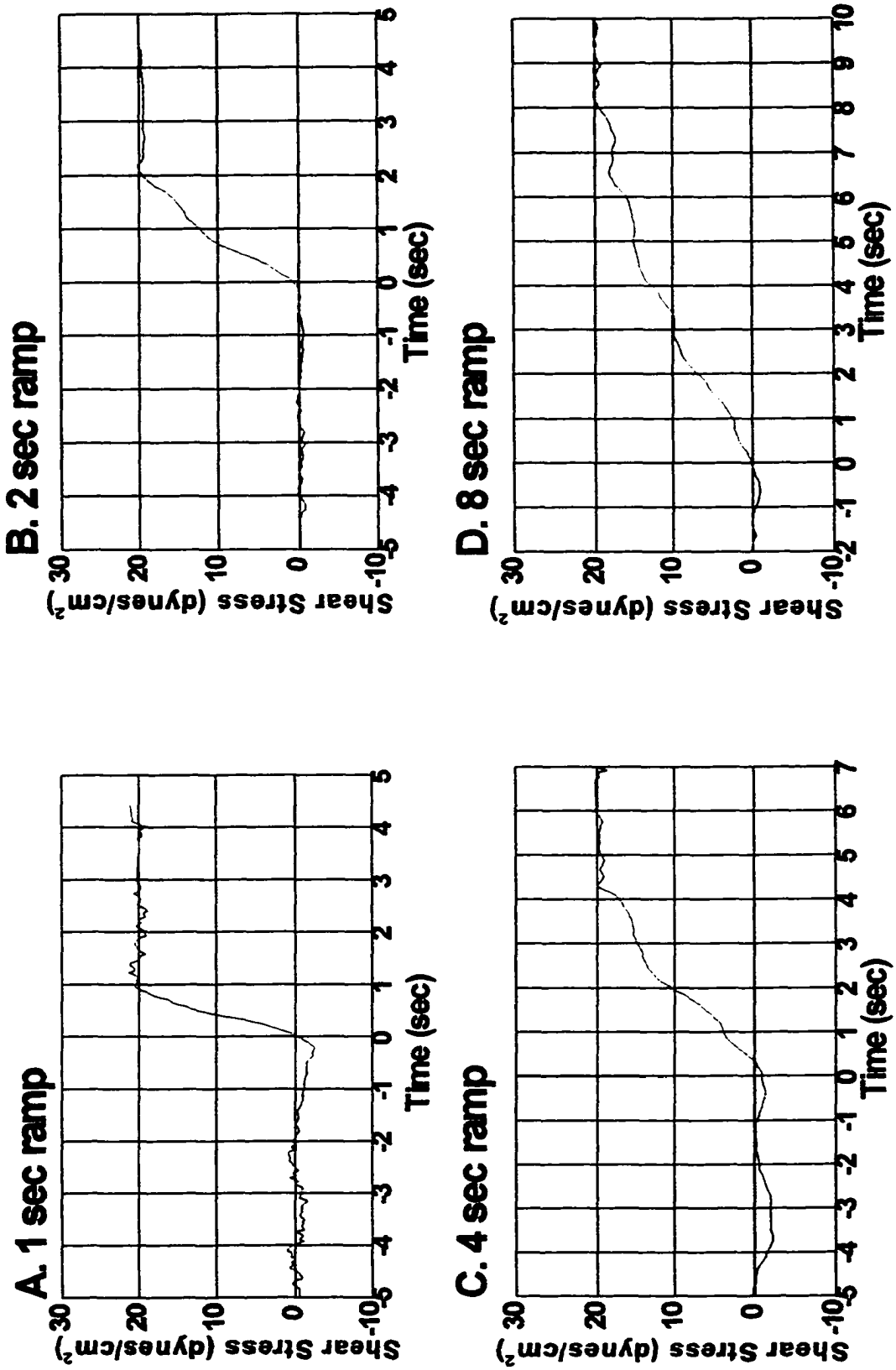

Figure 12: Representative Experimental Tracings

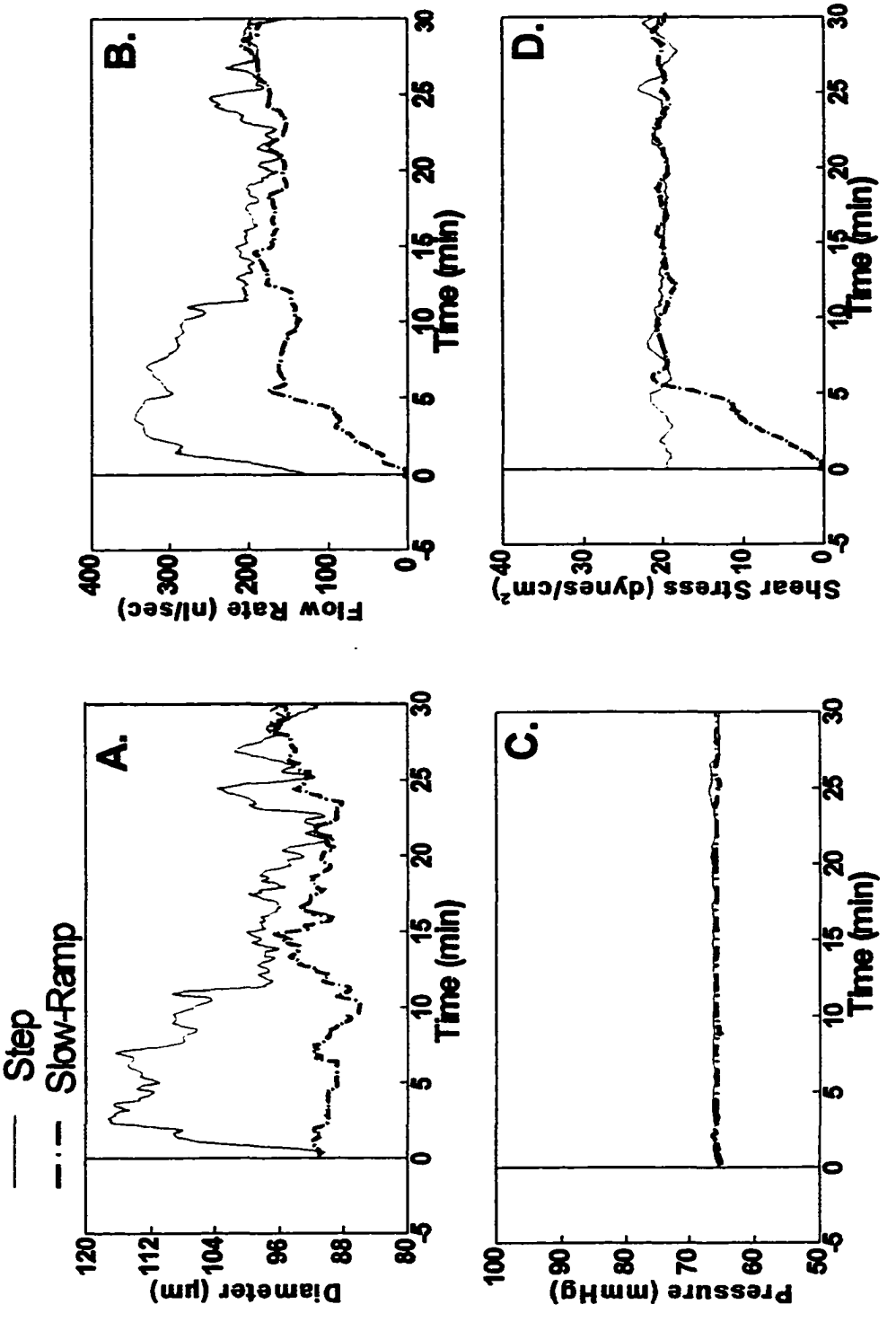

Figure 13: Response of vessels to a step or ramp in shear

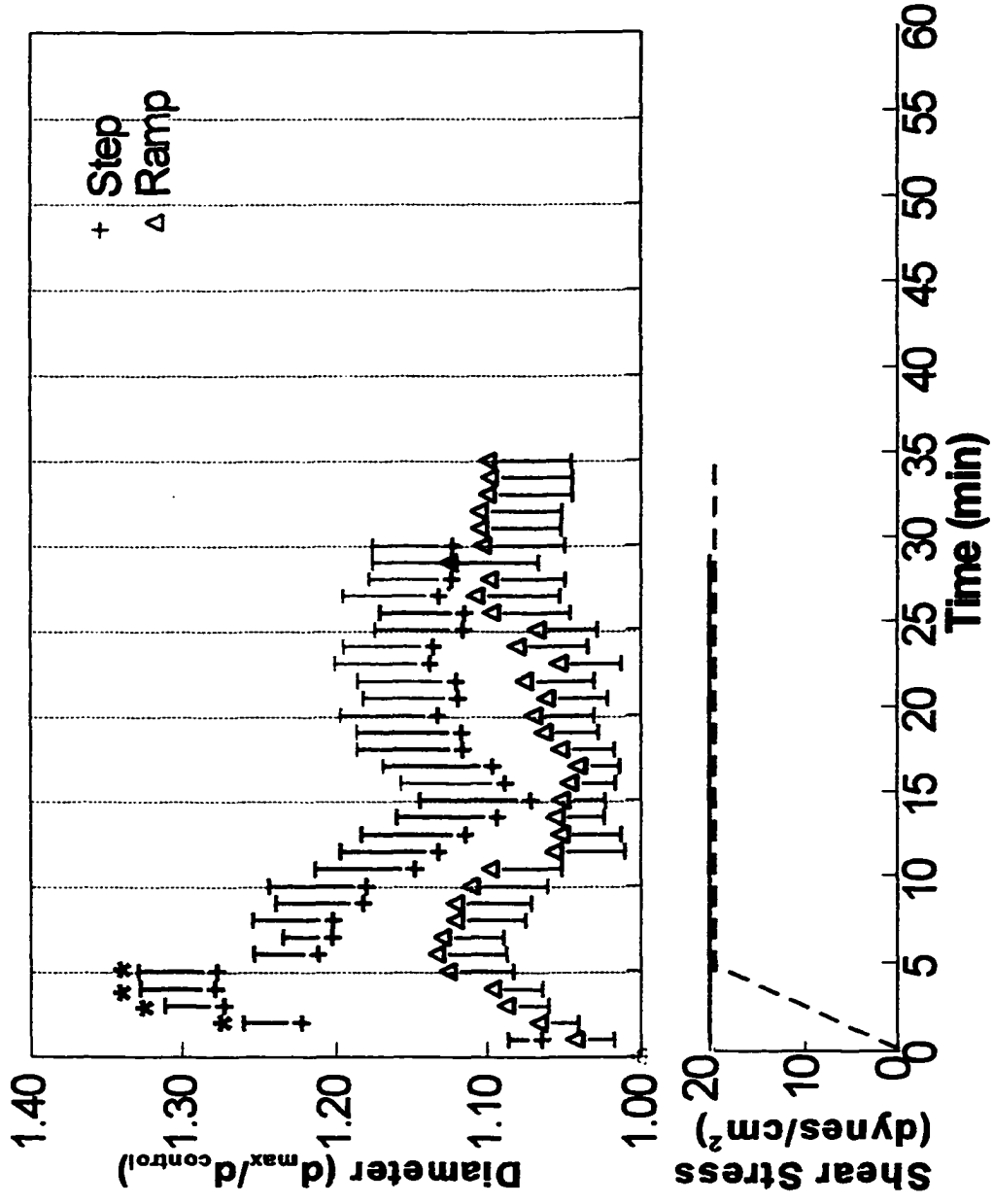

Figure 14: Curve fitting experimental data

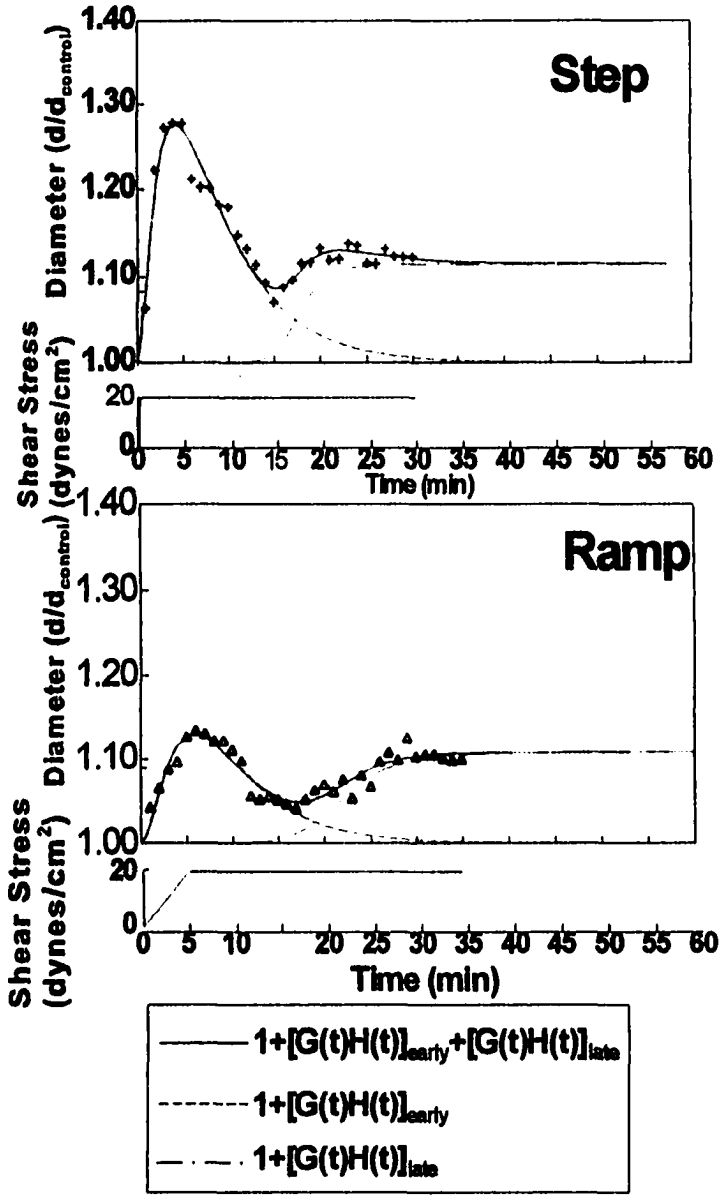

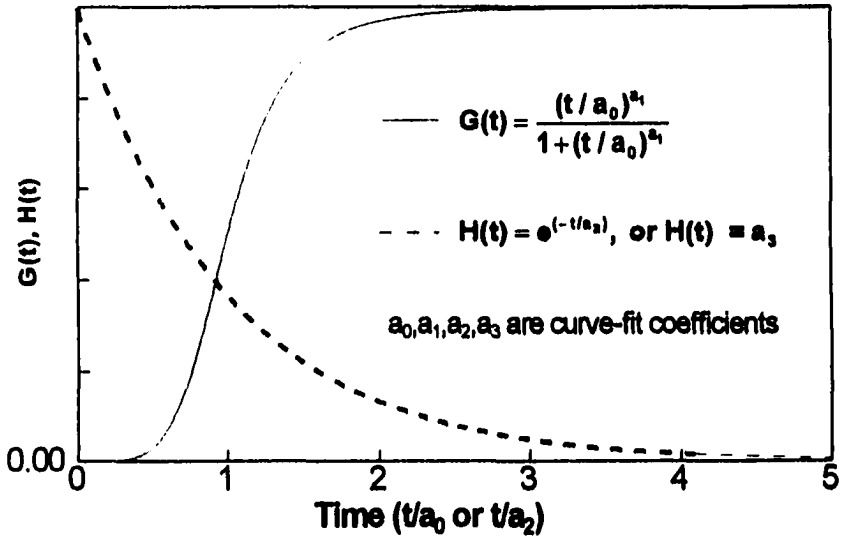

Figure 15: Effects of ramp duration on vessel diameter

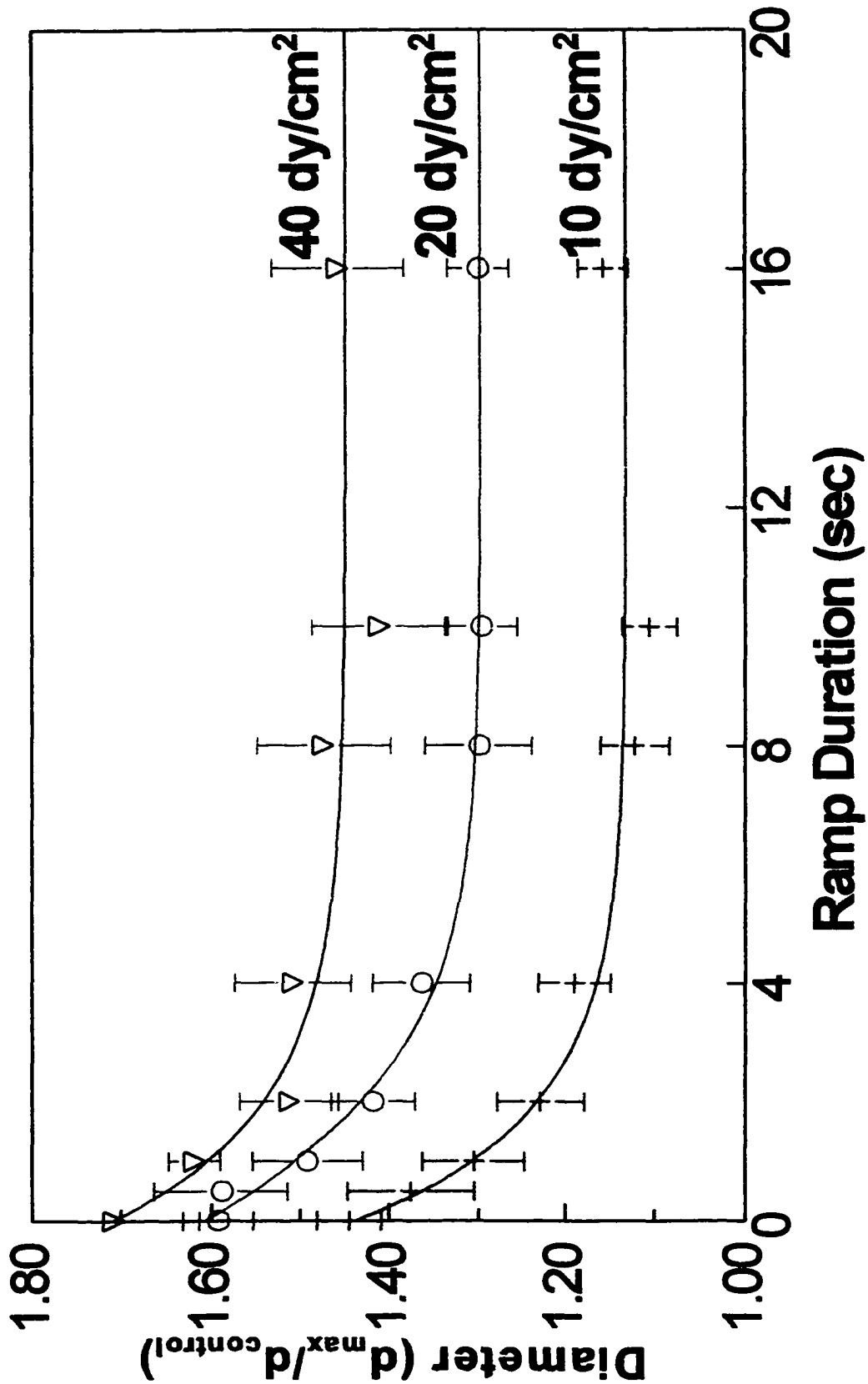

Figure 16: Diameter vs. TSG

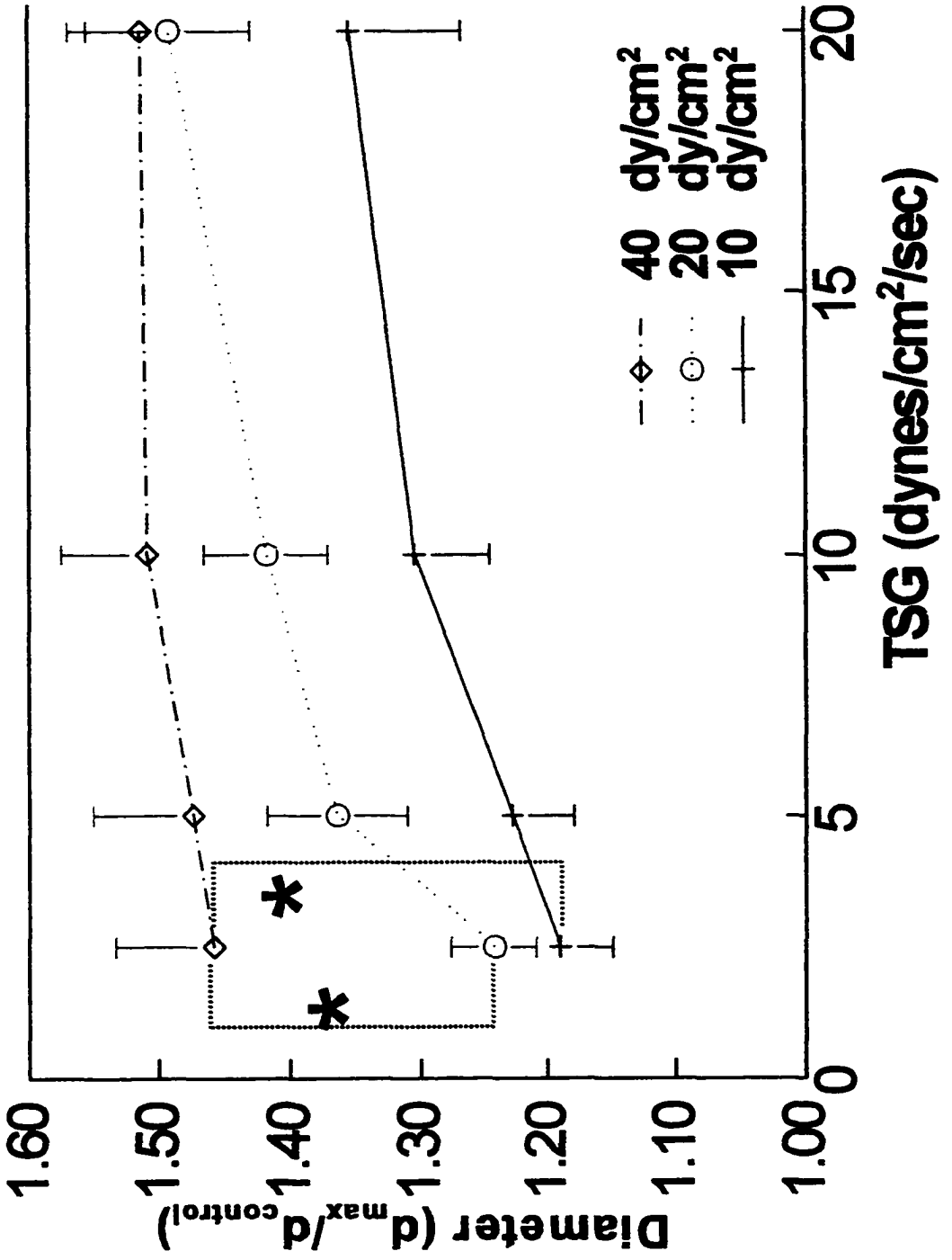

Figure 17: Diameter vs. Shear Magnitude

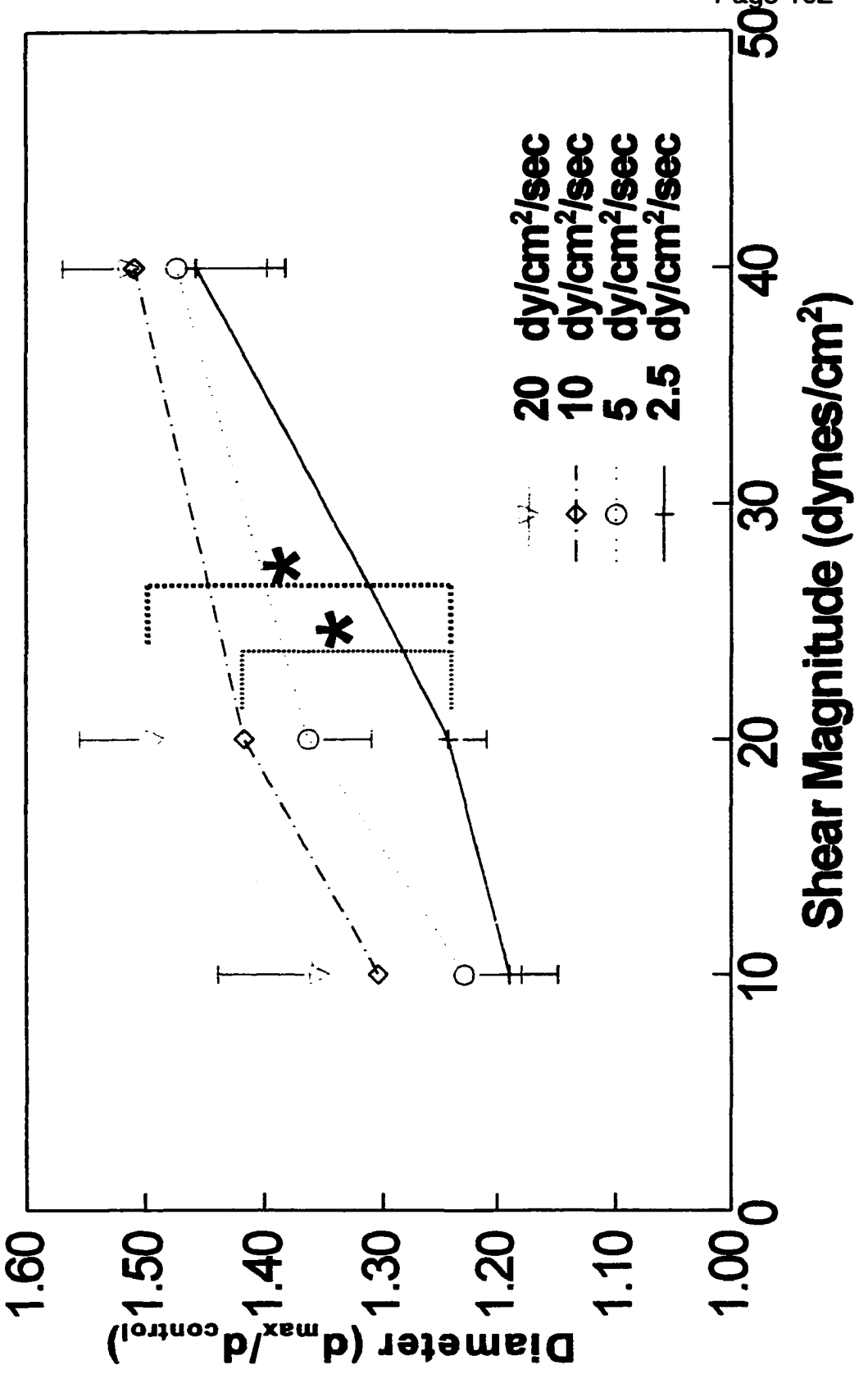

Figure 18: Membrane Structure and lipid-protein interaction

- τ increases GDP-$G_{\alpha\beta\gamma}$ ⇒ GTP-G_{α} + $G_{\beta\gamma}$ (activation)
  - Increased membrane cholesterol attenuates this activation
- $G_{\alpha q}$ (NO?, PTXi) associates with F-actin, $G_{i\alpha 3}$ (PGI_2?, PTXs) may not be associated with F-actin
  - $G_{\alpha q}$ impulse flow specific while $G_{i\alpha 3}$ may not be

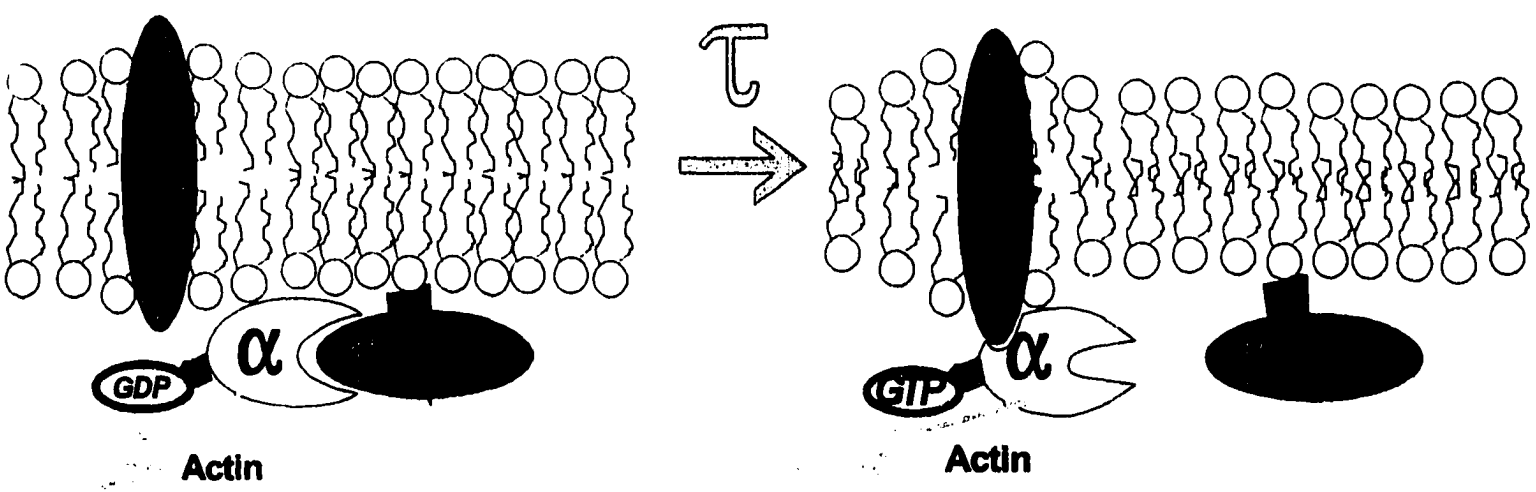

Figure 19: Fluorescence Recovery After Photobleaching and lipid mobility

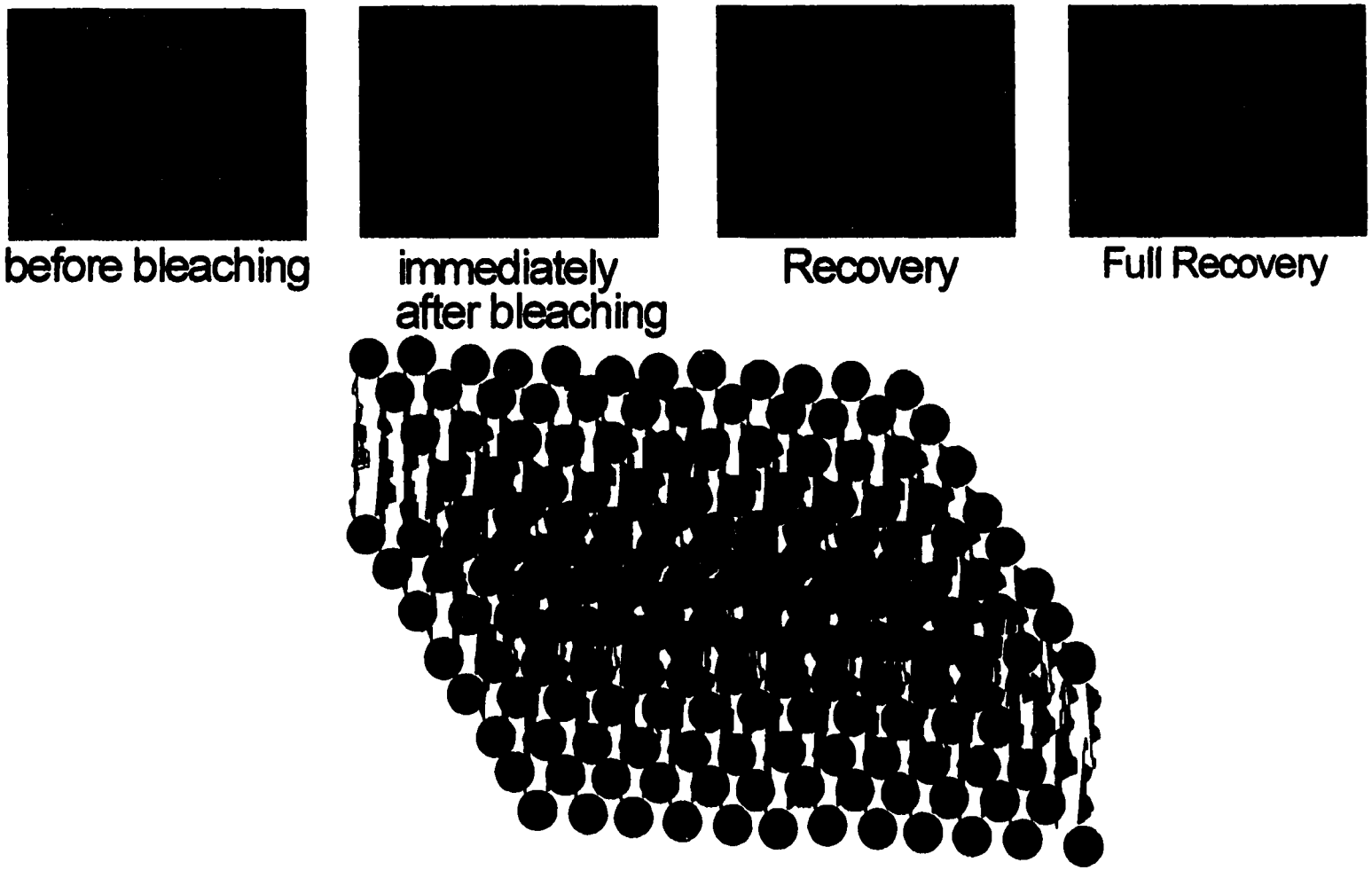

Figure 20: Determinants of membrane fluidity

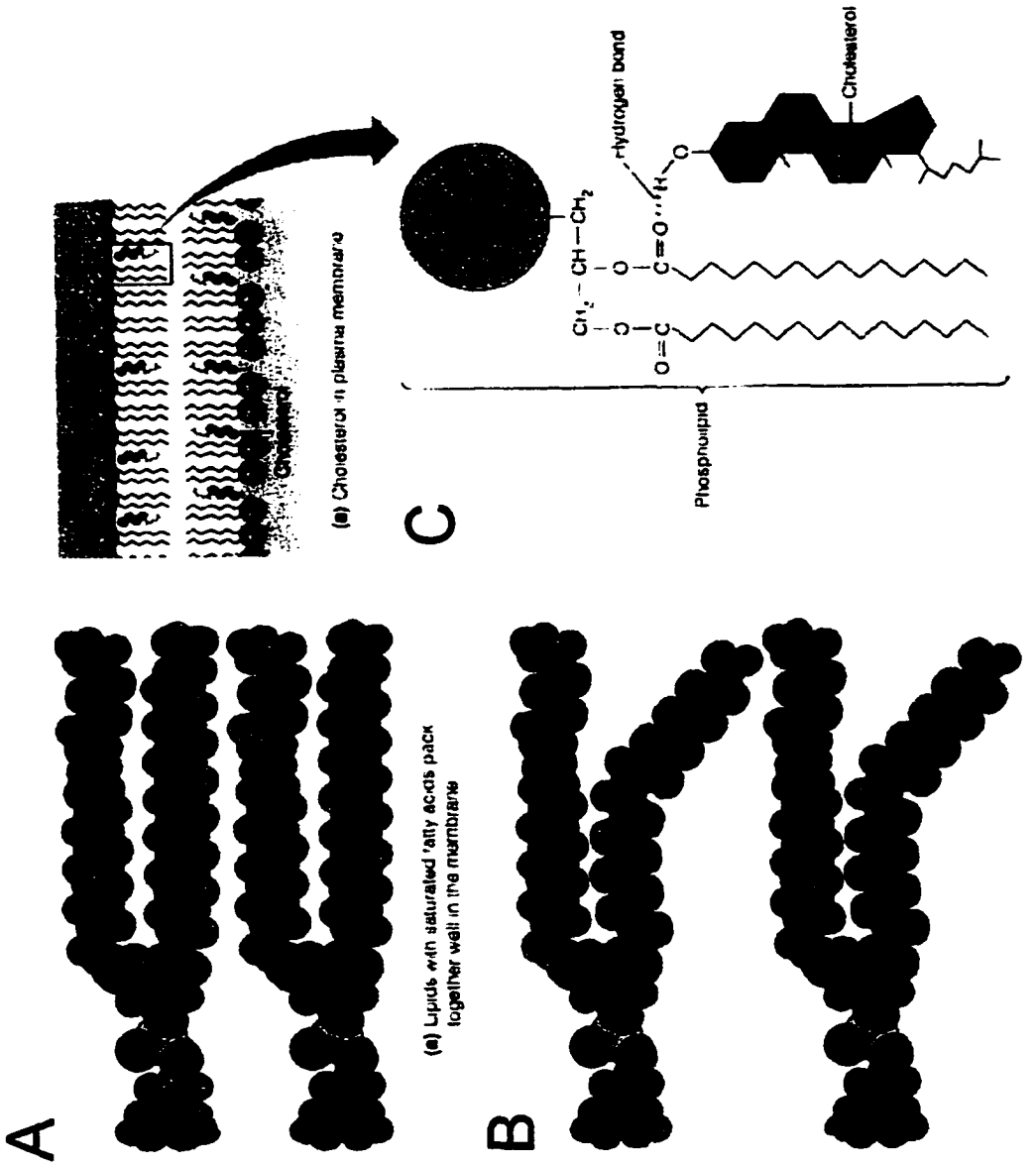

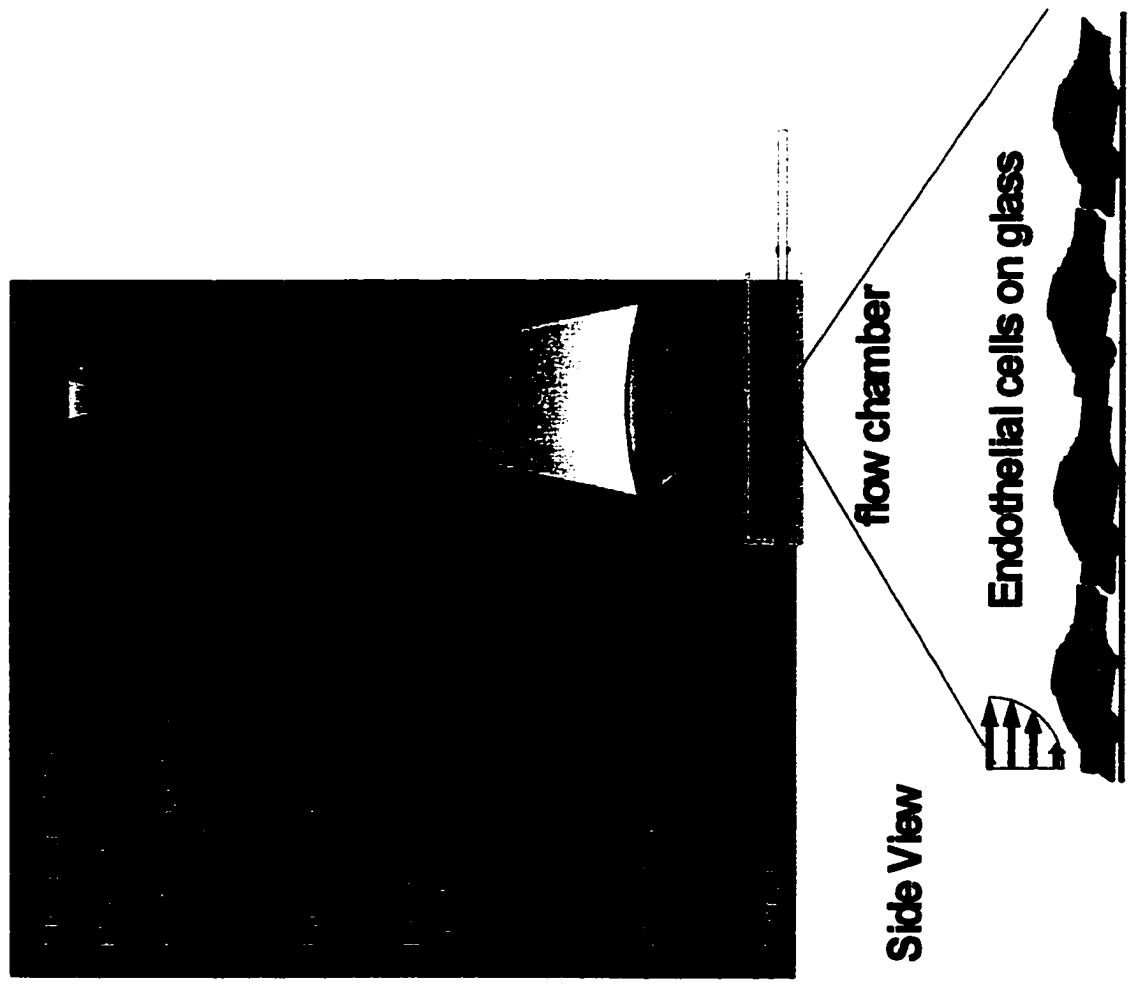

Figure 21: Confocal-FRAP setup

Figure 22: Stained BAEC's

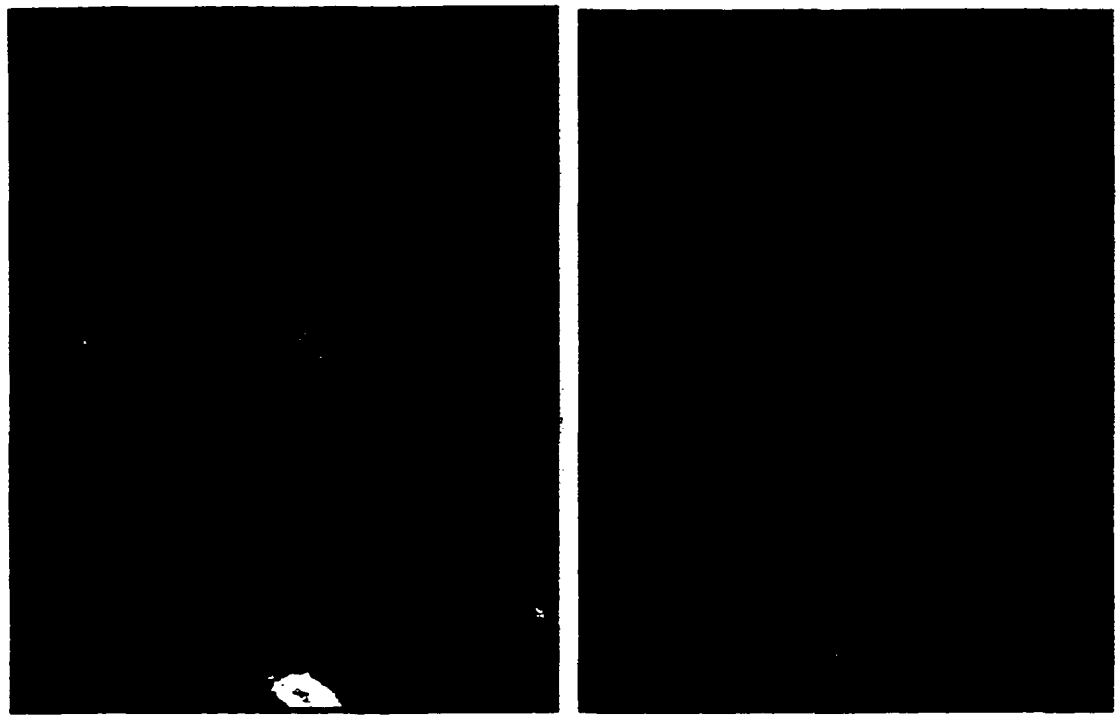

DiI (10^{-4}M): Lipid Probe

DTAF (10^{-5}M): Protein Stain

Figure 23: Evolution of concentration profile with time

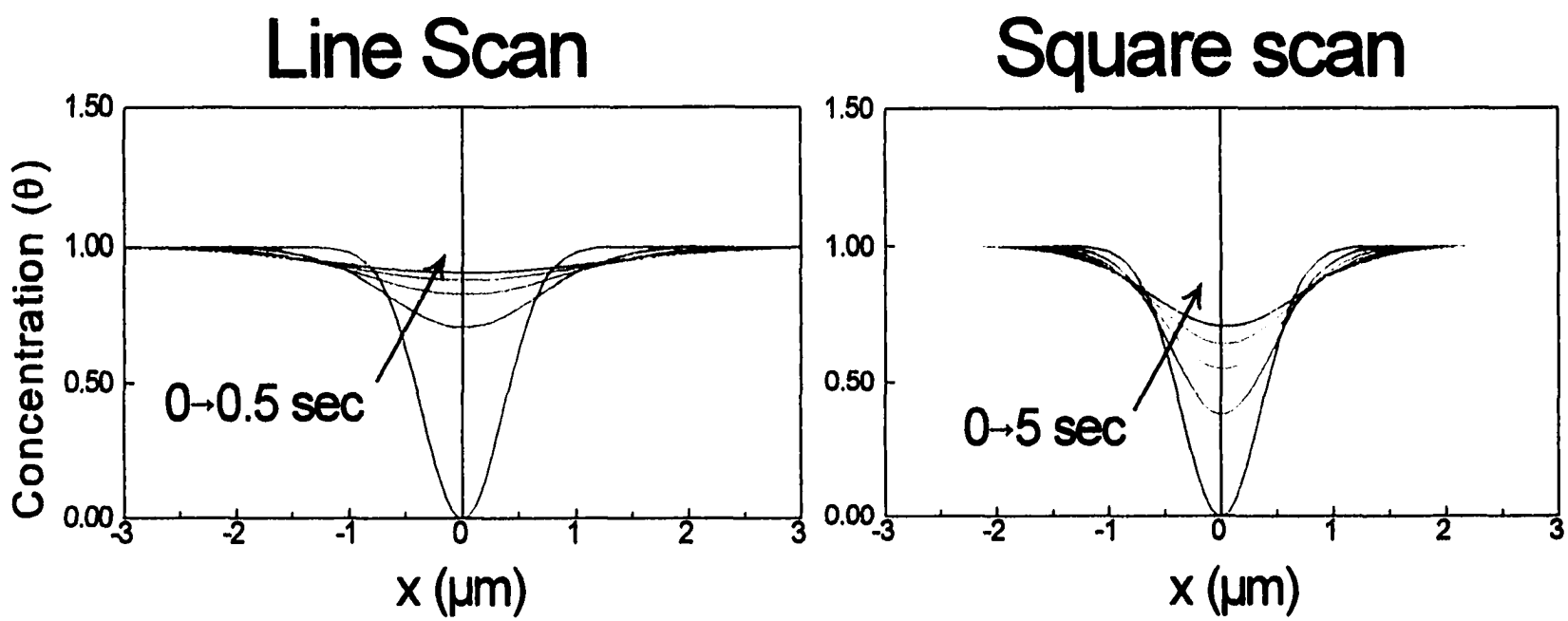

Figure 24: Decay curves describing photobleaching during monitoring

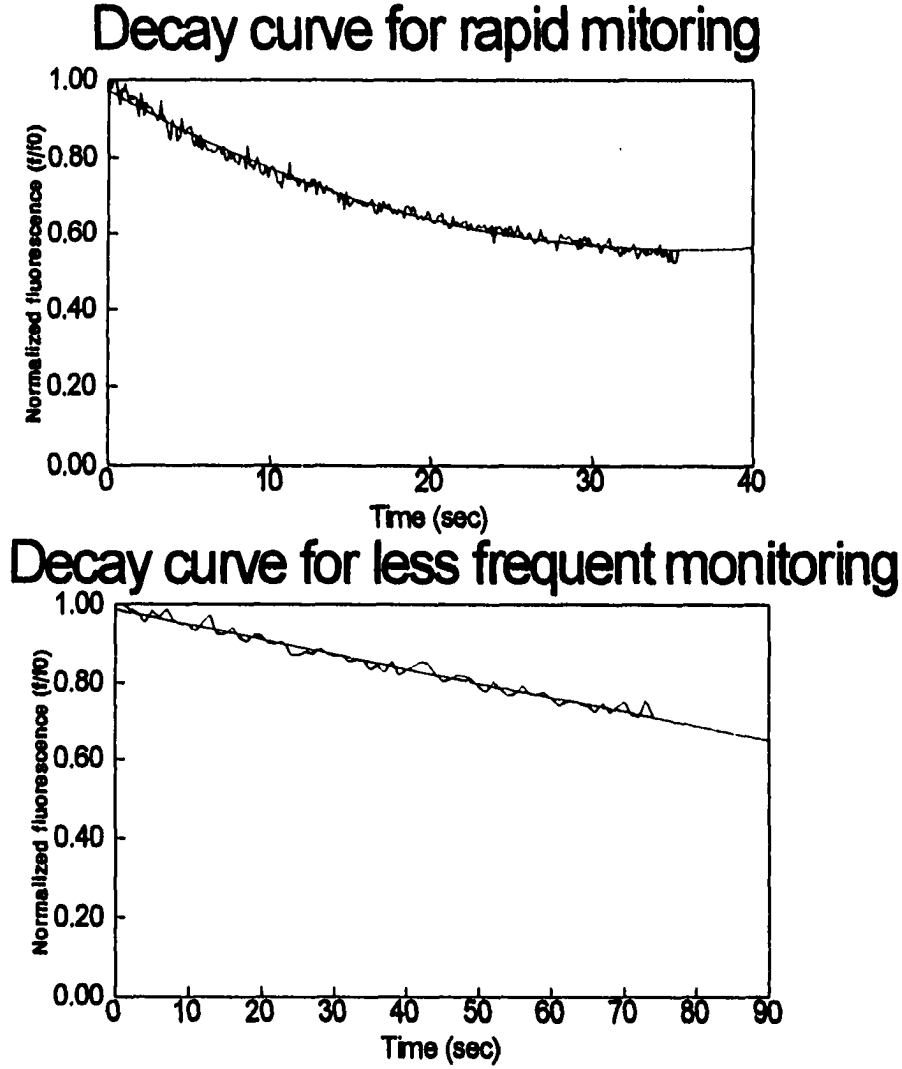

Figure 25: Recovery Curves (Square scan) : 8/28/98

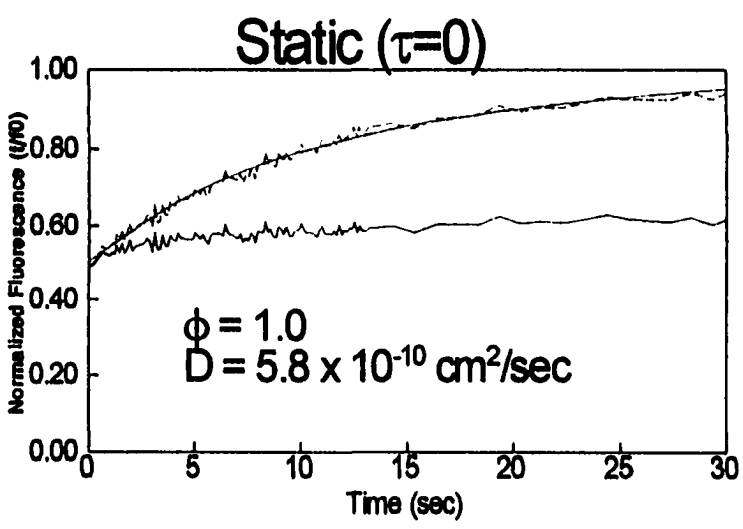

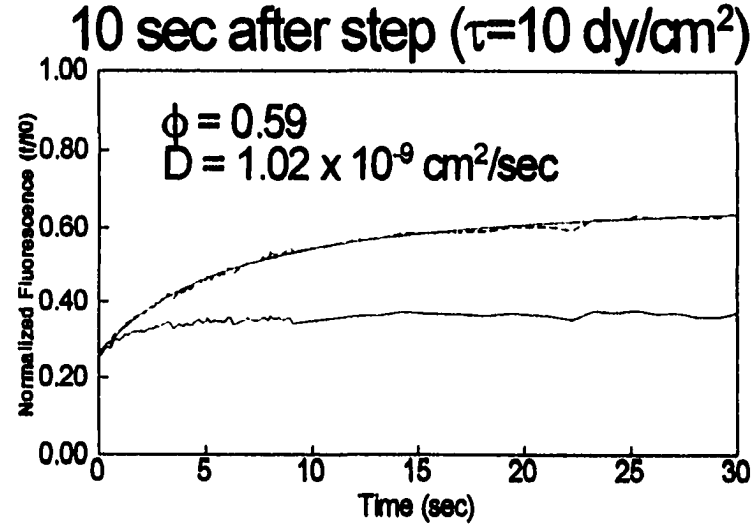

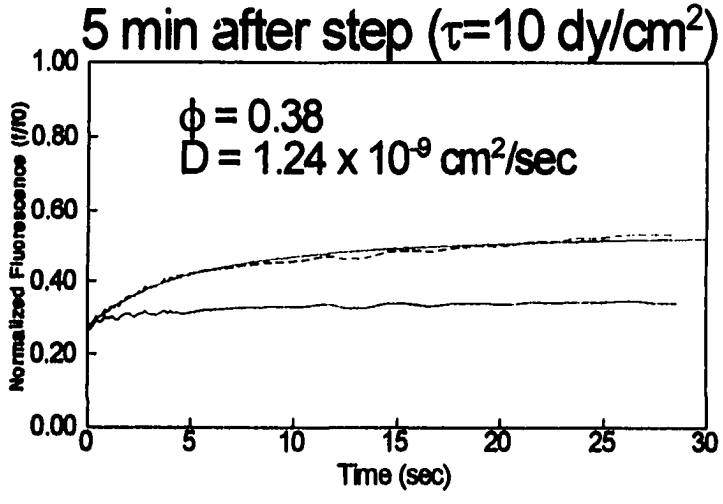

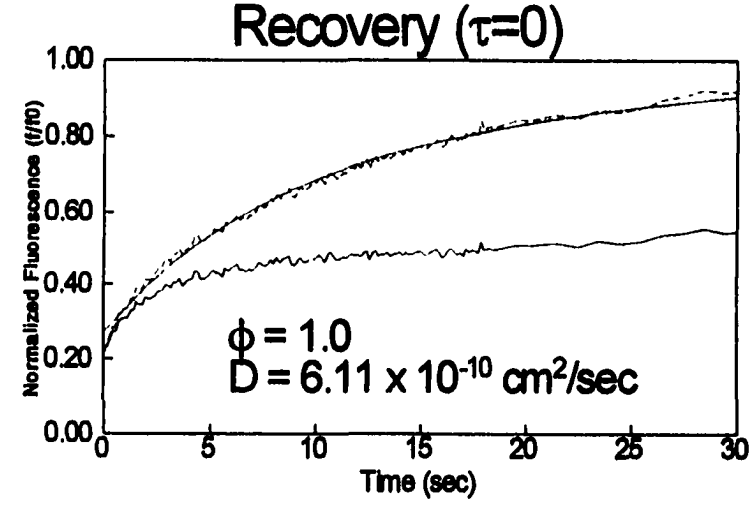

Figure 26: Recovery Curves (Square Scan) : 8/31/98

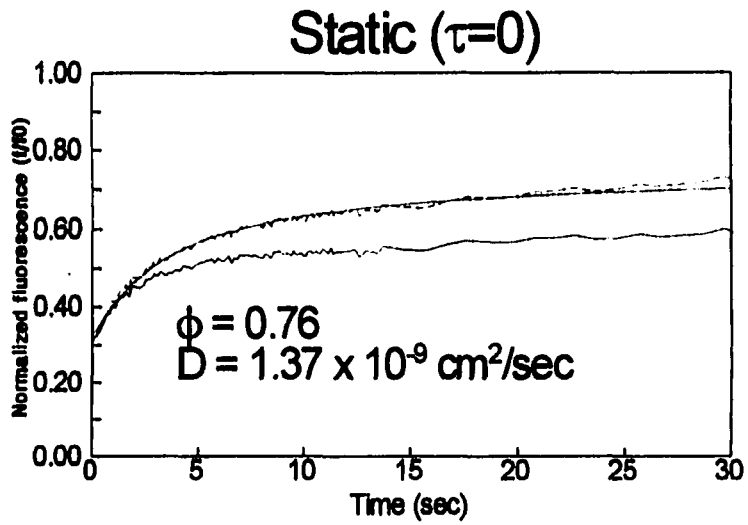

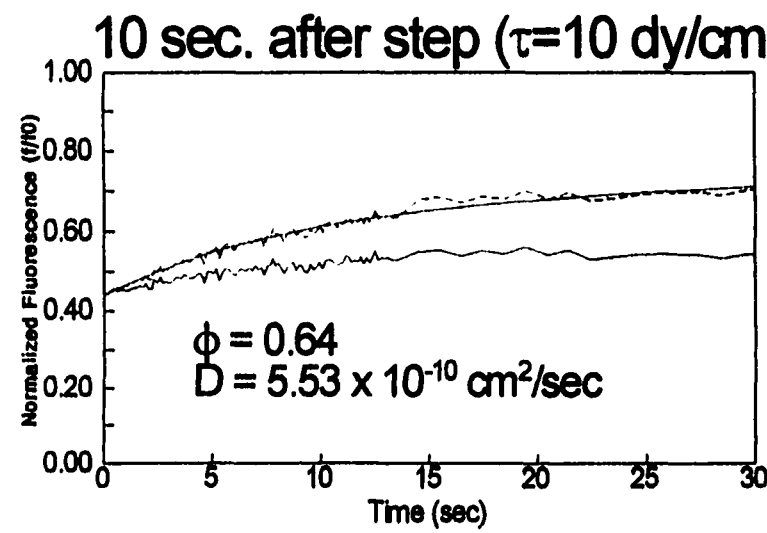

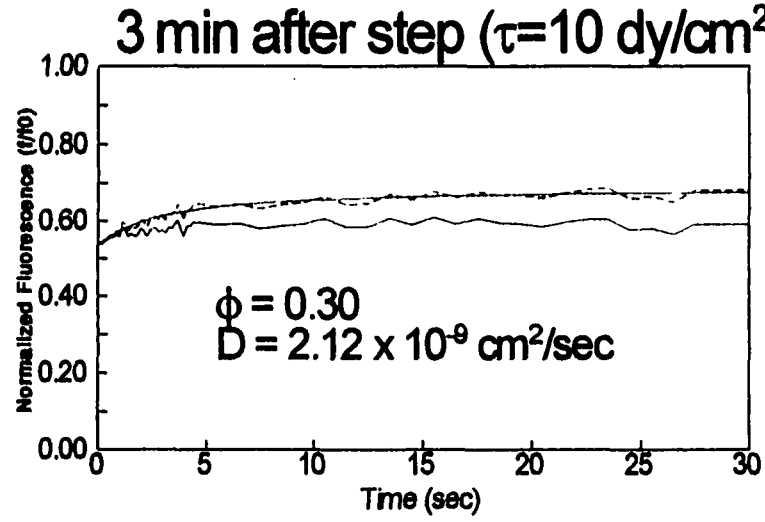

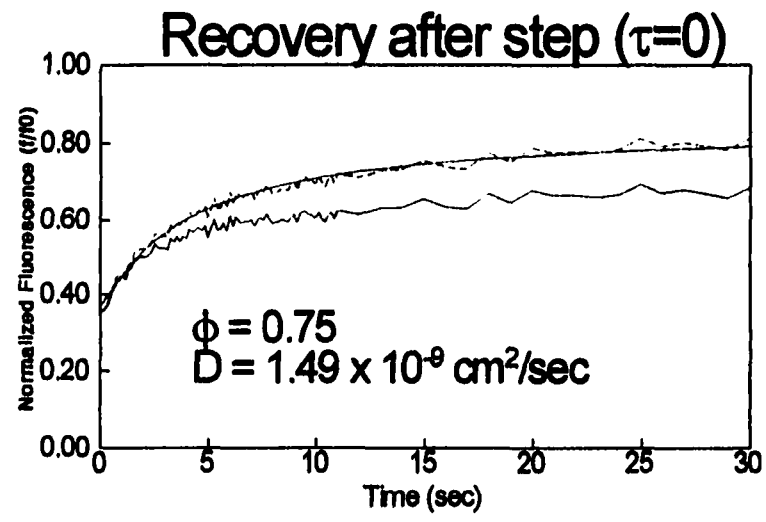

Figure 27: Recovery Curve (Line scan)

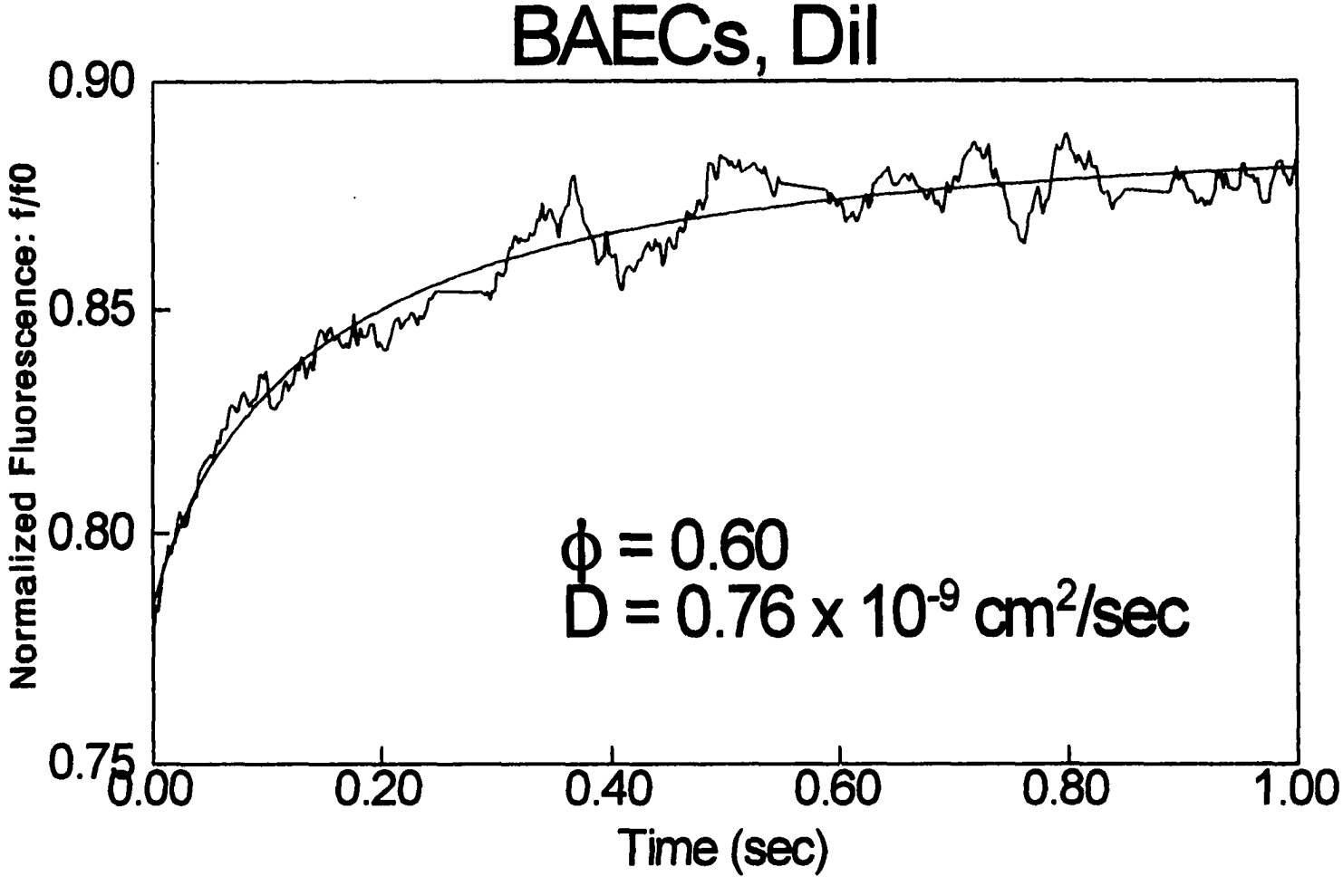

7. Reference List

1. **Ando, J., A. Ohtsuka, R. Korenaga, T. Kawamura, and A. Kamiya.** Wall shear stress rather than shear rate regulates cytoplasmic Ca^{++} responses to flow in vascular endothelial cells. *Biochem.Biophys.Res.Commun.* 190: 716-723, 1993.

2. **Axelrod, D., D.E. Koppel, J. Schlessinger, E. Elson, and W.W. Webb.** Mobility measurement by analysis of fluorescence photobleaching recovery kinetics. *Biophysical Journal* 16: 1055-1069, 1976.

3. **Becker, W.M., J.B. Reece, and M.F. Poenie.** *The World of the Cell.* Menlo Park, CA: Befamin/Cummings, 1996,

4. **Berthiaume, F. and J.A. Frangos.** Flow-induced prostacyclin production is mediated by a pertussis toxin-sensitive G protein. *FEBS Letters* 308: 277-279, 1992.

5. **Berthiaume, F. and J.A. Frangos.** Fluid flow increases membrane permeability to merocyanine 540 in human endothelial cells. *Biochimica et Biophysica Acta* 1191: 209-218, 1994.

6. **Blackman, B.R., L.E. Thibault, and K.A. Barbee.** Calcium response of endothelial cells to shear stress: A new insight to an old contraversy. *Annals of Biomedical Engineering* 25: S-38, Abst.# 224, 1997.(Abstract)

7. **Blonk, J.C.G., A. Don, H. Van Aalst, and J.J. Birmingham.** Fluorescence photobleaching recovery in the confocal scanning light microscope. *Journal of Microscopy* 169: 363-374, 1993.

8. **Boulanger, C. M. and Vanhoutte, P. M.** G Proteins and Endothelium-Dependent Relaxations. Journal of Vascular Research 34(3), 175-185. 1997.

9. **Davies, P.F.** Flow-mediated endothelial mechanotransduction. [Review] [407 refs]. *Physiological Reviews* 75: 519-560, 1995.

10. **Davies, P.F., A. Robotewskyj, and M.L. Griem.** Quantitative studies of endothelial cell adhesion. Directional remodeling of focal adhesion sites in response to flow forces. *J.Clin.Invest.* 93: 2031-2038, 1994.

11. **Davies, P.F. and S.C. Tripathi.** Mechanical stress mechanisms and the cell. An endothelial paradigm. *Circ.Res.* 72: 239-245, 1993.

12. **Dull, R.O. and P.F. Davies.** Flow modulation of agonist (ATP)-response (Ca2+) coupling in vascular endothelial cells. *Am.J.Physiol.* 261: H149-H1541991.

13. **Ethier, C.R., P. Ajersch, and R. Pirog.** An improved ocular perfusion system. *Current Eye Research* 12: 765-770, 1993.

14. **Falcone, J.C., M.J. Davis, and G.A. Meininger.** Endothelial independence of myogenic response in isolated skeletal muscle arterioles. *Am.J.Physiol.Heart Circ.Physiol.* 260: H130-H1351991.

15. **Falcone, J.C., L. Kuo, and G.A. Meininger.** Endothelial cell calcium increases during flow-induced dilation in isolated arterioles. *Am.J.Physiol.* 264: H653-H6591993.

16. **Fein, M., J. Unkeless, F.Y.S. Chuang, M. Sassaroli, R.d. Costa, H. Vaananen, and J. Eisinger.** Lateral Mobility of Lipid Analogues and GPI-Anchored Proteins in Supported Bilayers Determined By Fluorescent Bead Tracking. *J.Membr.Biol.* 35: 83-92, 1993.

17. **Firrell, J.C., H.H. Lipowsky, S. Usami, and S. Chien.** Segmental and total microvascular resistances during hemorrhagic hypotension in rabbit omentum. *Am.J.Physiol.* 247: H361-H3701984.

18. **Frangos, J.A., S.G. Eskin, L.V. McIntire, and C.L. Ives.** Flow effects on prostacyclin production by cultured human endothelial cells. *Science* 227: 1477-1479, 1985.

19. **Frangos, J. A. and Gudi, S.** Shear Stress Activates Reconstituted G-Proteins in the Absence of Protein Receptors By Modulating Lipid Bilayer Fluidity. FASEB J. 11(3), A521. 1997.

20. **Frangos, J.A., T.Y. Huang, and C.B. Clark.** Steady shear and step changes in shear stimulate endothelium via independent mechanisms--superposition of transient and sustained nitric oxide production. *Biochemical & Biophysical Research Communications* 224: 660-665, 1996.

21. **Fung, Y.C.** Bioviscoelastic Solids. In: *Biomechanics: Mechanical Properties of Living Tissues*, AnonymousNew York: Springer-Verlag, 1993, p. 242-320.

22. **Fung, Y.C. and S.Q. Liu.** Elementary mechanics of the endothelium of blood vessels. *J.Biomech.Eng.* 115: 1-12, 1993.

23. **Girard, P.R. and R.M. Nerem.** Endothelial cell signaling and cytoskeletal changes in response to shear stress. *Front.Med.Biol.Eng.* 5: 31-36, 1993.

24. **Girard, P.R. and R.M. Nerem.** Shear stress modulates endothelial cell morphology and F-actin organization through the regulation of focal adhesion-associated proteins. *J.Cell Physiol.* 163: 179-193, 1995.

25. **Gorczynski, R.M. and B.R. Duling.** Role of oxygen in arteriolar functional vasodilation in hamster striated muscle. *Am.J.Physiol.* 235: H505-H515: 1978.

26. **Grabowski, E.F., E.A. Jaffe, and B.B. Weksler.** Prostacyclin production by cultured endothelial cell monolayers exposed to step increases in shear stress. *Journal of Laboratory & Clinical Medicine* 105: 36-43, 1985.

27. **Gradshteyn, I.S. and I.M. Ryzhik.** *Table of Integrals, Series, and Products.* NY: Academic Press, 1980,

28. **Grande, P.O. and S. Mellander.** Characteristics of static and dynamic regulatory mechanisms in myogenic microvascular control. *Acta*

Physiologica Scandinavica 102: 231-245, 1978.

29. **Gudi, S., J.P. Nolan, and J.A. Frangos.** Modulation of GTPase activity of G proteins by fluid shear stress and phospholipid composition. *Proc.Natl.Acad.Sci.USA* 95: 2515-2519, 1998.

30. **Gudi, S.R., C.B. Clark, and J.A. Frangos.** Fluid flow rapidly activates G proteins in human endothelial cells. Involvement of G proteins in mechanochemical signal transduction. *Circulation Research* 79: 834-839, 1996.

31. **Hush, J.M., P. Wadsworth, D.A. Callaham, and P.K. Helper.** Quantification of microtubule dynamics in living plant cells using fluorescence redistribution after photobleaching. *Journal of Cell Science* 107: 775-784, 1994.(Abstract)

32. **Hutcheson, I.R. and T.M. Griffith.** Mechanotransduction through the endothelial cytoskeleton: mediation of flow- but not agonist-induced EDRF release. *British Journal of Pharmacology* 118: 720-726, 1996.

33. **Ikeoka, K., K. Nishigaki, M. Ohyanagi, and J.E. Faber.** In vitro analysis of alpha-adrenoceptor interactions with the myogenic response in resistance vessels. *J.Vasc.Res.* 29: 313-321, 1992.

34. **Jacobson, K.** Lateral Diffusion in Membranes. *Cell Motility* 3: 367-373, 1983.

35. **Jain, R.K., R.J. Stock, R.C. Srikanth, and M. Rueter.** Convection and diffusion measurements using fluorescence recovery after photobleaching and video frame analysis; in vitro calibration and assessment. *Microvascular Research* 39: 77-93, 1990.

36. **Johnson, P.C. and M. Intaglietta.** Contributions of pressure and flow sensitivity to autoregulation in mesenteric arterioles. *Am.J.Physiol.* 231(6): 1686-1698, 1976.

37. **Kamiya, A., R. Bukhari, and T. Togawa.** Adaptive regulation of wall shear stress optimizing the vascular tree function. *Bull.math.Bio.* 46, No. 1: 127-137, 1984.

38. **Kim, D.W., B.L. Langille, M.K. Wong, and A.I. Gotlieb.** Patterns of endothelial microfilament distribution in the rabbit aorta in situ. *Circulation Research* 64: 21-31, 1989.

39. **Knudsen, H.L. and J.A. Frangos.** Role of cytoskeleton in shear stress-induced endothelial nitric oxide production. *Am.J.Physiol.1997.Jul.* 273: H347-H3551997.

40. **Koller, A. and G. Kaley.** Endothelial regulation of wall shear stress and blood flow in skeletal muscle microcirculation. *Am.J.Physiol.* 260: H862-H868, 1991.

41. **Koller, A., D. Sun, A. Huang, and G. Kaley.** Corelease of nitric oxide and prostaglandins mediates flow- dependent dilation of rat gracilis muscle arterioles. *Am.J.Physiol.* 267: H326-H332, 1994.

42. **Koller, A., D. Sun, and G. Kaley.** Role of shear stress and endothelial prostaglandins in flow- and viscosity-induced dilation of arterioles in vitro. *Circ.Res.* 72: 1276-1284, 1993.

43. **Kuo, L., M.J. Davis, and W.M. Chilian.** Longitudinal gradients for endothelium-dependent and - independent vascular responses in the coronary microcirculation. *Circulation* 92: 518-525, 1995.

44. **Kwok, R. and E. Evans.** Thermoelasticity of large lecithin bilayer vesicles. *Biophysical Journal* 35: 637-652, 1981.

45. **Lee, S. and G.W. Schmid-Schonbein.** Biomechanical model for the myogenic response in the microcirculation: Part I--Formulation and initial testing. *Journal of Biomechanical Engineering* 118: 145-151, 1996.

46. **Lehr, H.A. and K. Messmer.** The microcirculation in atherogenesis. [Review] [61 refs]. *Cardiovascular Research* 32: 781-788, 1996.

47. **Macdonald, A.G.** The homeoviscous theory of adaptation applied to excitable membranes: A critical evaluation. *Biochim.Biophys.Acta Rev.Biomembr.* 1031: 291-310, 1990.

48. **Meininger, G.A.** Responses of sequentially branching macro- and microvessels during reactive hyperemia in the skeletal muscle. *Microvasc.Res.* 34: 29-45, 1987.

49. **Meininger, G.A., K.L. Fehr, and M.B. Yates.** Anatomic and hemodynamic characteristics of the blood vessels feeding the cremaster skeletal muscle in the rat. *Microvasc.Res.* 33: 81-97, 1987.

50. **Meininger, G.A., C.A. Mack, K.L. Fehr, and H.G. Bohlen.** Myogenic vasoregulation overrides local metabolic control in resting rat skeletal muscle. *Circ.Res.* 60: 861-870, 1987.

51. **Mouritsen, O.G. and M. Bloom.** Mattress model of lipid-protein interactions in membranes. *Biophysical Journal* 46: 141-153, 1984.

52. **Mouritsen, O.G. and M. Bloom.** Models of lipid-protein interactions in membranes. [Review] [75 refs]. *Annual Review of Biophysics & Biomolecular Structure* 22: 145-171, 1993.

53. **Muller, J.M., W.M. Chilian, and M.J. Davis.** Integrin signaling transduces shear stress--dependent vasodilation of coronary arterioles. *Circulation Research* 80: 320-326, 1997.

54. **Murray, C.D.** The physiological principle of minimum work. I. The vascular system and the cost of blood volume. *Physiology* 12: 207-214, 1926.

55. **Nagel, T., N. Resnick, W.J. Atkinson, C.F. Dewey, Jr., and M.A.J. Gimbrone.** Shear stress selectively upregulates intercellular adhesion molecule-1 expression in cultured human vascular endothelial cells. *J.Clin.Invest.* 94: 885-891, 1994.

56. **Olesen, S.P., D.E. Clapham, and P.F. Davies.** Haemodynamic shear stress activates a K^+ current in vascular endothelial cells. *Nature* 331: 168-170, 1988.

57. **Porret, C.-A., N. Stergiopulos, and J.-J. Meister.** Flow-driven diameter response in rat femoral arteries perfused in vitro. *Annals of Biomedical Engineering* 26: 526-533, 1998.

58. **Prasad, A.R., S.A. Logan, R.M. Nerem, C.J. Schwartz, and E.A. Sprague.** Flow-related responses of intracellular inositol phosphate levels in cultured aortic endothelial cells. *Circ.Res.* 72: 827-836, 1993.

59. **Reich, K.M., T.N. McAllister, S. Gudi, and J.A. Frangos.** Activation of G proteins mediates flow-induced prostaglandin E2 production in osteoblasts. *Endocrinology* 138: 1014-1018, 1997.

60. **Saito, Y., A. Eraslan, and R.L. Hester.** Role of EDRFs in the control of arteriolar diameter during increased metabolism of striated muscle. *Am.J.Physiol.* 267: H195-H2001994.

61. **Satcher, R.L., Jr. and C.F. Dewey, Jr.** Theoretical estimates of mechanical properties of the endothelial cell cytoskeleton. *Biophysical Journal* 71: 109-118, 1996.

62. **Sato, M., N. Ohshima, and R.M. Nerem.** Viscoelastic properties of cultured porcine aortic endothelial cells exposed to shear stress. *Journal of Biomechanics* 29: 461-467, 1996.

63. **Sato, M., D.P. Theret, L.T. Wheeler, N. Ohshima, and R.M. Nerem.** Application of the micropipette technique to the measurement of cultured porcine aortic endothelial cell viscoelastic properties. *Journal of Biomechanical Engineering* 112: 263-268, 1990.

64. **Schlessinger, J., D. Axelrod, D.E. Koppel, W.W. Webb, and E.L. Elson.** Lateral transport of a lipid probe and labled proteins on the cell membrane. *Science* 21: 307-309, 1977.

65. **Schmid-Schonbein, G.W., T. Kosawada, R. Skalak, and S. Chien.** Membrane model of endothelial cells and leukocytes. A proposal for the origin of a cortical stress. *Journal of Biomechanical Engineering* 117: 171-178, 1995.

66. **Shinitzky, M.** The lipid regulation of receptor functions. *Biomembranes and Receptor Mechanisms* 7: 135-141, 1987.

67. **Shyy, Y.-J. and S. Chien.** Role of integrins in cellular responses to mechanical

stress and adhesion. *Current Opinion in Cell Biology* 9: 707-713, 1997.

68. **Shyy, Y.J., H.J. Hsieh, S. Usami, and S. Chien.** Fluid shear stress induces a biphasic response of human monocyte chemotactic protein 1 gene expression in vascular endothelium. *Proc.Natl.Acad.Sci.USA* 91: 4678-4682, 1994.

69. **Singer, S.J. and G.L. Nicolson.** The fluid mosaic model of the structure of cell membranes. *Science* 175: 7201972.

70. **Storrie, B., R. Pepperkok, E.H.K. Stelzer, and T.E. Kreis.** The intrcellular mobility of a viral membrane glycoprotein measured by confocal microscope fluorescence recovery after photobleaching. *Journal of Cell Science* 107: 1309-1319, 1994.

71. **Sun, D., A. Huang, A. Koller, and G. Kaley.** Short-term daily exercise activity enhances endothelial NO synthesis in skeletal muscle arterioles of rats. *J.Appl.Physiol.* 76: 2241-2247, 1994.

72. **Takahashi, M., T. Ishida, O. Traub, M.A. Corson, and B.C. Berk.** Mechanotransduction in endothelial cells: temporal signaling events in response to shear stress. [Review] [55 refs]. *Journal of Vascular Research* 34: 212-219, 1997.

73. **Taylor, C.W.** The role of G proteins in transmembrane signalling. [Review] [165 refs]. *Biochemical Journal* 272: 1-13, 1990.

74. **Trudell, J.R.** Role of Membrane Fluidity in Anesthetic Action. In: *Drug and Anesthetic Effects on Membrane Structure and Function*, edited by R.C. Aloia, C.C. Curtain, and L.M. Gordon. New York: Wiley-Liss, Inc., 1991, p. 1-14.

75. **Wallenstein, S., C.L. Zucker, and J.L. Fleiss.** Some statistical methods useful in circulation research. *Circ.Res.* 47 (1): 1-9, 1980.

76. **Wang, D.L., B.-S. Wung, Y.-J. Shyy, C.-F. Lin, Y.-J. Chao, S. Usami, and S. Chien.** Mechanical strain induces monocyte chemotactic protein-1 gene expression in endothelial cells: Effects of mechanical strain on monocyte

adhesion to endothelial cells. *Circ.Res.* 77: 294-302, 1995.

77. **Wang, N., J.P. Butler, and D.E. Ingber.** Mechanotransduction across the cell surface and through the cytoskeleton [see comments]. *Science* 260: 1124-1127, 1993.

78. **Weinbaum, S.** 1997 Whitaker distinguished lecture: models to solve mysteries in biomechanics at the cellular level: a new view of fiber matrix layers. *Annals of Biomedical Engineering* 26: 627-643, 1998.

79. **Wiesner, T.F., B.C. Berk, and R.M. Nerem.** A mathematical model of the cytosolic-free calcium response in endothelial cells to fluid shear stress. *Proceedings of the National Academy of Sciences of the United States of America* 94: 3726-3731, 1997.

80. **Zhu, L., Lemons, D., and Weinbaum, S.** A New Approach for Predicting the Enhancement in the Effective Conductivity of Perfused Muscle Tissue Due to Hyperthermia. Annals of Biomedical Engineering 23, 1-12. 1995. (GENERIC Ref Type: Journal (Full)

IMAGE EVALUATION
TEST TARGET (QA-3)

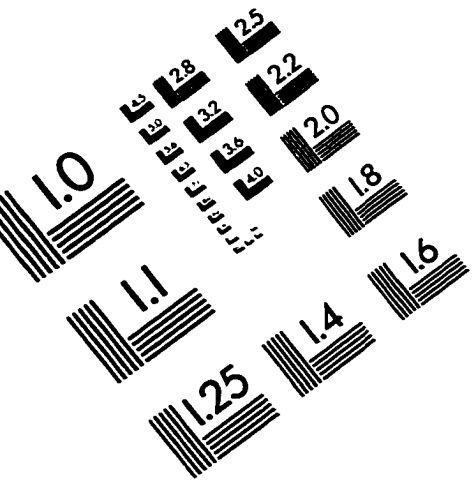

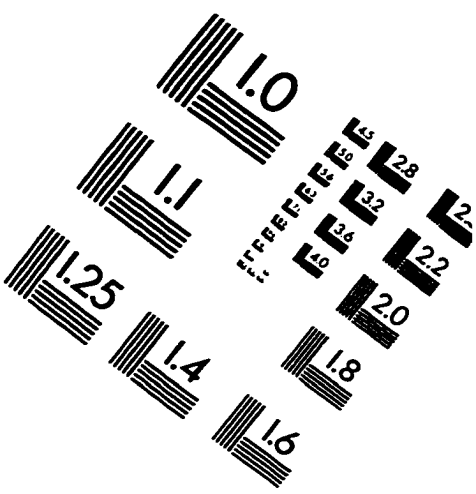

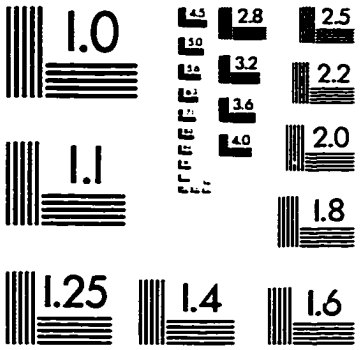

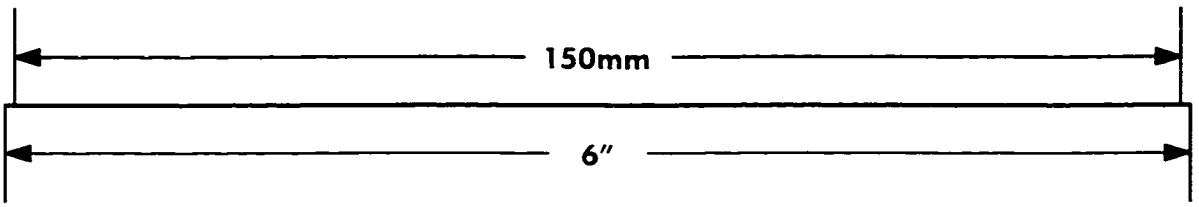

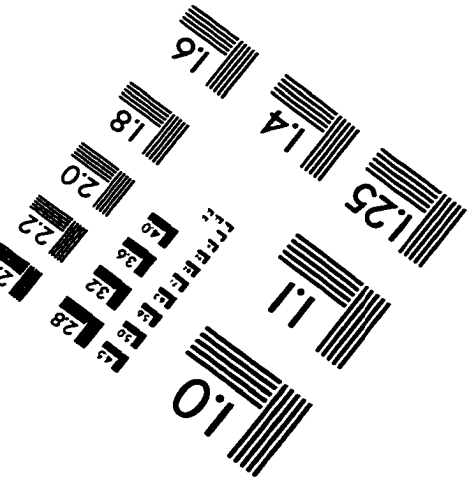

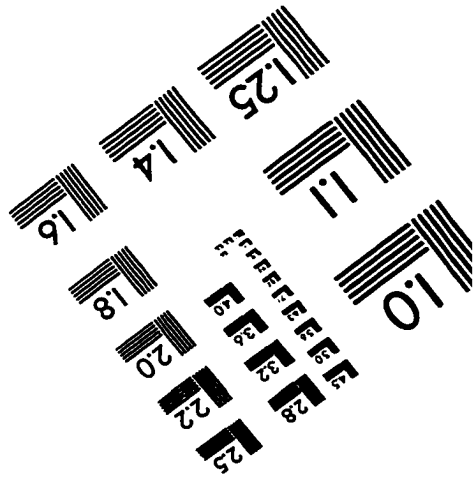

APPLIED IMAGE . Inc
1653 East Main Street
Rochester, NY 14609 USA
Phone: 716/482-0300
Fax: 716/288-5989